



Geomechanical Effects of Cumulative Fluid Injection  
through Hydraulic Fracturing in the Kiskatinaw  
Seismic Monitoring and Mitigation Area (KSMMA),  
British Columbia

for the BC Oil and Gas Research and Innovation Society

*ER-Seismic-2022-04*

**Final Report**

by

Enlighten Geoscience Ltd.

July 28, 2022

## Disclaimer and Document Authentication

All work performed for this project and information provided in this report is of the highest technical quality possible given data availability, quality, limitations and uncertainties at the time the work was completed. Enlighten Geoscience Ltd. cannot guarantee the accuracy of the material included in this document, and any conclusions or recommendations provided could change upon inclusion of new data and/or knowledge relevant to the investigation.

This report was written as a contribution to understanding induced seismicity in the Kiskatinaw Seismic Monitoring and Mitigation Area. The authors of, and contributors to, this report make no guarantees regarding the predictability or consequences of induced seismicity and its associated risks, nor the economic valuation of associated assets affected by induced seismicity.

This project was performed in Alberta for an entity in British Columbia. This document is therefore being authenticated per guidelines of both the Association of Professional Engineers and Geoscientists of Alberta and Engineers and Geoscientists BC.

## Executive Summary

This report describes the work undertaken for the British Columbia Oil and Gas Research and Innovation Society (BC OGRIS) by Enlighten Geoscience Ltd. (Enlighten) to investigate the relationship between fluid injected into the Montney formation during hydraulic fracturing operations and induced seismicity in the Kiskatinaw Seismic Monitoring and Mitigation Area (KSMMA) in Northeast BC. The purpose of this work is to advance research that government and regulatory agencies may use to guide current policies for managing induced seismicity risk and safeguarding the public.

The study presented herein is composed of two parts. The first part is a KSMMA-wide accounting of fluids both injected into and extracted from the Montney over time (2008 to 2020), both for the whole Montney and individual Montney stratigraphic intervals. For this regional analysis, the following data were mapped and analyzed: volume of fluid injected, volume of fluid produced, net fluid volume and pore pressure. The results are presented as time-series animations clearly illustrating both yearly and cumulative changes.

The second part of the study is a detailed analysis of stress and induced seismicity related to hydraulically fractured completions on wells drilled from a pad located at 03-09-081-17W6. Diagnostic Fracture Injection Test (DFIT) data were interpreted for minimum principal stress, and hydraulic fracturing stage data were analyzed to identify changes in stress during completions that may be related to induced seismic events. The seismic events associated with the pad completions were analyzed by investigating variations in earthquake b-values as a function of time.

Data for the fluids mapping were compiled from several different databases and screened for quality and consistency. Liquids includes volumes reported as condensate, nC<sub>2</sub> to nC<sub>5</sub>, load fluid, water, oil, slickwater and other fluids. Fluid (pore) pressure data were derived from a database compiled by Enlighten for previous projects (Fox and Watson, 2019; Enlighten Geoscience, 2021). The database was updated to include any pressures reported since the last project. For the purposes of this study, the database includes data that show evidence of production-induced drawdown or injection-induced increase. The resulting fluids and pressure map set comprises over 550 individual image files that were used to create the animations. The individual PNG files and the animation MOV files are provided in the appendices. Hyperlinks to the MOV files are also included in the body of the report.

The animation of yearly liquids injection into the entire Montney illustrates a general increase in the amount of liquids injected from 2008 through 2017. The amount of liquid injected from 2018 through 2020 is generally lower. There is a significant decrease in liquids injection for 2020, likely reflecting the decrease in industry activity during that time. Although the intensity of liquids injection has varied from year to year, liquids production has resulted in a lower net liquids injection each year. A similar pattern occurs within each Montney stratigraphic interval, although it is important to note that these intervals have not, to date, been exploited equally. Mapping of the cumulative levels of liquids injection, production and net injection confirms that negative net injection levels in a series of years do not mask an overall net positive injection into the Montney, and more liquids have been produced from the Montney than injected into it. Although the Upper Montney has experienced the largest volume of liquid injection over a broad area, wells completed in this interval have experienced relatively low levels of associated induced seismic events. The pore pressure maps and animations illustrate the range of

pressure decline across the KSMMA. As the interval first brought on the production and the most widely exploited, the Upper Montney displays the most localities of reduced pressure. Decreasing pore pressure would serve to lower the risk of induced seismicity through a corresponding increase in effective normal stress on pre-existing fractures and faults. Earthquake data for the KSMMA are also presented as an annual time series revealing an increasing level of events greater than magnitude 2 that accompanied the increased development in the KSMMA up to the end of 2017 followed by a noticeable decrease in the number of larger events for 2018 through 2020.

The analysis of the 3-9 pad was partly focused on the wells that had complete DFIT data sets for interpretation. Reinterpreted closure pressures align better with early hydraulic fracture stage data than do operator-reported ISIP data from the DFITs. All of the pad wells associated with induced events, and many of the wells that are not, show a clear trend of increasing hydraulic fracturing stage ISIP with increasing stage number. There appears to be an increase in seismicity rate as ISIP approaches or even exceeds the vertical stress magnitude. For several of the non-seismogenic wells that don't show this increasing trend, early stage ISIPs start out higher than the vertical stress and remain high, and these wells tended to experience completion problems such as screen-outs.

Magnitude of completeness ( $M_c$ ), b-value and error in the b-value were calculated for 17 scenarios including the full KSMMA earthquake catalog, all earthquakes associated with the 3-9 pad wells, earthquakes associated with the 3-9 pad wells for time-limited occupations in 2019, 2020 and 2021 and events assigned to 3-9 pad wells targeting specific Montney stratigraphic intervals. For each of the pad occupations, event magnitudes,  $M_c$  and b-value were examined as a function of time. The upper Middle Montney completion zone has the highest b-values. This is consistent with KSMMA-wide experience for wells targeting this stratigraphic interval. In all three pad occupations, b-values decrease over time. In all three occupations the highest magnitude events are in the middle of the occupation. It is likely that seismicity mitigation measures contributed to the reduction of seismic events later in the occupations. The 2020 occupation had the highest number of associated seismic events. By illustrating these events occurring over time, it appears they occurred on a series of small, NE-SW oriented faults.

Both the KSMMA-wide mapping and the analysis of the 3-9 Pad in this study support the theory that temporary increases in pore pressure related to hydraulic fracturing in areas proximal to critically stressed faults is the primary driver of hydraulic-fracture induced seismicity rather than continuously increasing fluid volumes. The data do not indicate that seismicity rates or event magnitudes increase over time with ongoing hydraulic fracture-based field development. The work presented here demonstrates that the effects of Montney hydraulic fracturing flowback and production more than offset the cumulative effect of fluid injection during hydraulic fracturing. The resulting stress and pressure drops would likely serve to reduce seismic risk.

Additional appendices for this report include: a full DFIT database for the KSMMA (updated from Enlighten Geoscience, 2021); the full earthquake catalogue and catalogues of the events assigned to the 3-9 pad (including details of the assignment workflow); details regarding data sources and software used in the analysis; large-format maps, map shapefiles and data files; additional figures for the 3-9 pad analysis.

## Table of Contents

Disclaimer and Document Authentication.....	i
Executive Summary.....	ii
Table of Contents.....	iv
List of Figures.....	vi
List of Tables.....	viii
I. Introduction.....	1
Study Motivation.....	1
II. Study Area.....	2
KSMMA and Study Area Definition.....	2
Structural Setting.....	3
‘3-9 Pad’ Selection.....	5
III. Project Data.....	8
Stratigraphic Assignment of Data.....	8
Fluid Injection and Production.....	8
Hydrodynamics.....	10
Seismic Catalogue.....	11
Assignment of Seismic Events to 3-9 Pad.....	11
DFIT Analysis.....	11
IV. Liquids Volume, Pressure and Seismicity Mapping.....	12
Mapping Workflow.....	12
Imaging Horizontal Well Data.....	12
Heatmap Layers.....	13
Contour Map Layers.....	13
Post Data Layers.....	13
Map Animations.....	14
Maps.....	14
Montney Liquids Injection, Production and Net Injection.....	14
Entire Montney.....	14
Montney Stratigraphic Intervals.....	22
Volumes Summary.....	42

Montney Pressure vs Depth.....	42
Montney Seismicity.....	46
V. 3-9 Pad Analysis .....	48
DFIT and Hydraulic Fracturing Stage Data Analysis .....	48
Earthquake b-value Analysis .....	56
VI. Conclusions and Recommendations.....	64
VII. Acknowledgements .....	66
VIII. Appendices .....	66
Appendix A: Databases .....	66
Appendix B: Data Sources and Software .....	66
Appendix C: Maps and Mapping Data .....	66
Appendix D: 3-9 Pad ISIP and Seismicity Plots.....	67
IX. References .....	67

## List of Figures

Figure 1. Map of Study Area including important geographical features. ....	3
Figure 2. Map of key faults in and around the KSMMA. ....	4
Figure 3. Montney comparative type section. ....	9
Figure 4. Map of Montney yearly liquids injection for 2020. ....	15
Figure 5. Map of Montney yearly liquids production for 2020. ....	16
Figure 6. Map of Montney yearly net liquids for 2020. ....	17
Figure 7. Map of Montney cumulative liquids injection through the end of 2020. ....	19
Figure 8. Map of Montney cumulative liquids production through the end of 2020. ....	20
Figure 9. Map of Montney net cumulative liquids through the end of 2020. ....	21
Figure 10. Cumulative completed length by stratigraphic interval. ....	22
Figure 11. Map of lower Middle Montney yearly liquids injection for 2020. ....	24
Figure 12. Map of lower Middle Montney yearly liquids production for 2020. ....	25
Figure 13. Map of lower Middle Montney yearly net liquids for 2020. ....	26
Figure 14. Map of lower Middle Montney cumulative liquids injection for 2020. ....	27
Figure 15. Map of lower Middle Montney cumulative liquids production for 2020. ....	28
Figure 16. Map of lower Middle Montney cumulative net liquids for 2020. ....	29
Figure 17. Map of upper Middle Montney yearly liquids injection for 2020. ....	30
Figure 18. Map of upper Middle Montney yearly liquids production for 2020. ....	31
Figure 19. Map of upper Middle Montney yearly net liquids for 2020. ....	32
Figure 20. Map of upper Middle Montney cumulative liquids injection for 2020. ....	33
Figure 21. Map of upper Middle Montney cumulative liquids production for 2020. ....	34
Figure 22. Map of upper Middle Montney cumulative net liquids for 2020. ....	35
Figure 23. Map of Upper Montney yearly liquids injection for 2020. ....	36
Figure 24. Map of Upper Montney yearly liquids production for 2020. ....	37
Figure 25. Map of Upper Montney yearly net liquids for 2020. ....	38
Figure 26. Map of Upper Montney cumulative liquids injection for 2020. ....	39
Figure 27. Map of Upper Montney cumulative liquids production for 2020. ....	40
Figure 28. Map of Upper Montney cumulative net liquids for 2020. ....	41
Figure 29. Map of Montney pressure vs depth gradient for 2020. ....	43
Figure 30. Map of lower Middle Montney pressure vs depth gradient for 2020. ....	44
Figure 31. Map of upper Middle Montney pressure vs depth gradient for 2020. ....	45
Figure 32. Map of Upper Montney pressure vs depth gradient for 2020. ....	46
Figure 33. Map of Montney earthquakes greater than magnitude 2 for 2020. ....	47

Figure 34. Comparison of how operator-picked ISIP values and PTA-based FFEP values correlate with closure pressure for the 3-9 DFITs. ....	49
Figure 35. DFIT FFEP, operator-picked DFIT ISIP and hydraulic fracturing stage ISIP as a function of fracture stage. ....	51
Figure 36. Number of induced seismic events as a function of stage number for the seismogenic wells on the 3-9 pad. ....	51
Figure 37. ISIP, induced seismic event count and event magnitude distribution as a function of stage number in well 104/09-34-080-17W6/00. ....	52
Figure 38. Map of well 104/09-34-080-17W6/00 and its associated induced seismic events. ....	52
Figure 39. ISIP, induced seismic event count and event magnitude distribution as a function of stage number in well 103/16-34-080-17W6/00. ....	53
Figure 40. Map of well 103/16-34-080-17W6/00 and its associated induced seismic events. ....	53
Figure 41. FFEP values from the 3-9 DFITs as a function of time. ....	56
Figure 42. Magnitude of completeness, number of events with magnitudes above $M_c$ and b-values for all of the scenarios. ....	58
Figure 43. Details for the 2019 occupation of the 3-9 pad. ....	59
Figure 44. Details for the 2020 occupation of the 3-9 pad. ....	60
Figure 45. Details for the 2021 occupation of the 3-9 pad. ....	61
Figure 46. Map of seismic events during the 2020 pad occupation. ....	63
Figure 47. Map of seismic events associated with Stage 51 of the completion of 104/09-34-080-17W6/00 (WA 36433) during the 2020 occupation of the 3-9 pad. ....	64

## List of Tables

Table 1. List of wells drilled off of 3-9 pad.....	7
Table 2. List of wells with DFITS evaluated for this study.....	12
Table 3. Summary of cumulative liquids for the KSMMA.....	42
Table 4. Scenario descriptions for the b-value analysis.....	57

## I. Introduction

This report describes the work undertaken for the British Columbia Oil and Gas Research and Innovation Society (BC OGRIS) by Enlighten Geoscience Ltd. (Enlighten) to investigate the relationship between fluid injected into the Montney formation during hydraulic fracturing operations and induced seismicity in the Kiskatinaw Seismic Monitoring and Mitigation Area (KSMMA) in Northeast BC. The primary goal of the study was to use all available public data to determine spatial, stratigraphic and temporal changes in net fluid injected into and extracted from the Montney and then examine resulting changes in pore pressure and stress. The analysis was achieved both regionally over the entire KSMMA and specifically at one pad known to have associated induced seismicity during three periods of hydraulic fracturing completions from 2019 to 2021.

For the regional analysis, the following data were mapped and analyzed:

- Volume of fluid injected into each Montney stratigraphic unit
- Volume of fluid produced from each Montney stratigraphic unit
- Net fluid volume in each Montney stratigraphic unit
- Initial pore pressure and the effect of production-induced drawdown on the reservoir pressures

The pad-specific analysis was performed on a pad located at 03-09-081-17W6. Diagnostic Fracture Injection Test (DFIT) data were interpreted for minimum principal stress, and hydraulic fracturing stage data were analyzed to identify changes in stress during completions that may be related to induced seismic events. This analysis was subcontracted to Pressure Diagnostics Ltd. and performed by Kirby Nicholson, P.Eng. (Pressure Diagnostics Ltd.), a contributor to several technical articles on modern DFIT analysis and who also performed extensive DFIT analysis for two previous KSMMA studies by Enlighten (Fox and Watson, 2019; Enlighten Geoscience, 2021). The seismic events associated with the pad completions were analyzed by investigating variations in earthquake b-values as a function of time. This analysis was performed by Dr. Alireza Babaie Mahani, P. Geo. (Mahan Geophysical Consulting Inc.), who has authored and co-authored numerous papers on induced seismicity in the KSMMA.

### Study Motivation

Induced seismicity has been a growing concern throughout North America and around the world as increasing numbers of seismic events related to oil and gas development have been occurring in areas with little or no natural historic seismicity. Induced earthquakes were initially limited to events related to large-scale wastewater injection projects, which typically were injecting into deep geological formations. Over the past decade, however, the widespread use of large-scale, multi-stage hydraulic fracturing in oil and gas wells has also led to induced earthquakes. In British Columbia, induced seismicity from hydraulic fracturing (HFIS) has been occurring related to development of the Horn River and Montney plays. Although the earthquakes have mostly been limited to nuisance events, there remains concern surrounding the unknown potential for larger ones. HFIS in the KSMMA specifically has been the subject of numerous studies and publications in recent years. Despite abundant research, however, the identification of the causal mechanism behind the induced seismicity has proven very difficult.

Injected fluid volume is often assigned responsibility for induced earthquakes. In many cases of seismicity induced by wastewater disposal, there does appear to be a link between injected volumes and induced earthquakes, but the actual physical process responsible for the earthquakes is the resulting increase in subsurface fluid pressure, which is often more closely related to injection rates than volumes (Lagenbruch et al., 2018). Since injected volume is one of the commonly reported data points from hydraulic fracturing operations, it is often included in so-called “machine learning” studies of HFIS and generally is one of the parameters that correlates the highest with HFIS. For example, in the Duvernay play in Alberta, the number of induced earthquakes was found to have a linear relationship with injection volume (Schultz et al., 2018), and an analysis of eight earthquake clusters related to hydraulic fracturing operations in the KSMMA hinted at a similar relationship (Babaie Mahani, 2021). This has led to publications postulating that fluid volume during hydraulic fracturing, particularly cumulative volume, is a primary catalyst for induced seismicity and may even have a link to earthquake magnitude (e. g., Chapman, 2021). However, unlike wastewater injection, hydraulic fracturing occurs for a short duration in a formation where fluids are also being produced, so it is important to better understand the balance of fluids going in and coming out and its impact on subsurface pressure.

## II. Study Area

### KSMMA and Study Area Definition

In order to accomplish the goals of the study fully and completely, it was essential to consider data within a suitable buffer outside of the KSMMA. In comparing this study to previous studies, it is important to note that the boundary of the KSMMA was slightly modified on April 19, 2021.

As with Enlighten (2021), the Study Area, or Area of Interest (AOI), is defined by the following corners:

- SE: 93-P-09
- SW: 93-P-11
- NE: Twp. 85, Rge. 13W6 (portion east of British Columbia/Alberta boundary)
- NW: Twp. 85, Rge. 22W6

Figure 1 displays the AOI and includes as reference points:

- Revised KSMMA Boundary (as of April 19, 2021)
- Previous KSMMA Boundary
- Cities of Ft. St. John (northwest) and Dawson Creek (southeast)
- Alaska Highway

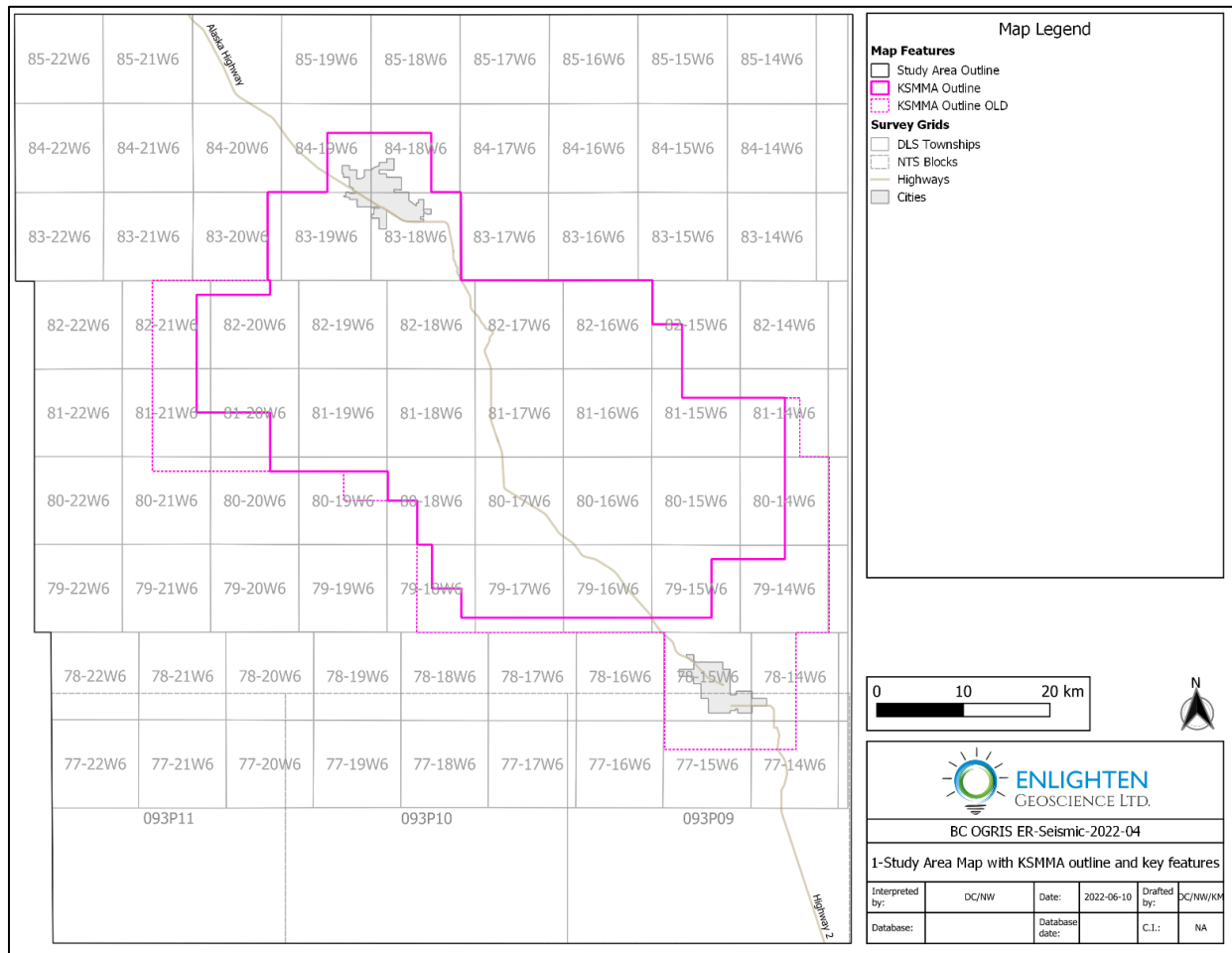


Figure 1. Map of Study Area including important geographical features.

## Structural Setting

The KSMMA has seen a complex tectonic history through a number of structural episodes including:

- Uplift of the Peace River Arch (PRA) during the Precambrian (O’Connell, 1994)
- Post-Devonian down-casting of the PRA to form the Dawson Creek Graben Complex (DCGC) (Barclay et al., 1990)
- Compression during the Columbia and Laramide orogenies leading to modification of existing structures to transpression features (O’Connell, 1994; Norgaard, 1997)
- Post-Laurentian differential uplift and erosion (Koohzare et al., 2008)

Hayes et al. (2021) and Fox and Watson (2019) provide a more detailed discussion regarding the structural setting of the KSMMA.

Enlighten Geoscience (2021) presented a set of key faults in the study area collated from public domain sources. This fault distribution is presented in Figure 2 and has been incorporated into the analysis for this report for the purposes of continuity of structural interpretation between projects. For the

purposes of this study each fault was named and assigned a numeric code for ease of description. These values are stored in the attribute table of the fault shapefile in Appendix C.

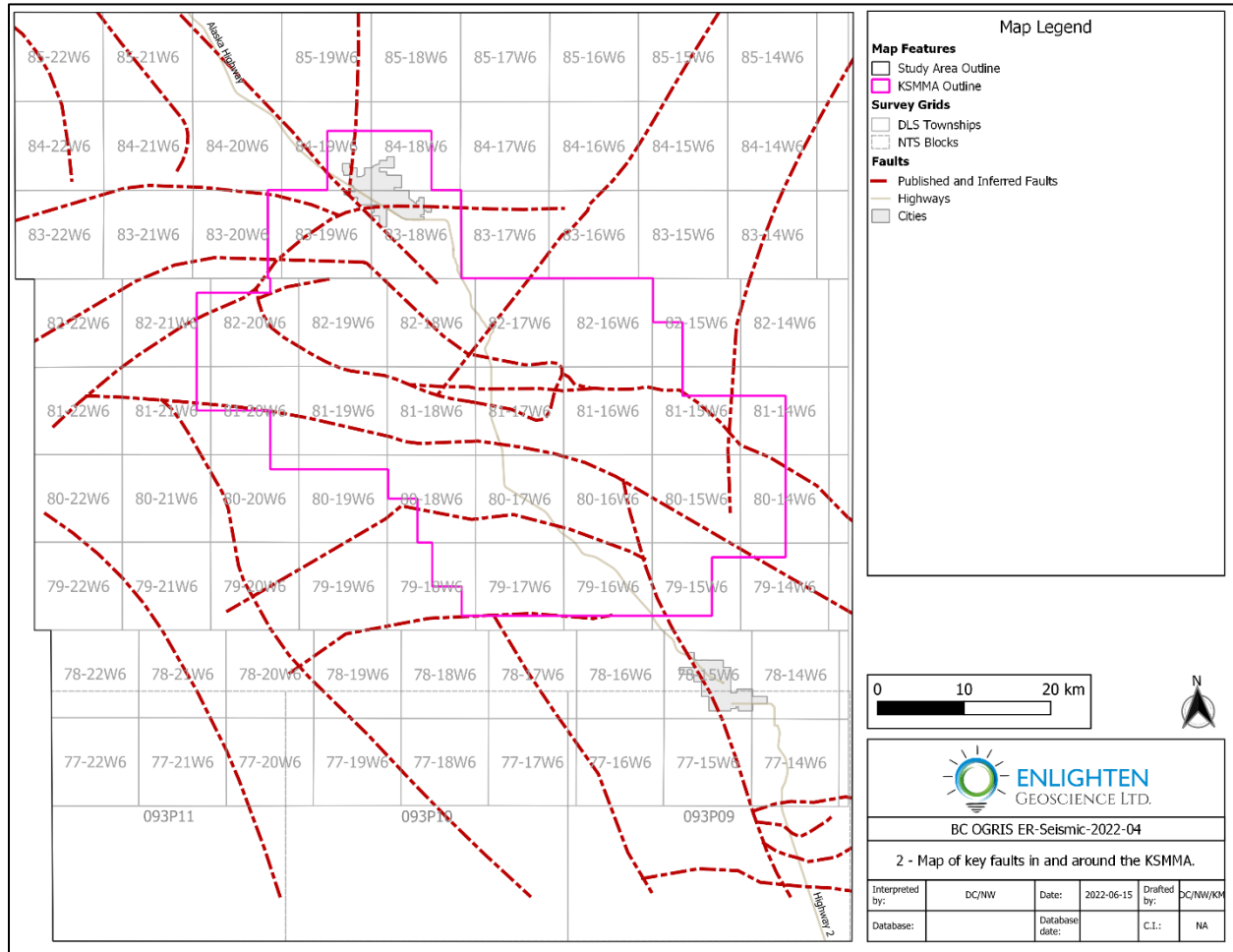


*Figure 2. Map of key faults in and around the KSMMA.*

Given that induced seismicity in the KSMMA is understood to be the result of reactivation of pre-existing faults (Roth et al., 2022), the development of the best possible structural interpretation is central to the goal of mitigating induced seismicity. The development of a structural model with the preferred level of sophistication is limited by a number of factors:

- While reflection seismic techniques are a powerful tool for the identification of structural features, the cost to licence data is prohibitive and vendor concerns regarding the protection of their intellectual property prevent the dissemination of the interpretations into the public domain.
- Oil and gas operators have in-house structural interpretations based on seismic and wellbore data. These operators are, for understandable, competitive reasons, unable to share these proprietary interpretations in the public domain.

- The operator interpretations are, furthermore, focussed on their properties and do not significantly extend those boundaries, meaning they are limited in the ability to provide a cohesive structural understanding of the entire KSMMA.
- Even if these interpretations were available, coalescing these models into a coherent structural model would be difficult (Wozniakowska et al. (2021)). Several structural features, such as strike-slip faults or faults with vertical throw below the resolution of the seismic, are difficult to conclusively identify using reflection seismic data.

The issues in published structural interpretations (imprecise fault location, differing structural interpretation styles and lack of ease of reproducibility) have been recognized in the past. The concept of “structural corridors” was introduced by Wozniakowska et al. (2021) as a method to circumvent this issue. While this approach has merits on a regional basis, the application of Coulomb frictional failure theory (i.e., the calculation of critical perturbation pressure or fault slip probability) to assess the risk of slip on faults due to an increase in fluid pressure benefits from the most detailed local structural model possible.

It is possible to create a structural model of this calibre though the use of all available wellbore data (e.g., detailed stratigraphic tops, image logs and drilling data), geophysical data other than seismic (i.e., aeromagnetic and gravity data) and the application of the concept of balanced structural cross sections and mapping. Potential additional sources of structural data have been identified during the development of this report. These data are:

- Linear trends of induced seismic events as a function of time — maps of earthquake events and resource development on a yearly basis illustrate several linear features that are likely indicative of a fault reactivated by hydraulic fracturing.
- The occurrence of kicks, inflows and other drilling events (Drilling Kicks and Blowouts by Area database, BCOGC-41720) — these events, if related to drilling through a fault, can provide the location and depth of a fault.

Incorporating these data into a structural interpretation has the potential to greatly improve the fault mapping of the KSMMA.

### ‘3-9 Pad’ Selection

The general criteria for choosing a pad for detailed analysis included:

- Pads with wells that had associated induced seismic events (wells termed *seismogenic*) in the early stages of a completion and therefore not likely related to large cumulative volumes of injected fluids liquids
- Pads with multiple occupations (periods of hydraulic fracturing completions) and a decreasing number of associated seismic events
- Pads including a significant number of wells which were completed without associated induced seismic events (wells termed *non-seismogenic*)
- Pads allowing a comparison of seismic events associated with completions in different stratigraphic intervals of the Montney

A number of well pads were initially identified by the BC OGC for the pad-based analysis. The surface locations of these pads are:

- 03-09-081-17W6
- 04-08-081-17W6
- 16-06-081-17W6
- 09-04-081-16W6
- 09-03-080-16W6
- 12-31-079-14W6
- 03-15-080-15W6
- 05-22-080-15W6
- 15-01-081-17W6
- 01-10-081-16W6
- 05-04-081-16W6

The available data in the vicinity of the suggested pads was reviewed to understand the feasibility of developing an analysis of each pad. This data review included tabulating all DFIT data in the vicinity of the pad wells and entering them into the Enlighten DFIT database (Enlighten Geoscience, 2021). The resulting, expanded database is included in Appendix A1.

All available hydraulic fracturing data for the pad wells was acquired from a series of public domain and commercial sources, collated, databased and cross-referenced for quality. It is not possible to include a copy of the resulting database as part of this report due to intellectual property concerns of data vendors.

Based on these considerations, the pad at 03-09-081-17W6 was chosen for analysis and is referred to in the remainder of this report as the 3-9 pad. The wells drilled off of the 3-9 pad with data available at the time of the study are listed in Table 1. Wells in which DFITs were run are marked with an asterisk.

WA#	UWI	Well Name	Stratigraphic Interval
36406	103/16-34-080-17W6/00*	OVV HZ TOWERLAKE AB03-09-081-17	Upper Montney
36407	104/16-34-080-17W6/00	OVV HZ TOWERLAKE AC03-09-081-17	Upper Montney
36408	100/15-08-081-17W6/00*	OVV HZ TOWERLAKE 03-09-081-17	Upper Montney
36409	103/13-08-081-17W6/00*	OVV HZ TOWERLAKE A03-09-081-17	Upper Montney
36410	102/13-08-081-17W6/00*	OVV HZ TOWERLAKE B03-09-081-17	Upper Montney
36411	102/16-07-081-17W6/00	OVV HZ TOWERLAKE C03-09-081-17	Upper Montney
36412	104/13-08-081-17W6/00*	OVV HZ TOWERLAKE D03-09-081-17	upper Middle Montney
36414	104/16-07-081-17W6/00*	OVV HZ TOWERLAKE F03-09-081-17	lower Middle Montney
36415	102/15-08-081-17W6/00*	OVV HZ TOWERLAKE G03-09-081-17	Upper Montney
36416	102/14-08-081-17W6/00	OVV HZ TOWERLAKE H03-09-081-17	Upper Montney
36417	100/14-08-081-17W6/00	OVV HZ TOWERLAKE I03-09-081-17	upper Middle Montney
36418	103/16-07-081-17W6/00	OVV HZ TOWERLAKE J03-09-081-17	upper Middle Montney
36419	100/16-08-081-17W6/00	OVV HZ TOWERLAKE K03-09-081-17	upper Middle Montney
36420	102/16-08-081-17W6/00	OVV HZ TOWERLAKE L03-09-081-17	Upper Montney
36421	103/16-08-081-17W6/00	OVV HZ TOWERLAKE M03-09-081-17	upper Middle Montney
36422	103/14-08-081-17W6/00	OVV HZ TOWERLAKE N03-09-081-17	lower Middle Montney
36423	105/13-08-081-17W6/00	OVV HZ TOWERLAKE O03-09-081-17	lower Middle Montney
36424	100/02-09-081-17W6/00	OVV HZ TOWERLAKE P03-09-081-17	Upper Montney
36424	103/15-08-081-17W6/02	OVV HZ TOWERLAKE P03-09-081-17	lower Middle Montney
36425	100/03-09-081-17W6/00	OVV HZ TOWERLAKE Q03-09-081-17	Upper Montney
36425	104/15-08-081-17W6/02	OVV HZ TOWERLAKE Q03-09-081-17	lower Middle Montney
36426	104/16-08-081-17W6/00	OVV HZ TOWERLAKE R03-09-081-17	lower Middle Montney
36427	102/09-34-080-17W6/00*	OVV HZ TOWERLAKE S03-09-081-17	Upper Montney
36428	100/08-34-080-17W6/00*	OVV HZ TOWERLAKE T03-09-081-17	Upper Montney
36429	103/08-34-080-17W6/00	OVV HZ TOWERLAKE U03-09-081-17	lower Middle Montney
36430	100/13-34-080-17W6/00*	OVV HZ TOWERLAKE V03-09-081-17	upper Middle Montney
36431	102/08-34-080-17W6/00*	OVV HZ TOWERLAKE W03-09-081-17	lower Middle Montney
36432	103/09-34-080-17W6/00*	OVV HZ TOWERLAKE X03-09-081-17	Upper Montney
36433	104/09-34-080-17W6/00*	OVV HZ TOWERLAKE Y03-09-081-17	lower Middle Montney
36434	100/16-34-080-17W6/00*	OVV HZ TOWERLAKE Z03-09-081-17	Upper Montney
36435	102/16-34-080-17W6/00*	OVV HZ TOWERLAKE AA03-09-081-17	Upper Montney
40772	100/01-03-081-17W6/00*	OVV HZ TOWER LAKE AD03-09-081-17	Upper Montney
40773	102/01-03-081-17W6/00*	OVV HZ TOWER LAKE AE03-09-081-17	Upper Montney

*Table 1. List of wells drilled off of 3-9 pad.*

### III. Project Data

Details regarding the data sources and software used in this project are provided in Appendix B.

#### Stratigraphic Assignment of Data

All Montney data (e.g., completion interval, producing zone and pressure test interval) were assigned to the following stratigraphic intervals based on Davies et al. (2018), including nomenclature:

- Upper Montney (UM)
- upper Middle Montney (uMM)
- lower Middle Montney (lMM)
- Lower Montney (LM)

Vertical stratigraphic data assignments were based on correlation of petrophysical logs to the stratigraphic model. As illustrated by the composite stratigraphic table provided in Figure 3 (Euzen et al. (2021)), the three unconformity-bounded third-order sequences defined in Davies et al. (2018) model correspond with those defined in Euzen et al. (2018), Moslow et al. (2018) and Zonneveld and Moslow (2018).

Data for vertical wells were assigned based on which intervals were completed and produced from, or which intervals were tested for pressure. Data from horizontal wells were assigned to Montney intervals by comparison of the data elevation to the geospatial grids of the elevations of the top of the interval. Depending on the location of the data and the data type, the assignments were based on either the True Vertical Depth (TVD) at the mid-point of the completion interval (e.g., a pressure test of the entire wellbore) or the TVD at the Surface-hole (SH) or Bottom-hole (BH) locations. For example, a DFIT run at the toe of a horizontal would be placed at the BH coordinates of the well, while a pressure recorder in the vertical or moderately deviated section of the well would be placed at the SH location.

#### Fluid Injection and Production

Discussions of the effect of fluid injection during hydraulic fracturing operations often only consider fluid injection without addressing the produced fluid to determine the net fluid injection. Additionally, the analysis of net fluid injection is often based on approximations of the volume of fluid injection and fluid production over a broad area rather than a precise allocation of liquids injected and produced. The stratigraphic and temporal implications of the fluid injection and production are also rarely considered. Any of these factors can potentially contribute to misleading conclusions regarding fluid injection.

The data for a more precise analysis often exists but is generally maintained in isolated databases. As an example, fluid injection during a hydraulic fracturing operation (whether a horizontal or vertical well) is recorded in the completion reports. Similarly, the fluid produced during the post-fracturing (well clean-up) phase (“load fluid”) is also primarily included in the completion and well test reports. Fluid injected into the formation subsequent to the completion for the purposes of a secondary recovery or water disposal scheme is included in the well injection reports. After a well is placed on production, water volumes, including any residual load fluid not recovered during the well clean-up phase, are included in the post-completion well production reports. Any hydrocarbon liquids produced are included in the well

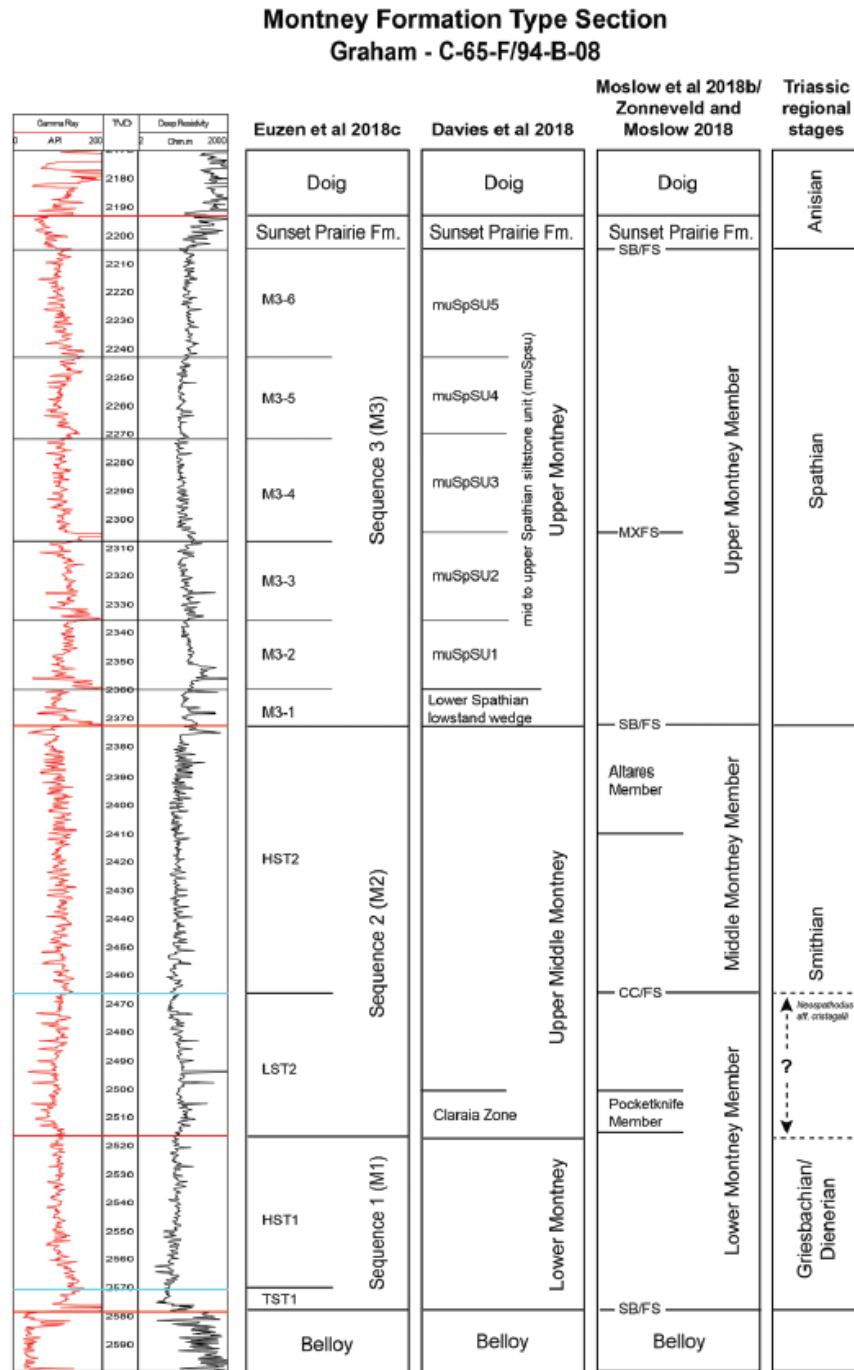


Figure 3. Montney comparative type section. Euzen et al. (2021)

test and production reports. In order to execute this project, the data from all of these various data sources needed to be collated and cross-referenced to minimize the potential to miss or double-count any of the liquids volumes.

The following tasks were completed to create the injection and production database:

- The period analyzed was set to extend from 2008 (the generally accepted initiation of hydraulic fracturing of horizontal wells in the KSMMA) to 2020 (the last year for which comprehensive data were available).
- Well completions and hydraulic fracturing data were downloaded from the following sources:
  - hydraulic\_fracture\_csv file from the BC OGC Data Centre
  - FracFocus data from the BC OGC Data Centre
  - gDCWeb™ website

Data from the gDCWeb were preferentially utilized for hydraulic fracturing data due to the greater comprehensiveness of the dataset in general and the 2008 to 2012 period in particular. BCOGC data was used where gDCWeb data was incomplete or inconsistent.

- The data in the “WELL - LOAD FLUID (M3)” and “WELL - LOAD FLUID REC (M3)” columns in the csv file exported via the gDCWeb were designated as the best summary of the total liquid and produced respectively (J. Xie – personal communication).
- Production and post-completion injection data were downloaded from Petro Ninja™
- All production and injection data were reviewed for quality and consistency (e.g., unit consistency, no missing or contradictory data).
- Production and injection data was collated and summed on an annualized basis.

Liquids includes volumes reported as condensate, nC<sub>2</sub> - nC<sub>5</sub>, load fluid, water, oil, slickwater and other fluids.

## Hydrodynamics

The goal of the hydrodynamics evaluations in the previous Enlighten projects in the KSMMA (Fox and Watson, 2019; Enlighten Geoscience, 2021) was to define the initial pore pressure state (i.e., the nature of the Montney pore pressure prior to significant activity). In developing those models, pressure data was evaluated to exclude values that resulted from poor quality tests or represented reservoirs that had experienced production-induced drawdown (PID).

The current study aims to understand the impact of fluid injection and transient pressure change at different time intervals in Montney development in the KSMMA area. To achieve this, the previous pressure database was updated, and the initial pressure state of the Montney in the region was re-evaluated. The updating of the pressure file included a thorough document search to identify any pressures not captured in the digital databases. Screening was again performed for poor quality tests (i.e.: misruns or incomplete buildups), but in this case tests indicating production-induced drawdown (PID) or injection-induced increase (III) were included in order to estimate the yearly changes in pore pressure for this study.

It was determined that the impact of Montney development on the pressure setting was negligible prior to 1999, so this was the year used as a baseline (Original Pressure State) for measuring changes in reservoir conditions. The yearly pressure data was inspected to identify the high-quality tests that are most likely to represent reservoir conditions at that time. Where a wellbore had tests over several years, a linear yearly pressure decline was calculated to estimate the pressure value for that wellbore for each

year. The final pressure test value is applied to any subsequent years (e.g., if a pressure of 12.2 kPa/m was reported in 2017 and no further tests were done, the value 12.2 was used for 2018, 2019, and 2020). If a wellbore only had one test, that value is used for all years of the yearly pressure mapping from 1999 through to 2020.

The authors determined this procedure was the best method to honour the data for the goals of the current study. The results and mapping of PID in the various Montney intervals should be considered as being more indicative in nature than predictive. This analysis could be enhanced in a future study by incorporating a more detailed reservoir engineering analysis including extrapolated pressure declines and other reservoir engineering analyses.

## Seismic Catalogue

Mahan Geophysical Consulting Inc. provided a catalogue of earthquake events over the AOI. This data was included in the seismicity maps over the Study Area and was used as an input for the b-value analysis for the 3-9 pad. A copy of the catalogue is provided in Appendix A2.

## Assignment of Seismic Events to 3-9 Pad

The BC OGC has been collaborating with Ryan Visser of the BC Seismic Research Consortium to develop an algorithm to improve the association of induced seismic events with specific wells and corresponding completion stages. This technique was utilized by Ryan Visser to identify the seismogenic wells and stages for the 3-9 pad analysis. Fracturing operations were ongoing at the 3-9 Pad in multiple Montney stratigraphic units. Best efforts have been made to attribute the events to the most likely causal well and stage, but it should be recognized that some uncertainty exists. It is important to stress that the Upper Montney and the upper Middle Montney are associated with significantly fewer, less frequent and lower magnitude events than the lower Middle Montney.

Copies of the well assignments and the workflow are provided in Appendix A2.

## DFIT Analysis

In previous Enlighten KSSMA studies (Fox and Watson, 2019; Enlighten Geoscience, 2021), all available DFITs in the KSMMA Montney were consistently evaluated and databased. Data files for this evaluation were downloaded from Petro Ninja and the BC OGC eLibrary. Some of the wells included in those analyses were on the 3-9 pad. The methods set out in those studies were applied to additional 3-9 pad DFITs available for this study. The resulting data were added to an updated DFIT database available in Appendix A1. A full list of wells with analyzed DFITs on the 3-9 pad is provided in Table 2. Other wells indicated in Table 1 as having had DFITs run did not have a full, interpretable dataset available. Minimum requirements for full DFIT re-interpretation include:

- A .CSV or .PAS file including pumping and fall-off pressure data, usually recorded at a 1-second frequency
- Pressure gauge location (surface or downhole)
- True vertical depth of gauge and injection port (or measured depths with well deviation survey)
- Wellbore fluid density and injection fluid density at surface
- Injection rates and total volume

- Descriptions of operational issues, if available

The most common missing component in the public data set is the .CSV or .PAS file recorded during the DFIT, because these files were not required to be submitted by the regulator at the time of the tests.

WA#	UWI	Well Name	Stratigraphic Interval
36406	103/16-34-080-17W6/00	OVV HZ TOWERLAKE AB03-09-081-17	lower Middle Montney
36408	100/15-08-081-17W6/00	OVV HZ TOWERLAKE 03-09-081-17	Upper Montney
36409	103/13-08-081-17W6/00	OVV HZ TOWERLAKE A03-09-081-17	Upper Montney
36410	102/13-08-081-17W6/00	OVV HZ TOWERLAKE B03-09-081-17	Upper Montney
36412	104/13-08-081-17W6/00	OVV HZ TOWERLAKE D03-09-081-17	upper Middle Montney
36415	102/15-08-081-17W6/00	OVV HZ TOWERLAKE G03-09-081-17	Upper Montney
36427	102/09-34-080-17W6/00	OVV HZ TOWERLAKE S03-09-081-17	Upper Montney
36428	100/08-34-080-17W6/00	OVV HZ TOWERLAKE T03-09-081-17	Upper Montney
36434	100/16-34-080-17W6/00	OVV HZ TOWERLAKE Z03-09-081-17	Upper Montney
40772	100/01-03-081-17W6/00	OVV HZ TOWER LAKE AD03-09-081-17	Upper Montney
40773	102/01-03-081-17W6/00	OVV HZ TOWER LAKE AE03-09-081-17	Upper Montney

Table 2. List of wells with DFITS evaluated for this study.

As of May 31, 2022, the completion of the data search for this study, the files of 1,705 wells have been reviewed for DFIT data (including those for this and Enlighten’s two previous KSMMA projects). Of these wells (figures in parentheses indicate values from Enlighten Geoscience, 2021 report):

- 660 (474) wells have operator and/or service company closure pressure data
- 638 (96) wells have the original data files that would allow for detailed DFIT interpretation for closure pressure
- 729 (538) wells provide operator pore pressure data, including 83 (82) wells with pore pressure estimates corroborated by independent analysis of the DFIT (e.g., there is a service company or third-party report available in the data set)

## IV. Liquids Volume, Pressure and Seismicity Mapping

### Mapping Workflow

#### [Imaging Horizontal Well Data](#)

Proper mapping of data for horizontal wells poses significant challenges. An ideal dataset would include injection, production and pressure data assigned to each completion interval along the horizontal portion of the well. The data is only partially available to this level of detail. In addition, wellbore deviation surveys are not available for a significant subset of the horizontal wells. Given that the majority of the data comes from horizontals, it was important to handle this data in a consistent manner to best represent the geographical representation of the data.

Since detailed stage data was not available for each wellbore, the following process was used to distribute the production and injection data along horizontal wellbores: The data were evenly divided every 150 m along the path of the horizontal beginning at 450 m from the SH location through to the Measured Total Depth (MD) of the well (for wells in the AOI, the heel of a wellbore is typically 300 m to 450 m laterally from the SH location). As an example, for a 3,000 m horizontal well this process distributes the data evenly over 17 points along the wellbore at a 150 m spacing. If a well's deviation survey was unavailable, a line from the SH to BH locations was used to approximate the well path.

After the data was assigned a temporal, stratigraphic and geographical value, the following map layers were constructed:

- Heatmaps
- Contour Maps
- Post Maps

### [Heatmap Layers](#)

Geospatial grid algorithms commonly used to create contour maps are an inadequate tool for visualizing the injection and production data due to a tendency to fill regions with no wellbores with grid values or artefacts. For this reason, 'Heatmaps' were used to visualize the injection and production data using an algorithm incorporated within the QGIS mapping software used in this study. Heatmaps are an interpolation technique that is useful in outlining the density of input features within a confined geographical space.

A Dominion Land Survey (DLS) section (one square mile) is a common reference area for oil and gas operations. The Heatmaps were created using a one mile by one mile grid. Due to survey inconsistencies, the Earth's curvature and the size of the AOI, this grid does not precisely correspond to the DLS grid but does, however, represent a close approximation.

Yearly values and cumulative values to each year were used to create an annualized series of map layers displaying total fluid production, total fluid injection, and the net liquids injection.

### [Contour Map Layers](#)

The data for study components that reflect regionally extensive data sets (i.e., pore pressure) were gridded with the Minimum Curvature algorithm using Surfer™ that allowed the generation of contours and map colour fills.

Pressure vs Depth (PD) maps were generated for the original pressure state and for each year from 2008 through 2020 to represent the pore pressure during that year.

### [Post Data Layers](#)

Some data are best represented by a symbol at a specific geographic location. These data can include the earthquake catalogue or well locations and horizontal well paths.

## [Map Animations](#)

Animations of the yearly map layers for each of the data types were created by the following process:

- Maps pertaining to a particular year, stratigraphic interval and data class (e.g., 2008, uMM and Cumulative Liquids Injection) were printed to a Portable Network Graphics (PNG) file.
- The PNG files were then combined in order of increasing year into a MOV file using Windows Video Editor.
- Given the size of the MOV files, the animations are stored on a OneDrive folder which may be easily accessed through this [link](#). Individual files can be accessed through the links in the following sections. These links will be maintained until at least July 2024. All files are also available with the other project deliverables at the BC OGRIS website.
- The report figures consist of maps for the year 2020 for map classes requiring animations. The reader is encouraged to review the animations in conjunction with reviewing of the report.

## [Maps](#)

Developing the animations required the creation of over 550 individual image files. The individual PNG files are provided in Appendix C4. The images provided as map figures illustrate the values for the year 2020. A hyperlink to the MOV file for the subject map suite is provided immediately below the figure caption.

## [Montney Liquids Injection, Production and Net Injection](#)

Visualization of the liquids injection, production and net injection has been performed on both a yearly and cumulative basis for both the entire Montney and each Montney stratigraphic interval from 2008 to 2020. The discussion presented below utilizes static maps for 2020, but following each map is a link to an animation covering all years.

Yearly Net Liquids was calculated by subtracting the Yearly Liquids Injection grid from the grid for the Yearly Liquids Production. As a result, light to dark blue colours on the net injection maps indicate more injection than production, while orange colours indicate more production than injection. A similar methodology was used to create the Cumulative Net Liquids maps using the Cumulative Liquids Injection and Cumulative Liquids Production grids. Similar to the yearly maps, the blue hues represent areas with more cumulative injection while the orange hues represent Net Cumulative withdrawals from the formation.

### [Entire Montney](#)

Figure 4 provides the first heat map, which displays the annual water injection into the entire Montney in 2020. Its associated animation shows the same for each year from 2008 to 2020.

The animation of Montney liquids injection illustrates a general increase in the amount of liquids injected from 2008 through 2017. The amount of liquid injected from 2018 through 2020 is generally lower. It is possible this decrease is, in part, attributable to the mitigation measures put in place after the establishment of the KSMMA in May 2018. The significantly larger decrease in liquids injection for 2020 might reflect the decrease in industry activity related to the Covid-19 pandemic and the associated drop in natural gas liquids pricing, which is a key driver of activity in the KSMMA.

Figure 5 presents the yearly liquids production from the Montney for 2020, and its associated animation shows the same for each year from 2008 to 2020. The two data sets presented thus far illustrate that although the intensity of liquids injection has varied from year to year, liquids production has continued. This has resulted in in a lower net liquids injection. The net liquids injection map for 2020, shown in Figure 6, illustrates this for the year 2020. The associated animation shows net liquids injection for each year from 2008 to 2020. In general terms, a similar pattern occurs as the maps for each stratigraphic interval are considered (see below). A particular heat map square mile might initially display a positive level of liquids injection, but as the load fluid and production fluid are considered the net injection amount decreases and is generally a negative amount. Regardless of the stratigraphic interval or year considered, it is important to note that the injection activity is often located proximal to the fault traces indicated on the maps. The reasons for this concentration of exploration effort are unclear.

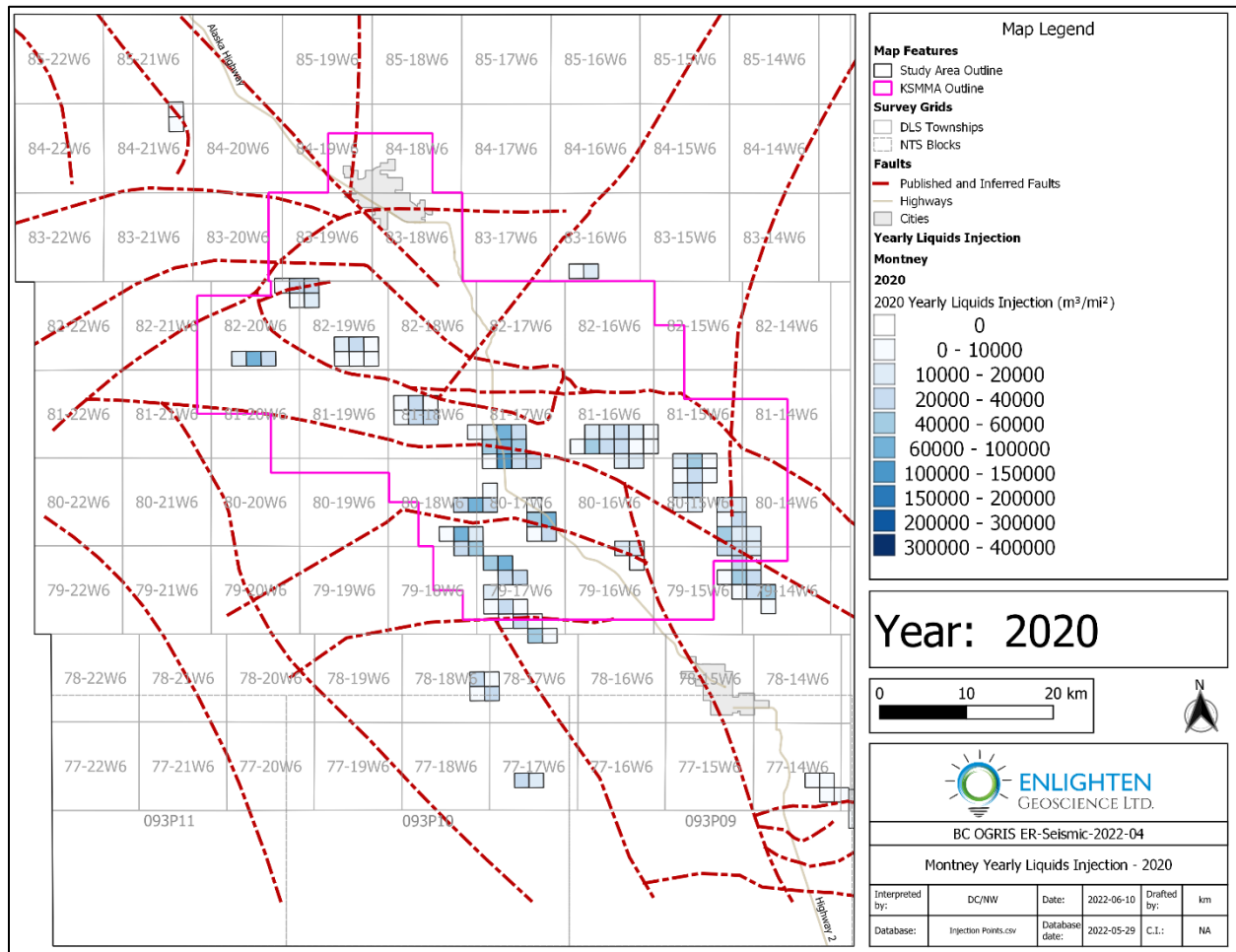


Figure 4. Map of Montney yearly liquids injection for 2020.

[Link to map animation of Montney yearly liquids injection from 2008 to 2020.](#)

*Geomechanical Effects of Cumulative Fluid Injection through Hydraulic Fracturing in the Kiskatinaw Seismic Monitoring and Mitigation Area, British Columbia (ER-Seismic-2022-04)*

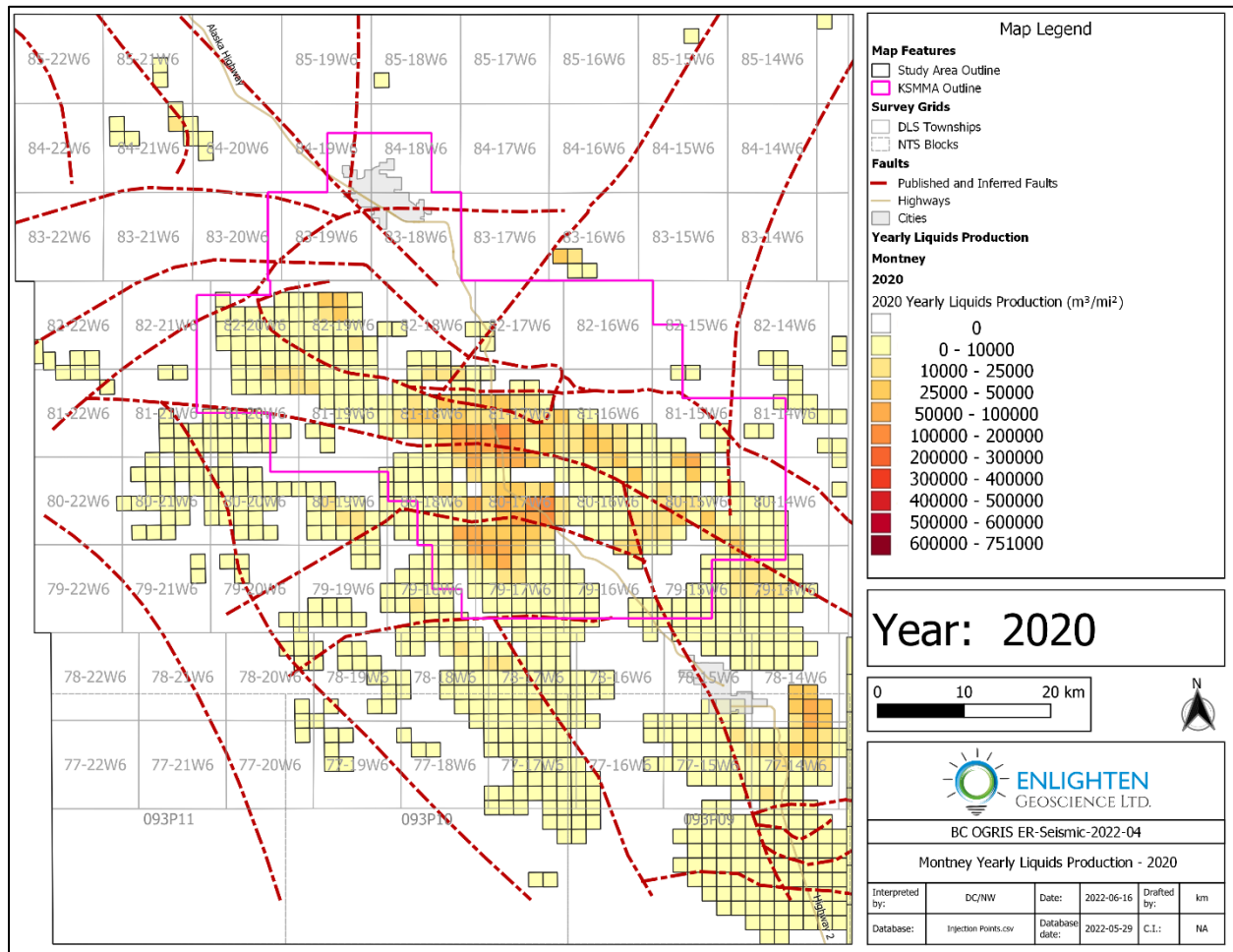


Figure 5. Map of Montney yearly liquids production for 2020.

[Link to map animation of Montney yearly liquid production from 2008 to 2020.](#)

Geomechanical Effects of Cumulative Fluid Injection through Hydraulic Fracturing in the Kiskatinaw Seismic Monitoring and Mitigation Area, British Columbia (ER-Seismic-2022-04)

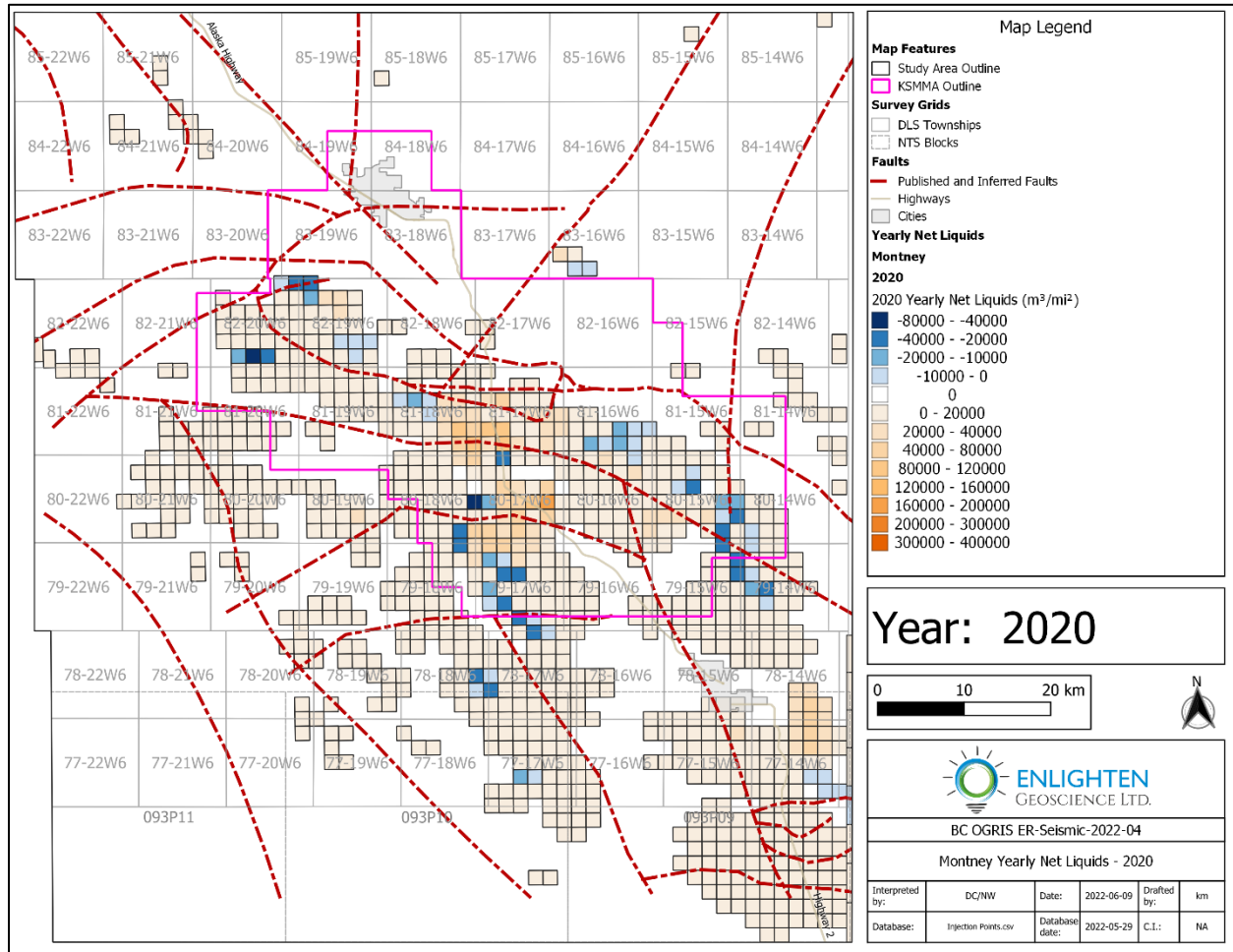


Figure 6. Map of Montney yearly net liquids for 2020.

[Link to map animation of Montney yearly net liquids from 2008 to 2020.](#)

Adding the volumes injected and produced on a year over year basis allows the cumulative levels of liquids injection, production and net injection to be calculated and mapped. This method of displaying the data allows for confirmation that negative net injection levels in a series of years do not mask an overall net positive injection into the Montney. Figures 7 through 9 display the Montney cumulative liquids injection, cumulative liquids production and cumulative net liquids injection for the period from 2008 to the end of 2020. The associated animations provide the same information up to and including each year from 2008 to 2020.

A significant volume of fluid has been injected into the KSMMA area Montney. Extracting values from the total Montney cumulative liquids injection geospatial grids indicates that, through to the end of 2020, 19,753,324 m<sup>3</sup> of liquids has been injected. While this is a large volume of liquids, it is important to realize that this fluid was introduced over a period of 13 years into an area of 2,012.6 km<sup>2</sup> and a rock volume of 629,044,586,040 m<sup>3</sup> distributed over four distinct stratigraphic intervals. To provide a sense of perspective, the total liquids injected into the entire Montney represents 0.0031% of the Montney rock volume underlying the KSMMA in contrast to the average porosity reported by the BCOGC for the Heritage Montney A Pool of 7.1%.

When the cumulative net liquids production to the end of 2020 is considered relative to the total porous rock volume of the Montney within the KSMMA in a similar fashion as with the cumulative net liquids injection to 2020, it illustrates that the cumulative liquids production was 41,048,119 m<sup>3</sup>.

*Geomechanical Effects of Cumulative Fluid Injection through Hydraulic Fracturing in the Kiskatinaw Seismic Monitoring and Mitigation Area, British Columbia (ER-Seismic-2022-04)*

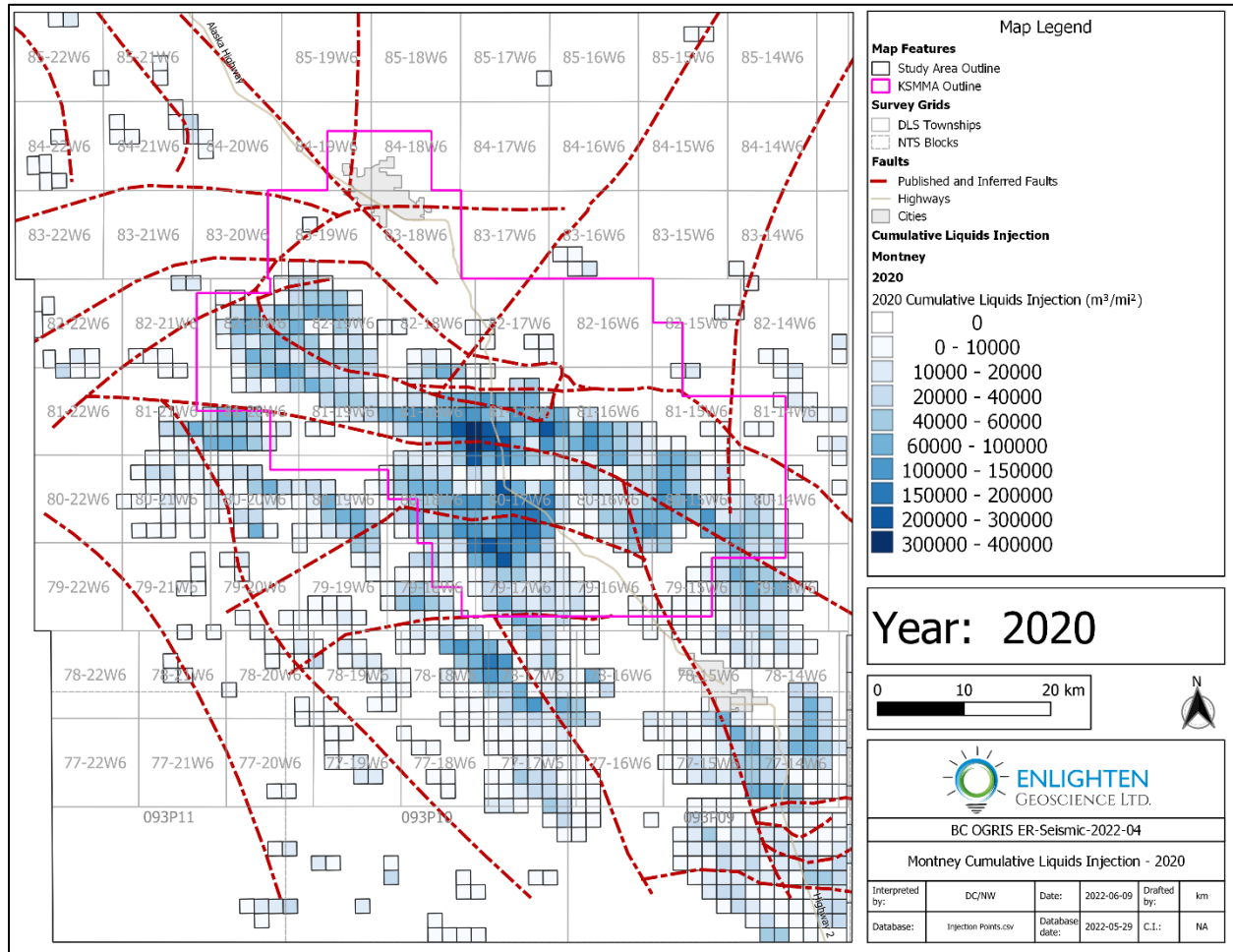


Figure 7. Map of Montney cumulative liquids injection through the end of 2020.

[Link to map animation of Montney cumulative liquids injection from 2008 to 2020.](#)

Geomechanical Effects of Cumulative Fluid Injection through Hydraulic Fracturing in the Kiskatinaw Seismic Monitoring and Mitigation Area, British Columbia (ER-Seismic-2022-04)

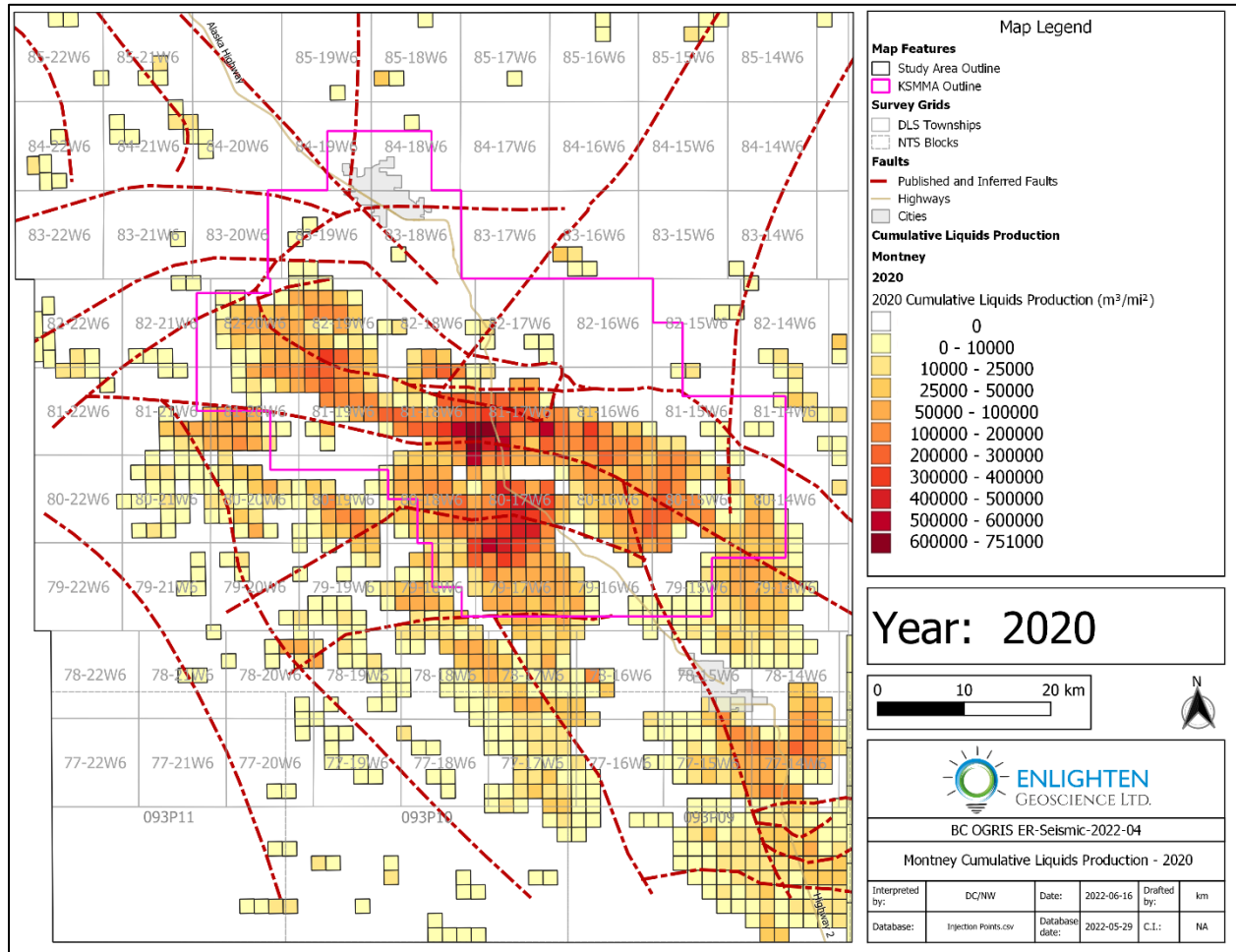


Figure 8. Map of Montney cumulative liquids production through the end of 2020.

[Link to map animation of Montney cumulative liquids production from 2008 to 2020.](#)

*Geomechanical Effects of Cumulative Fluid Injection through Hydraulic Fracturing in the Kiskatinaw Seismic Monitoring and Mitigation Area, British Columbia (ER-Seismic-2022-04)*

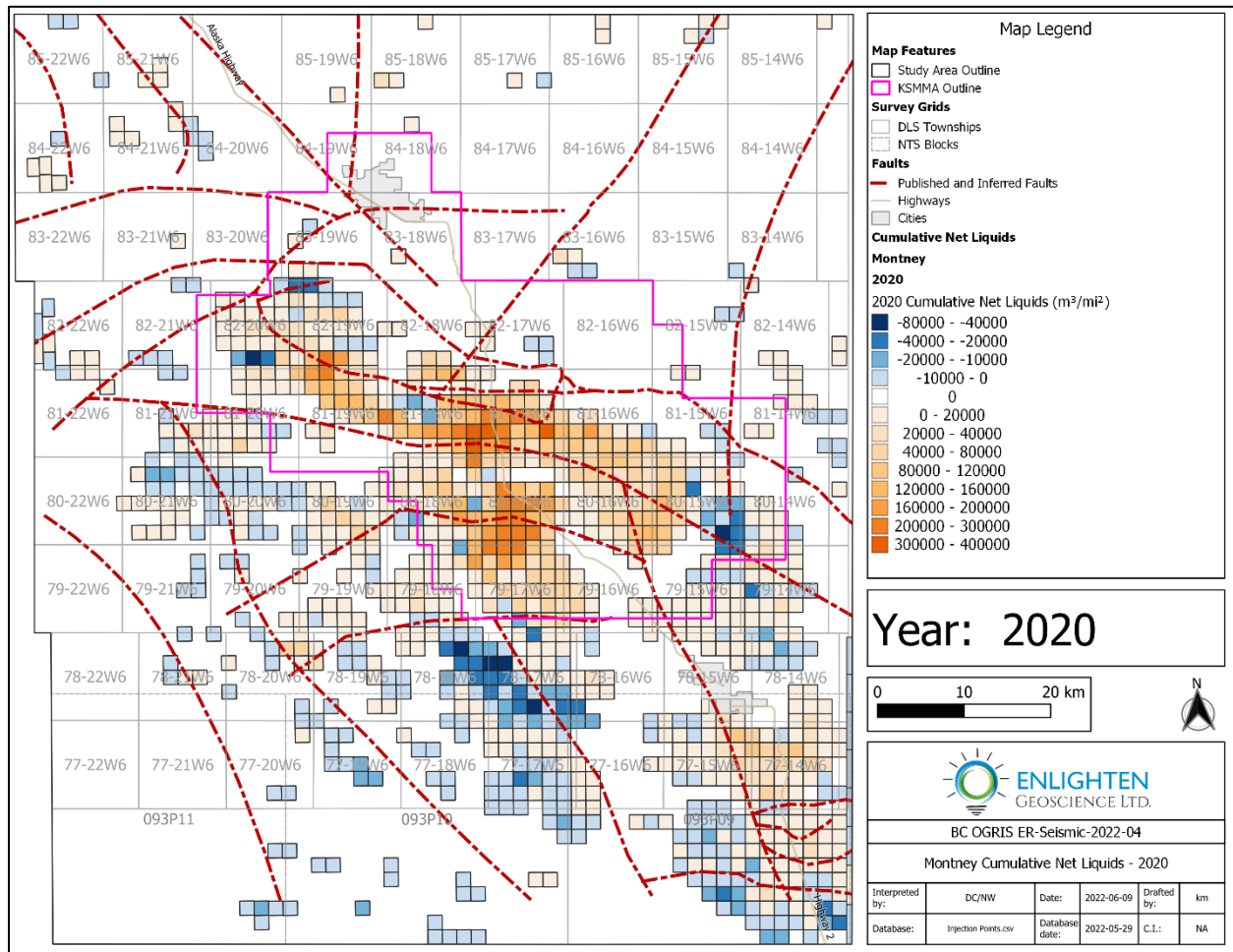


Figure 9. Map of Montney net cumulative liquids through the end of 2020.

[Link to map animation of Montney net cumulative liquids from 2008 to 2020.](#)

## Montney Stratigraphic Intervals

Patterns similar to what is seen in the entire Montney are seen in the maps and animations for each stratigraphic interval. Variations between the intervals, as discussed in this section, can be instructive as to the nature of liquids injection into the Montney play.

It should be noted that the individual Montney stratigraphic sequences have not, to date, been exploited equally. The UM has by far been the most thoroughly drilled and completed, followed by the IMM, uMM and LM. Figure 10 illustrates this discrepancy by tabulating the cumulative completion interval for each interval based on data provided by the gdcWeb.

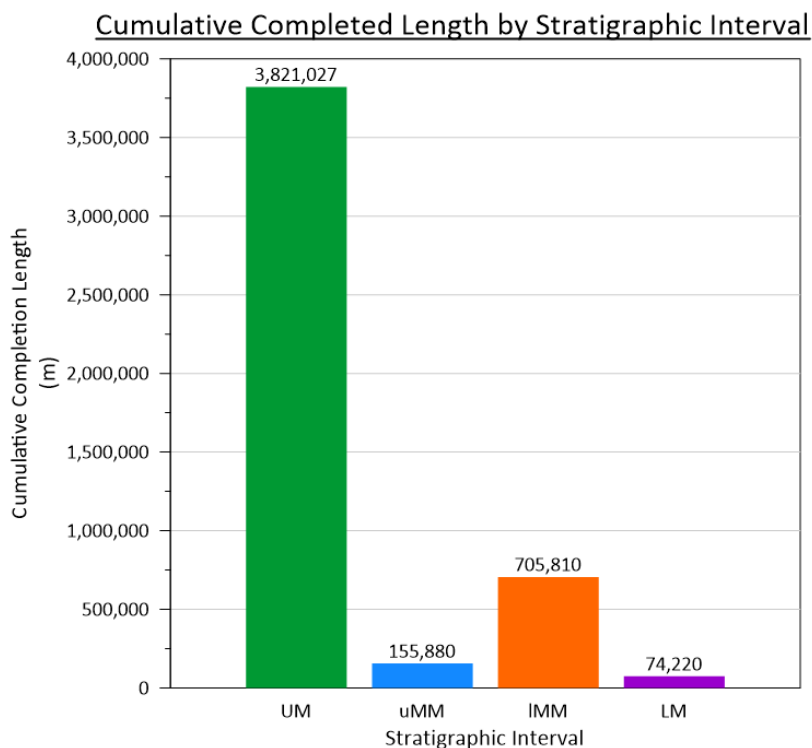


Figure 10. Cumulative completed length by stratigraphic interval.

### Lower Montney

The Lower Montney has been the target of a much lower level of industry activity to date. As a result, the maps of the yearly and cumulative LM liquids injection, production and net injection provide little data of relevance, and representative 2020 maps have not been included in the report. The Lower Montney maps and animations are included in Appendix C4, and the animations are available at the following links:

[Link to map animation of Lower Montney yearly liquid injection from 2008 to 2020.](#)

[Link to map animation of Lower Montney yearly liquids production from 2008 to 2020.](#)

[Link to map animation of Lower Montney yearly net liquids from 2008 to 2020.](#)

[Link to map animation of Lower Montney cumulative liquids injection from 2008 to 2020.](#)

[Link to map animation of Lower Montney cumulative liquids production from 2008 to 2020.](#)

[Link to map animation of Lower Montney cumulative net liquids from 2008 to 2020.](#)

### lower Middle Montney

In contrast to the very low level of liquids injection into the LM, the IMM is the second most targeted interval in the Montney play in the study area and has, as a consequence, seen a significant level of liquids injection and associated production (Figures 11 and 12, respectively). Although the IMM has developed into a productive interval, activity focused on the IMM was primarily located south and southeast of the KSMMA until 2014 with liquids injection not reaching a significant level in the KSMMA until 2017.

Notwithstanding the injection activity not ramping up until 2017, the yearly net injection map (Figure 13) records the same theme of negative net injection by the end of 2020 as was seen in the Montney as a whole. Similarly, the IMM cumulative liquids injection, cumulative liquids production and cumulative net injection (Figures 14, 15 and 16) display the similar theme of a negative cumulative net liquids by the end of 2020.

*Geomechanical Effects of Cumulative Fluid Injection through Hydraulic Fracturing in the Kiskatinaw Seismic Monitoring and Mitigation Area, British Columbia (ER-Seismic-2022-04)*

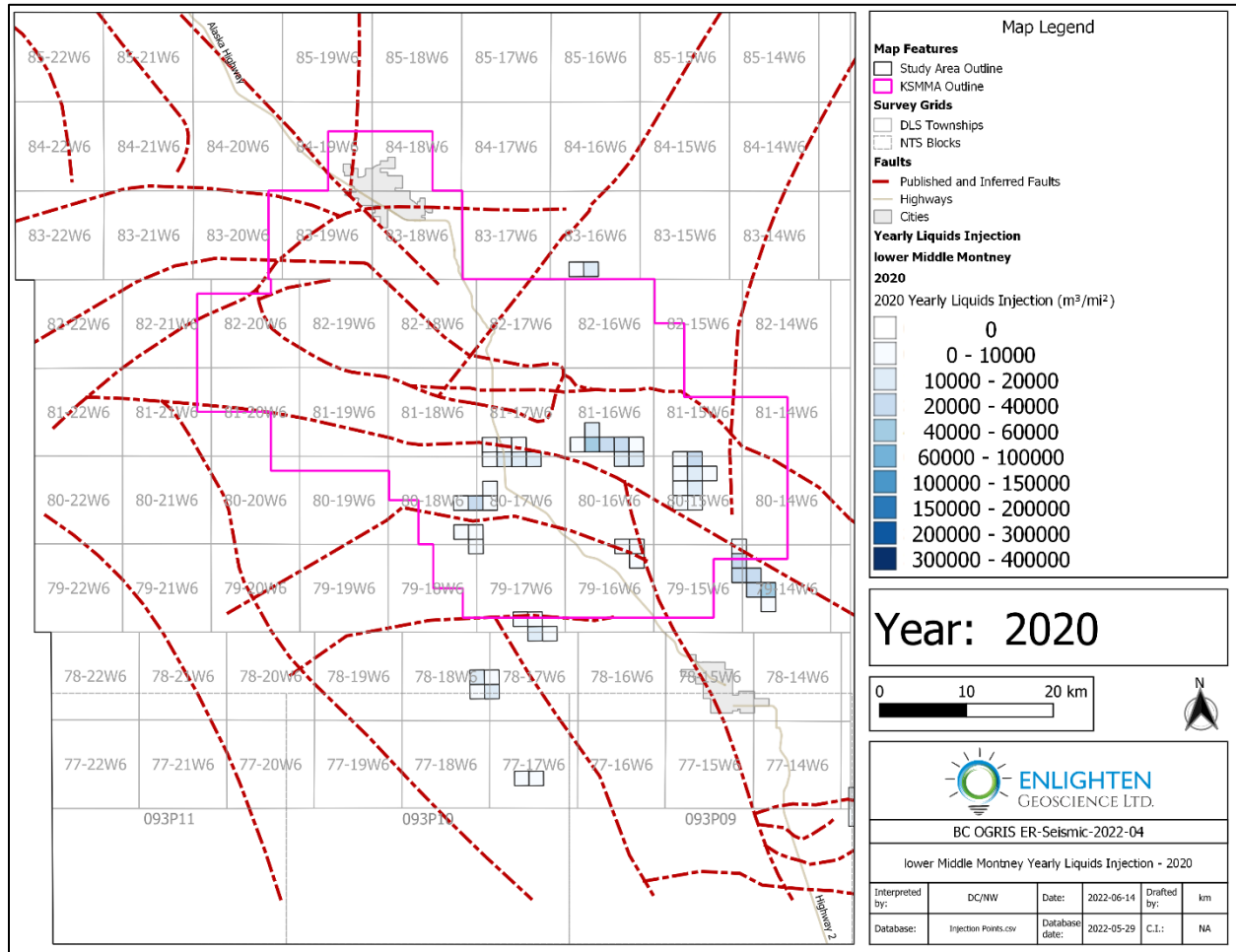


Figure 11. Map of lower Middle Montney yearly liquids injection for 2020.

[Link to map animation of lower Middle Montney yearly liquids injection from 2008 to 2020.](#)

*Geomechanical Effects of Cumulative Fluid Injection through Hydraulic Fracturing in the Kiskatinaw Seismic Monitoring and Mitigation Area, British Columbia (ER-Seismic-2022-04)*

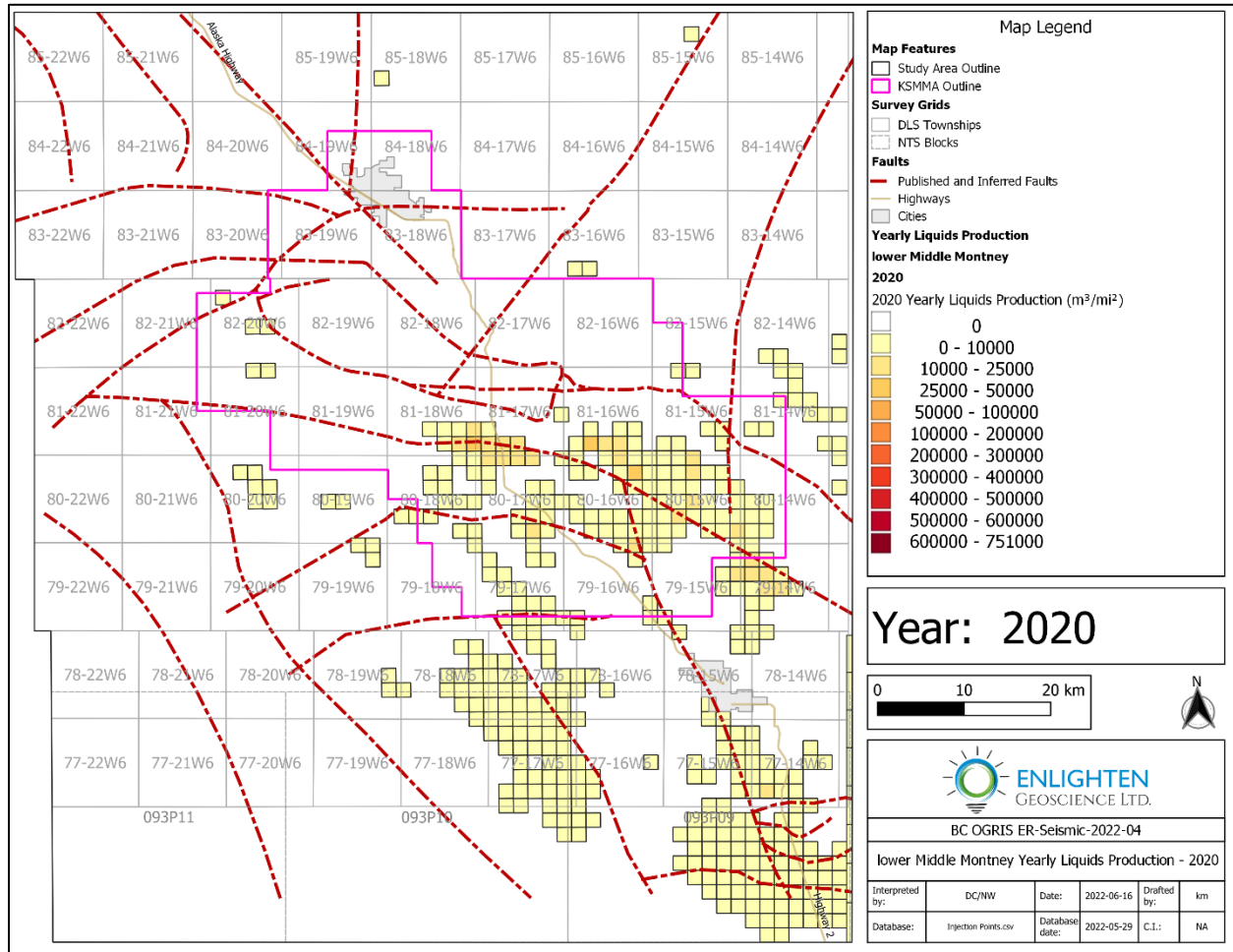


Figure 12. Map of lower Middle Montney yearly liquids production for 2020.

[Link to map animation of lower Middle Montney yearly liquids production from 2008 to 2020.](#)

*Geomechanical Effects of Cumulative Fluid Injection through Hydraulic Fracturing in the Kiskatinaw Seismic Monitoring and Mitigation Area, British Columbia (ER-Seismic-2022-04)*

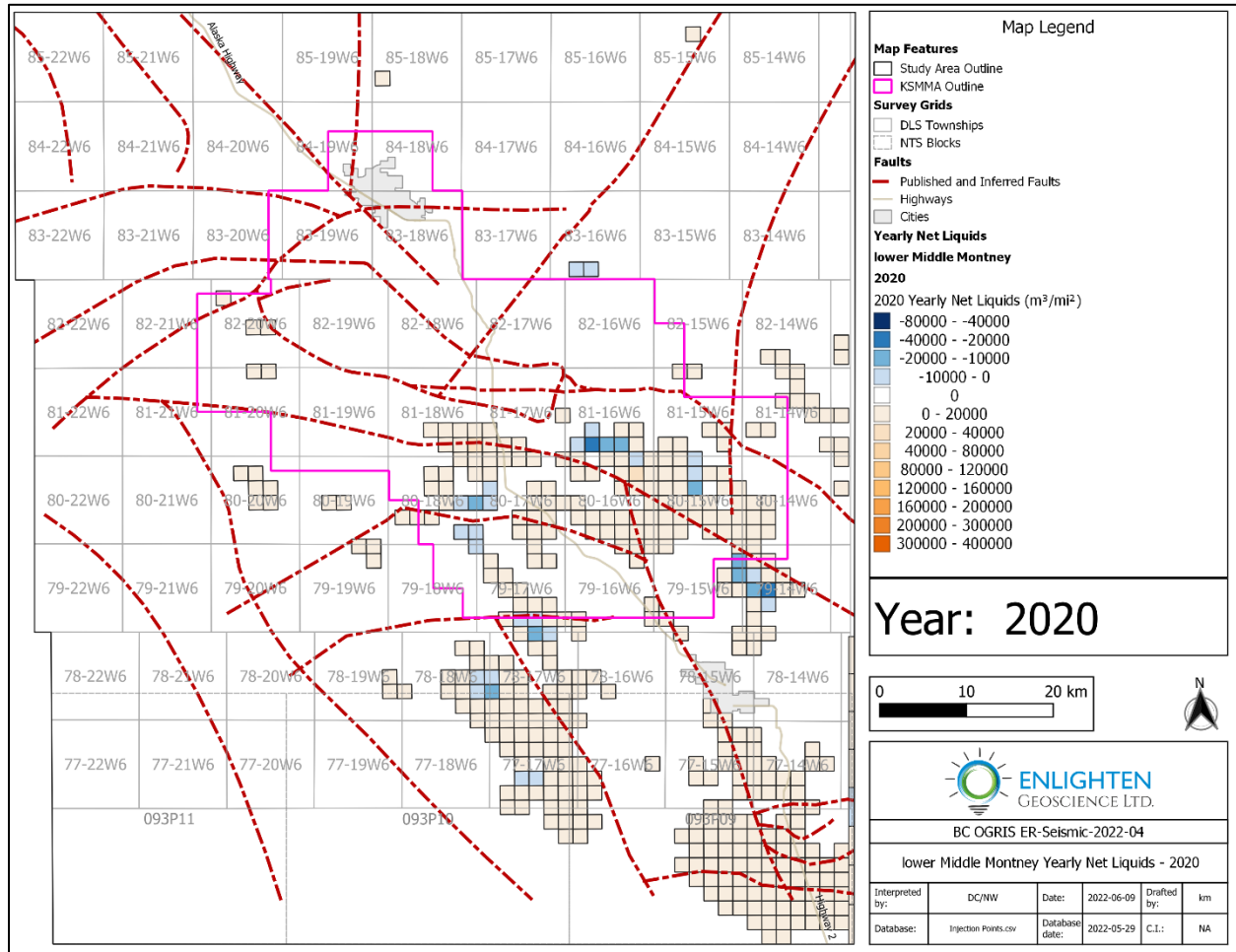


Figure 13. Map of lower Middle Montney yearly net liquids for 2020.

[Link to map animation of lower Middle Montney yearly net liquids from 2008 to 2020.](#)

*Geomechanical Effects of Cumulative Fluid Injection through Hydraulic Fracturing in the Kiskatinaw Seismic Monitoring and Mitigation Area, British Columbia (ER-Seismic-2022-04)*

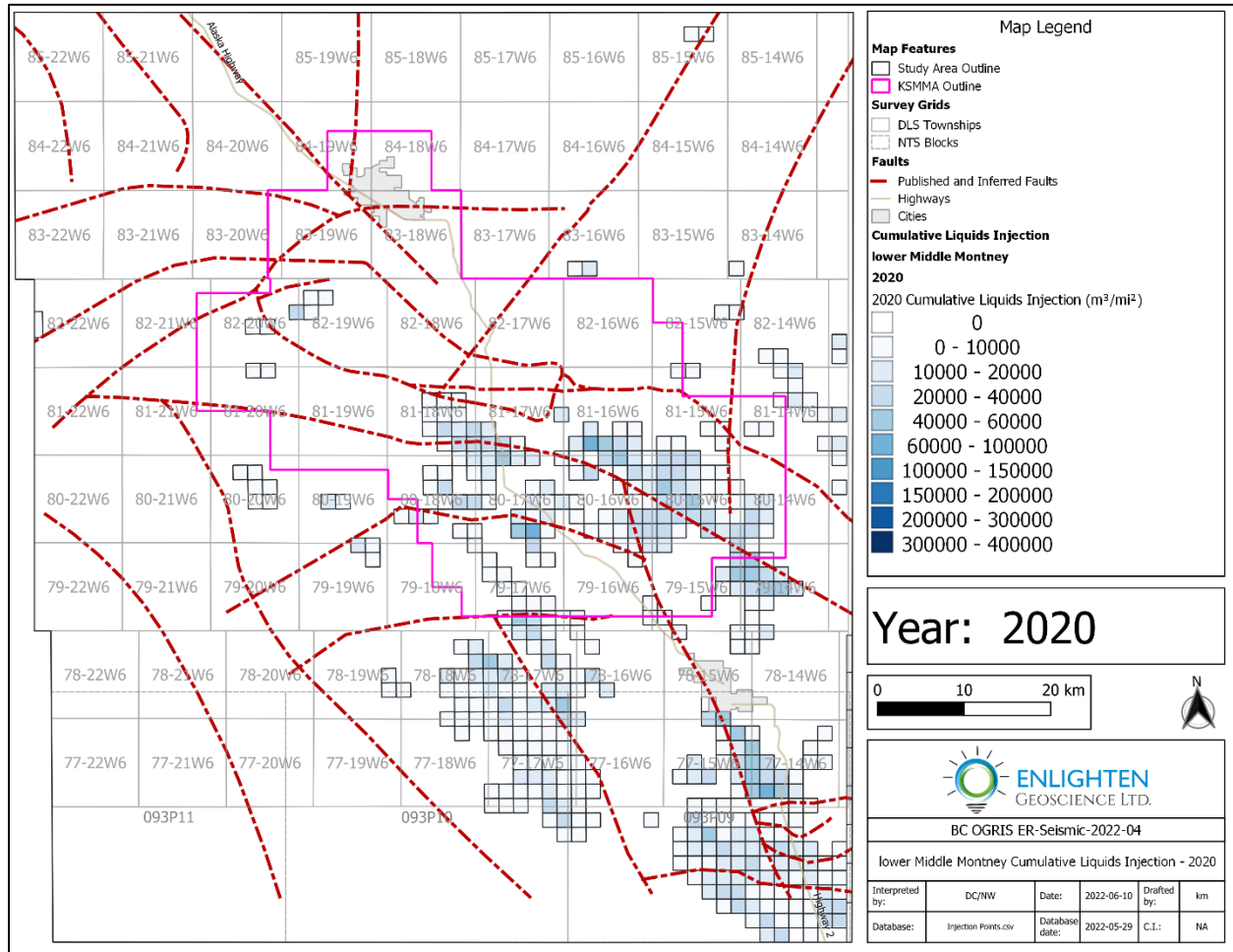


Figure 14. Map of lower Middle Montney cumulative liquids injection for 2020.

[Link to map animation of lower Middle Montney cumulative liquids injection from 2008 to 2020.](#)

*Geomechanical Effects of Cumulative Fluid Injection through Hydraulic Fracturing in the Kiskatinaw Seismic Monitoring and Mitigation Area, British Columbia (ER-Seismic-2022-04)*

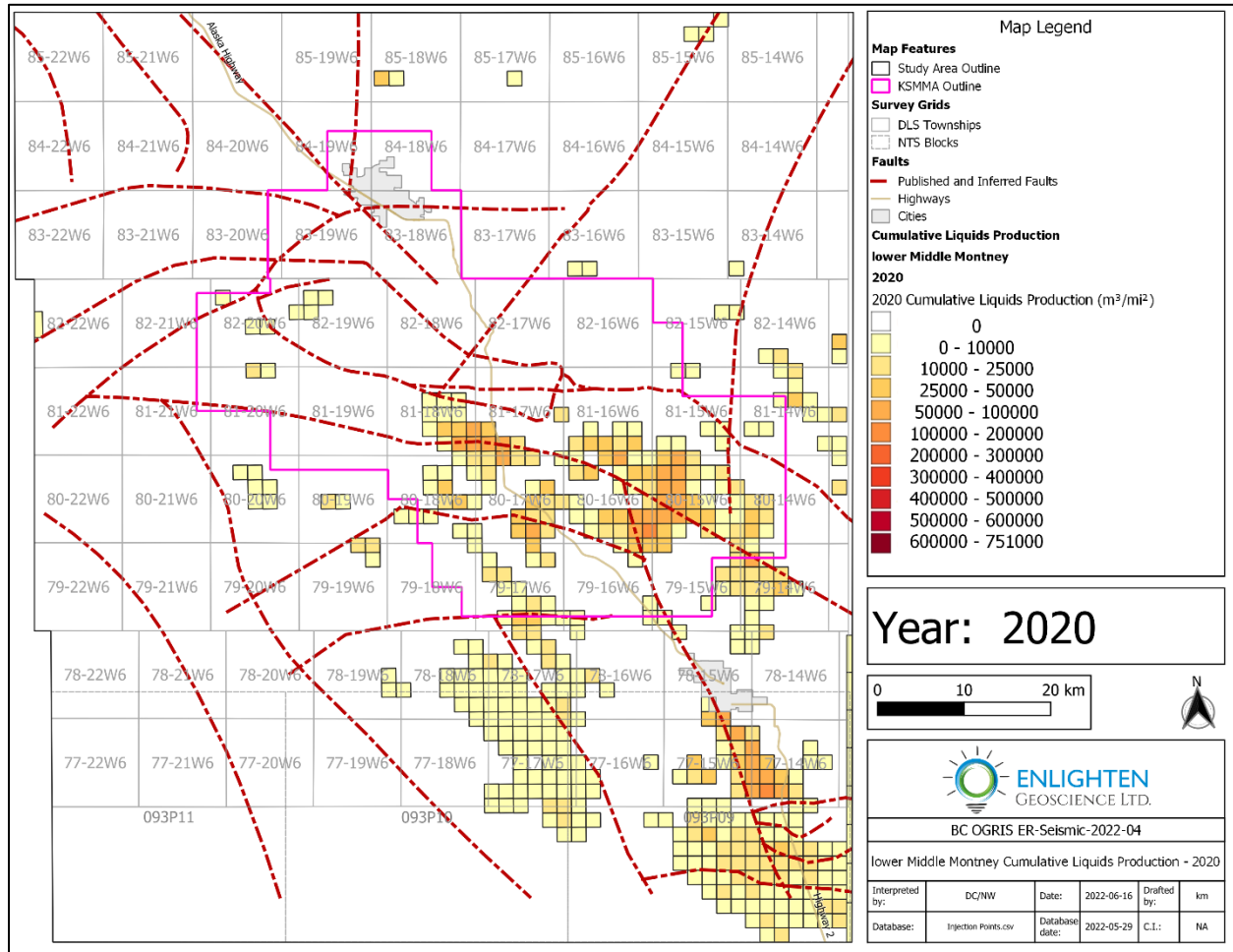


Figure 15. Map of lower Middle Montney cumulative liquids production for 2020.

[Link to map animation of lower Middle Montney cumulative liquids production from 2008 to 2020.](#)

*Geomechanical Effects of Cumulative Fluid Injection through Hydraulic Fracturing in the Kiskatinaw Seismic Monitoring and Mitigation Area, British Columbia (ER-Seismic-2022-04)*

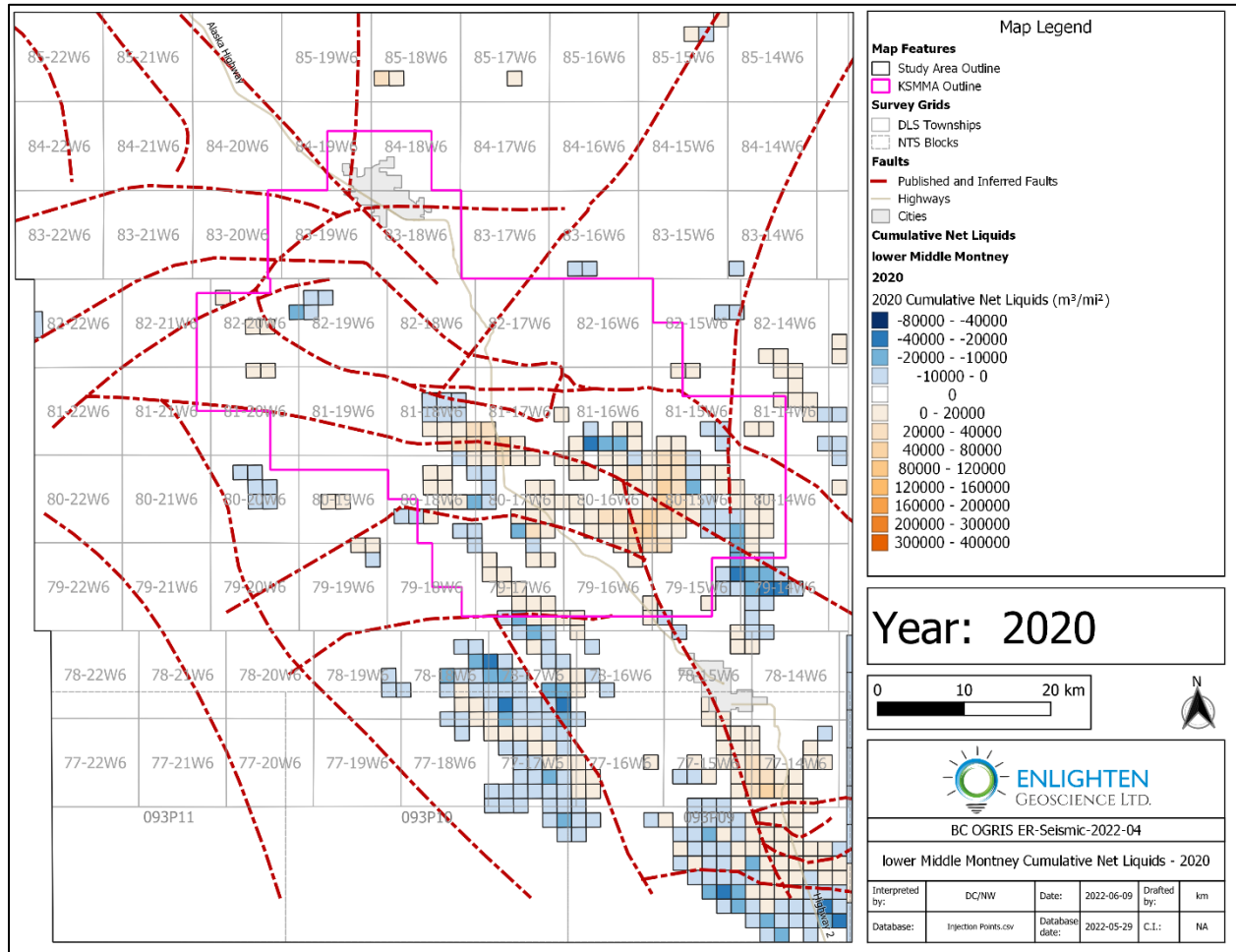


Figure 16. Map of lower Middle Montney cumulative net liquids for 2020.

[Link to map animation of lower Middle Montney cumulative net liquids from 2008 to 2020.](#)

upper Middle Montney

The uMM is, in a similar manner to the LM, a less exploited target than the IMM and uMM with only minor liquids injection occurring into the uMM up until 2018. Until that year, the injection activity occurred primarily outside of the KSMMA.

The yearly maps for liquids injection, liquids production and net liquids injection for the upper Middle Montney for 2020 are shown in Figures 17 through 19, and the cumulative maps are shown in Figures 20 to 22. Each map is followed by a link to the animation showing the same map type as a sequence over the years 2008 to 2020.

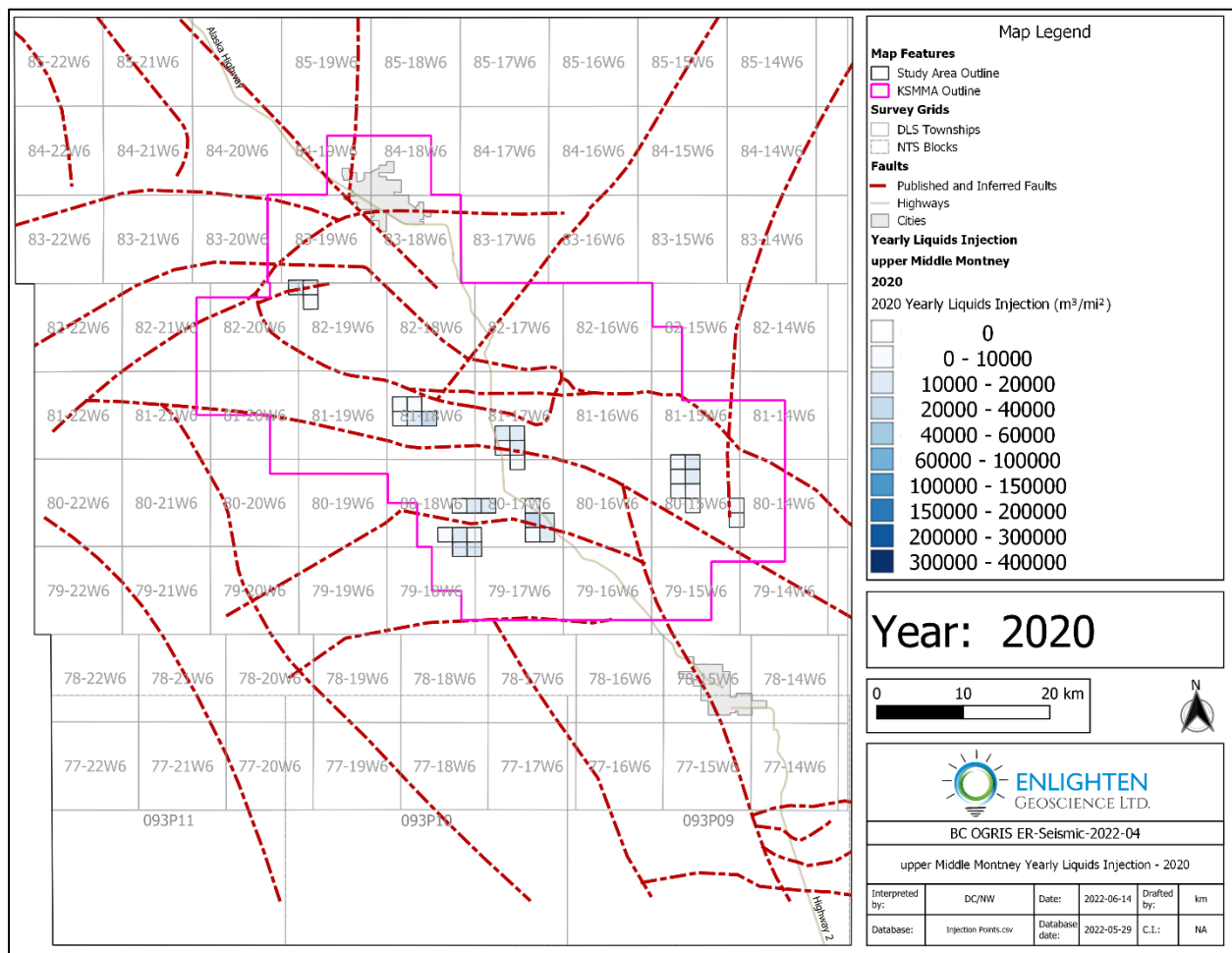


Figure 17. Map of upper Middle Montney yearly liquids injection for 2020.

[Link to map animation of upper Middle Montney yearly liquids injection from 2008 to 2020.](#)

*Geomechanical Effects of Cumulative Fluid Injection through Hydraulic Fracturing in the Kiskatinaw Seismic Monitoring and Mitigation Area, British Columbia (ER-Seismic-2022-04)*

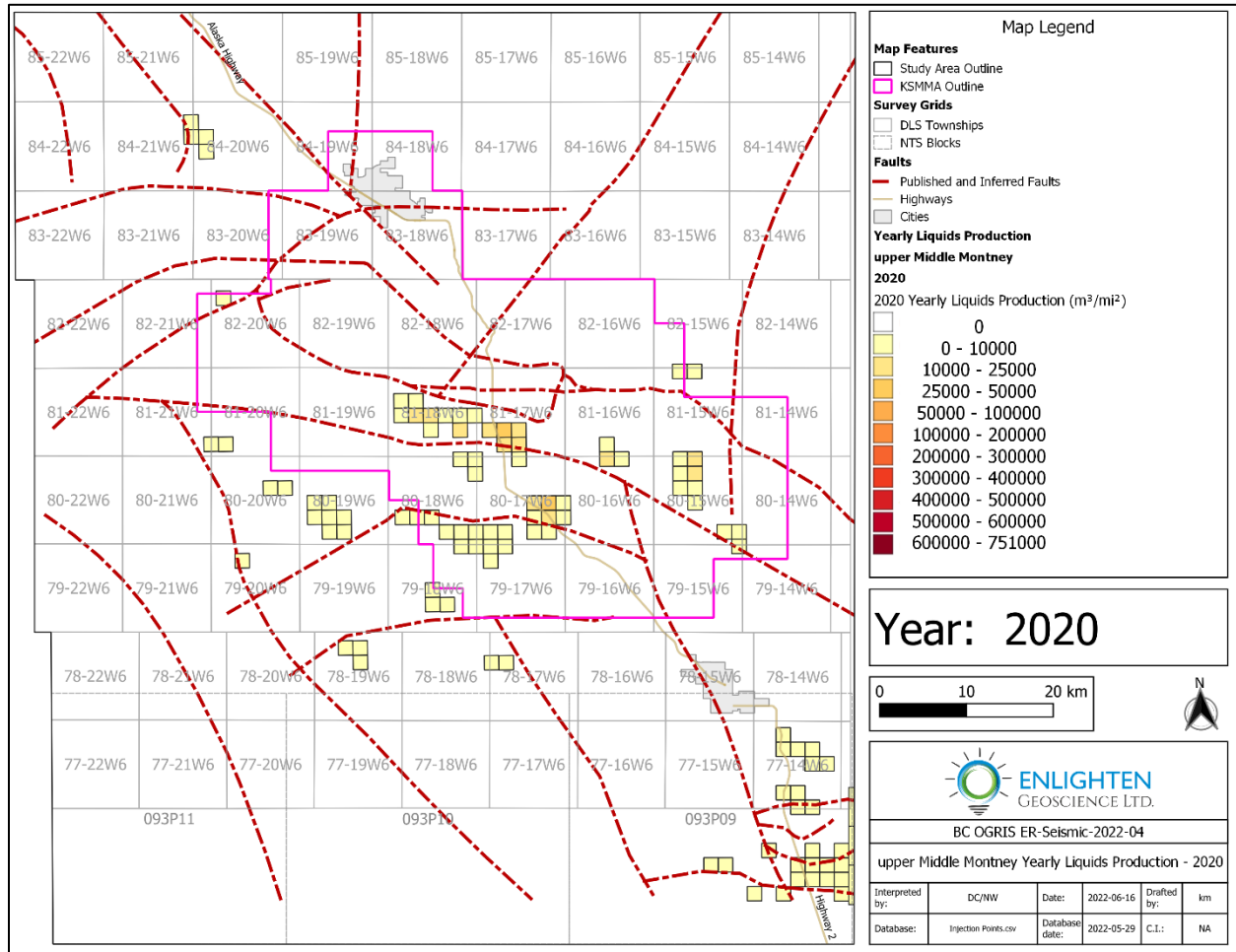


Figure 18. Map of upper Middle Montney yearly liquids production for 2020.

[Link to map animation of upper Middle Montney yearly liquids production from 2008 to 2020.](#)

*Geomechanical Effects of Cumulative Fluid Injection through Hydraulic Fracturing in the Kiskatinaw Seismic Monitoring and Mitigation Area, British Columbia (ER-Seismic-2022-04)*

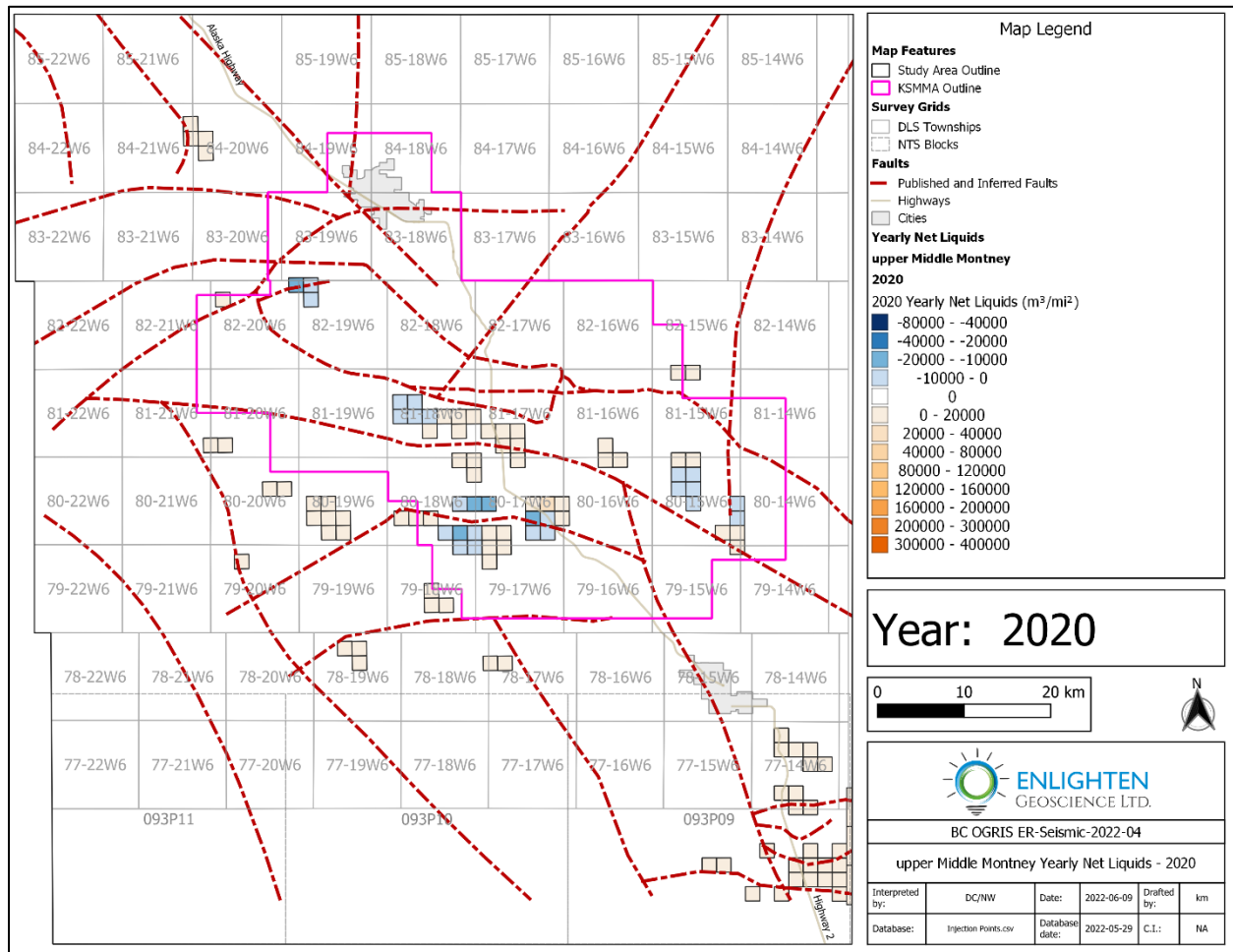


Figure 19. Map of upper Middle Montney yearly net liquids for 2020.

[Link to map animation of upper Middle Montney yearly net liquids from 2008 to 2020.](#)

*Geomechanical Effects of Cumulative Fluid Injection through Hydraulic Fracturing in the Kiskatinaw Seismic Monitoring and Mitigation Area, British Columbia (ER-Seismic-2022-04)*

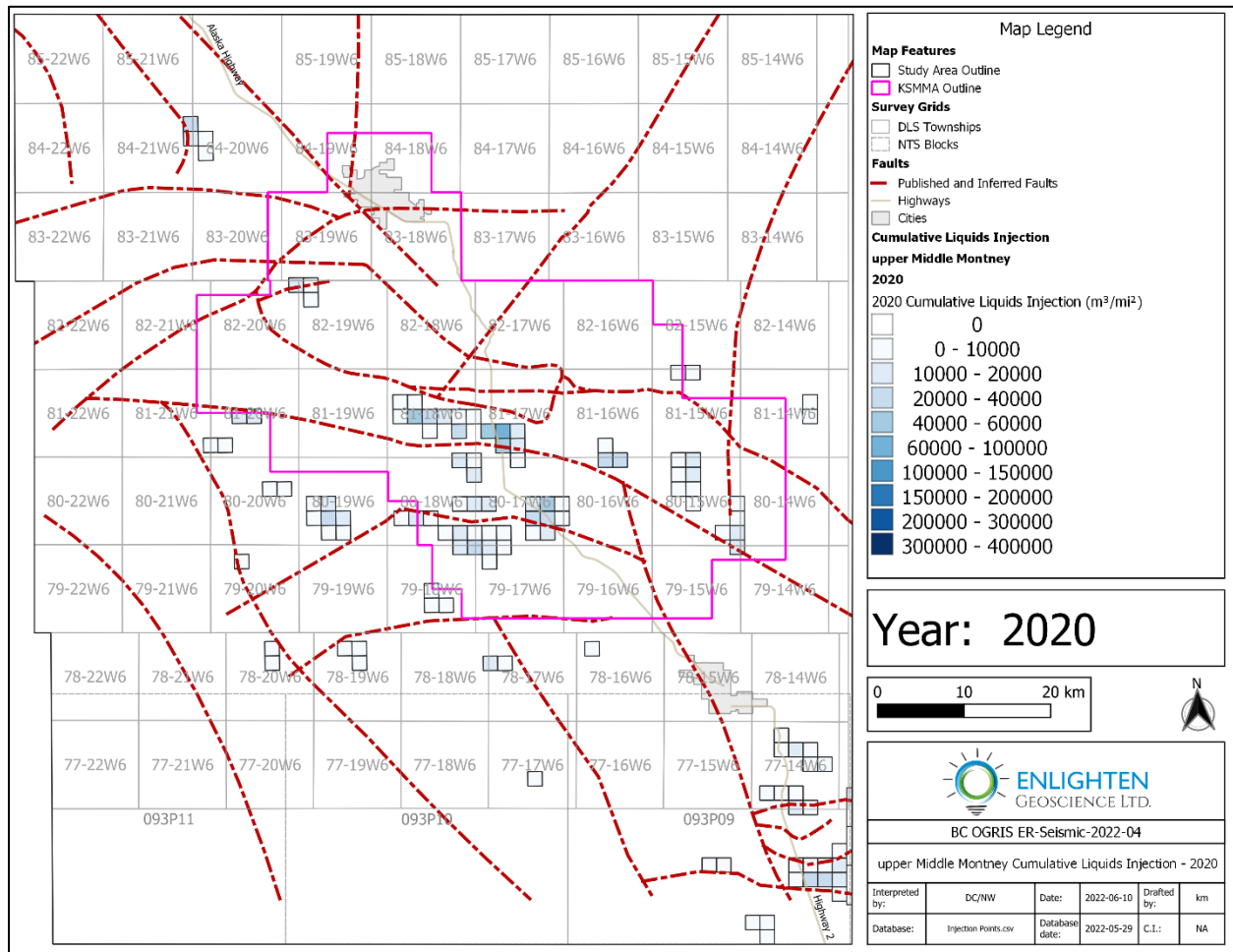


Figure 20. Map of upper Middle Montney cumulative liquids injection for 2020.

[Link to map animation of upper Middle Montney cumulative liquids injection from 2008 to 2020.](#)

*Geomechanical Effects of Cumulative Fluid Injection through Hydraulic Fracturing in the Kiskatinaw Seismic Monitoring and Mitigation Area, British Columbia (ER-Seismic-2022-04)*

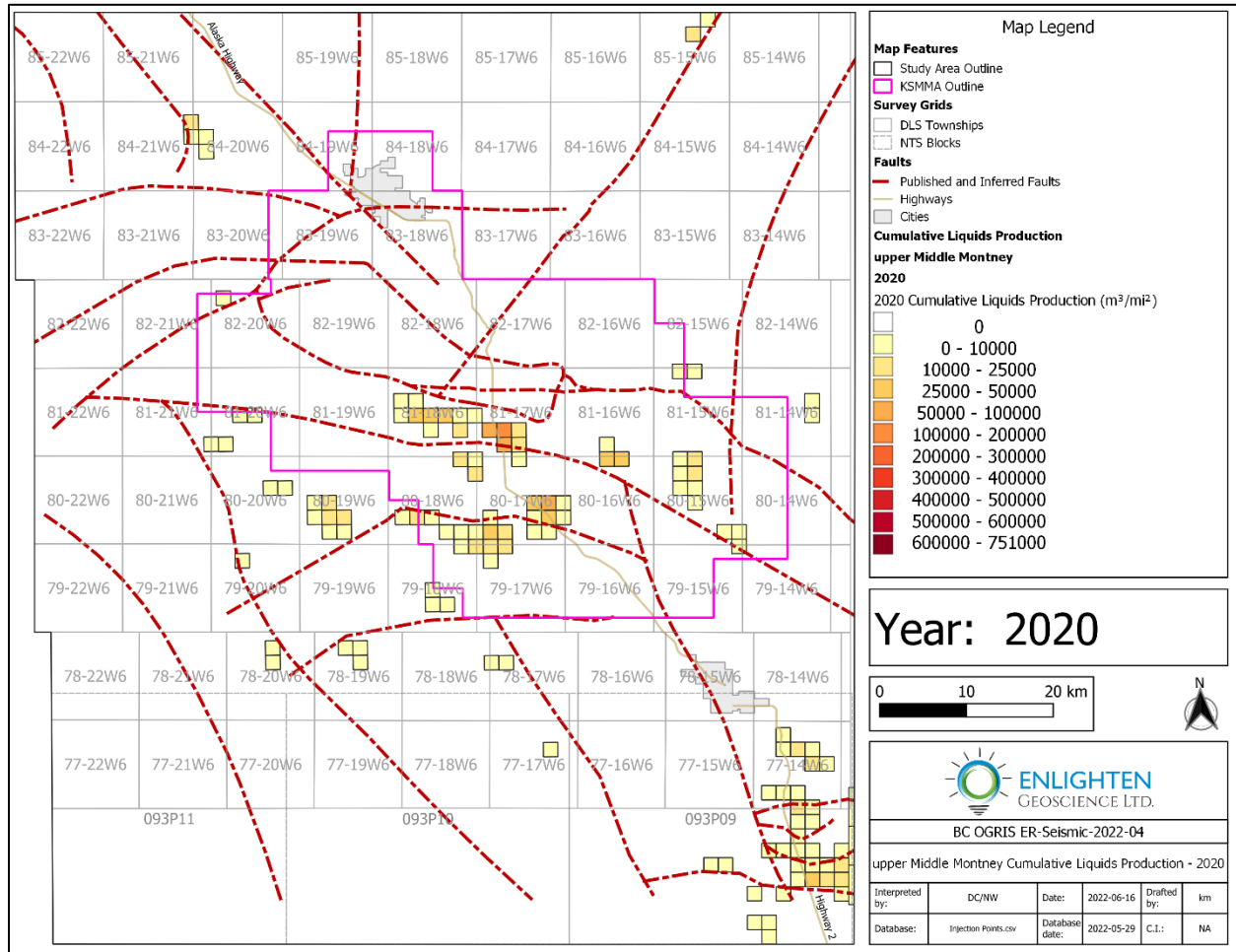


Figure 21. Map of upper Middle Montney cumulative liquids production for 2020.

[Link to map animation of upper Middle Montney cumulative liquids production from 2008 to 2020.](#)

*Geomechanical Effects of Cumulative Fluid Injection through Hydraulic Fracturing in the Kiskatinaw Seismic Monitoring and Mitigation Area, British Columbia (ER-Seismic-2022-04)*

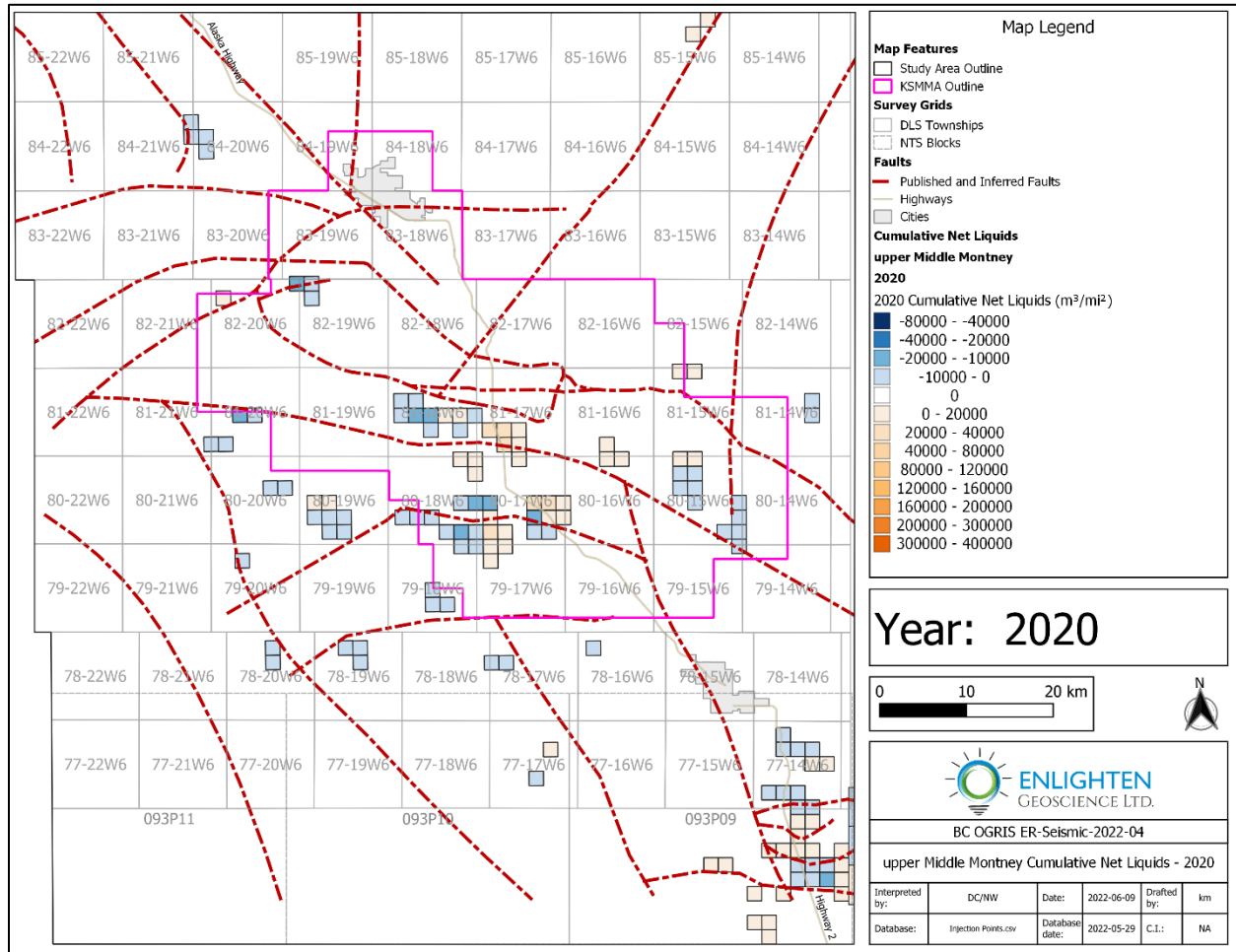


Figure 22. Map of upper Middle Montney cumulative net liquids for 2020.

[Link to map animation of upper Middle Montney cumulative net liquids from 2008 to 2020.](#)

Upper Montney

The map suite for the UM is of particular interest given the level of injection experienced over the time period considered by the study. The yearly liquids injection, yearly liquids production, yearly net liquids injection, cumulative liquids injection, cumulative liquids production and cumulative net liquids injection for 2020 are shown in Figures 23 through 28. The associated animations show each map type as a sequence from 2008 to 2020.

The Upper Montney was the initial focus of the original Montney development effort and has remained of central interest to operators. As such the injection occurred both within and beyond the bounds of the KSMMA throughout the 2008 to 2020 period.

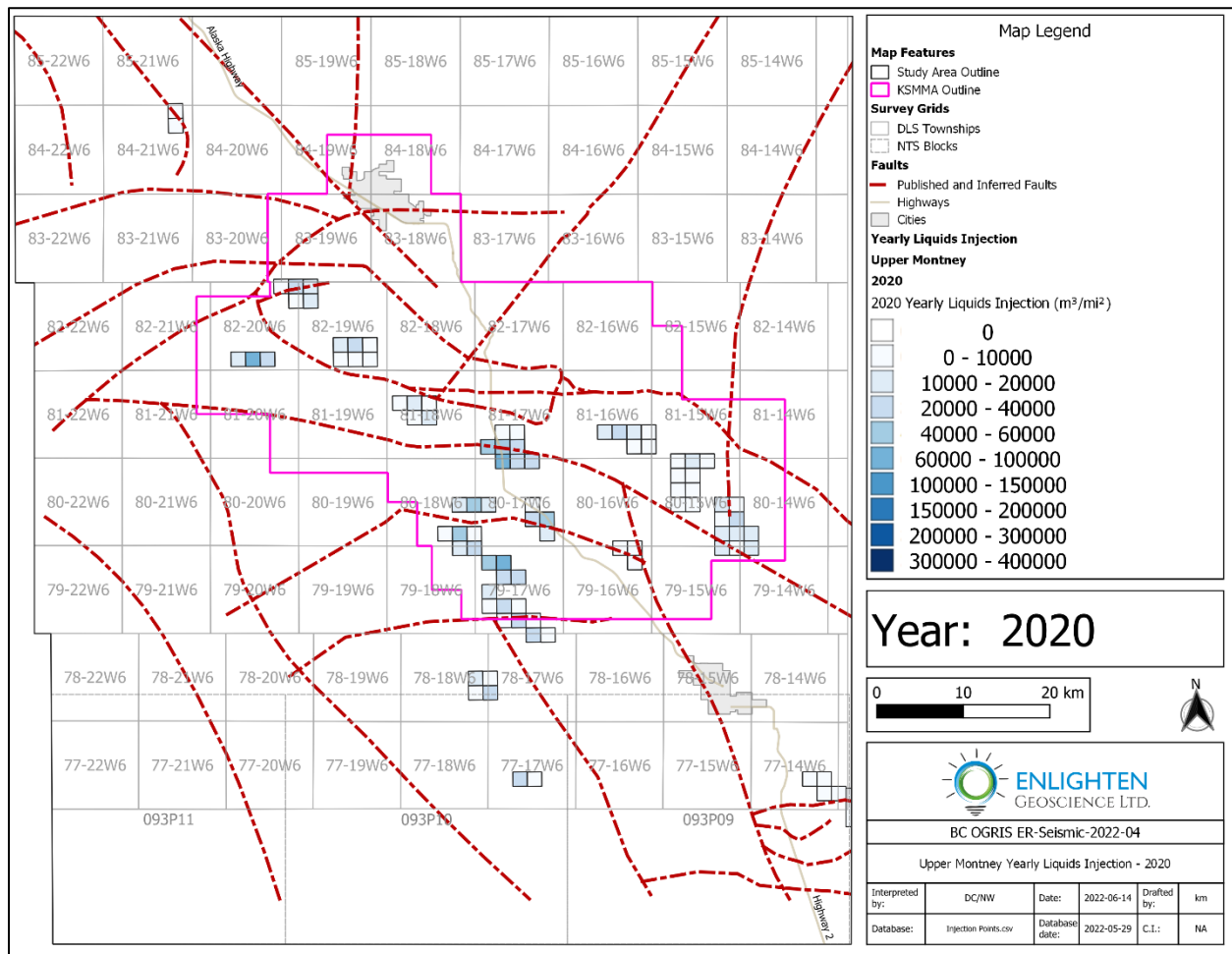


Figure 23. Map of Upper Montney yearly liquids injection for 2020.

[Link to map animation of Upper Montney yearly liquids injection from 2008 to 2020.](#)

Geomechanical Effects of Cumulative Fluid Injection through Hydraulic Fracturing in the Kiskatinaw Seismic Monitoring and Mitigation Area, British Columbia (ER-Seismic-2022-04)

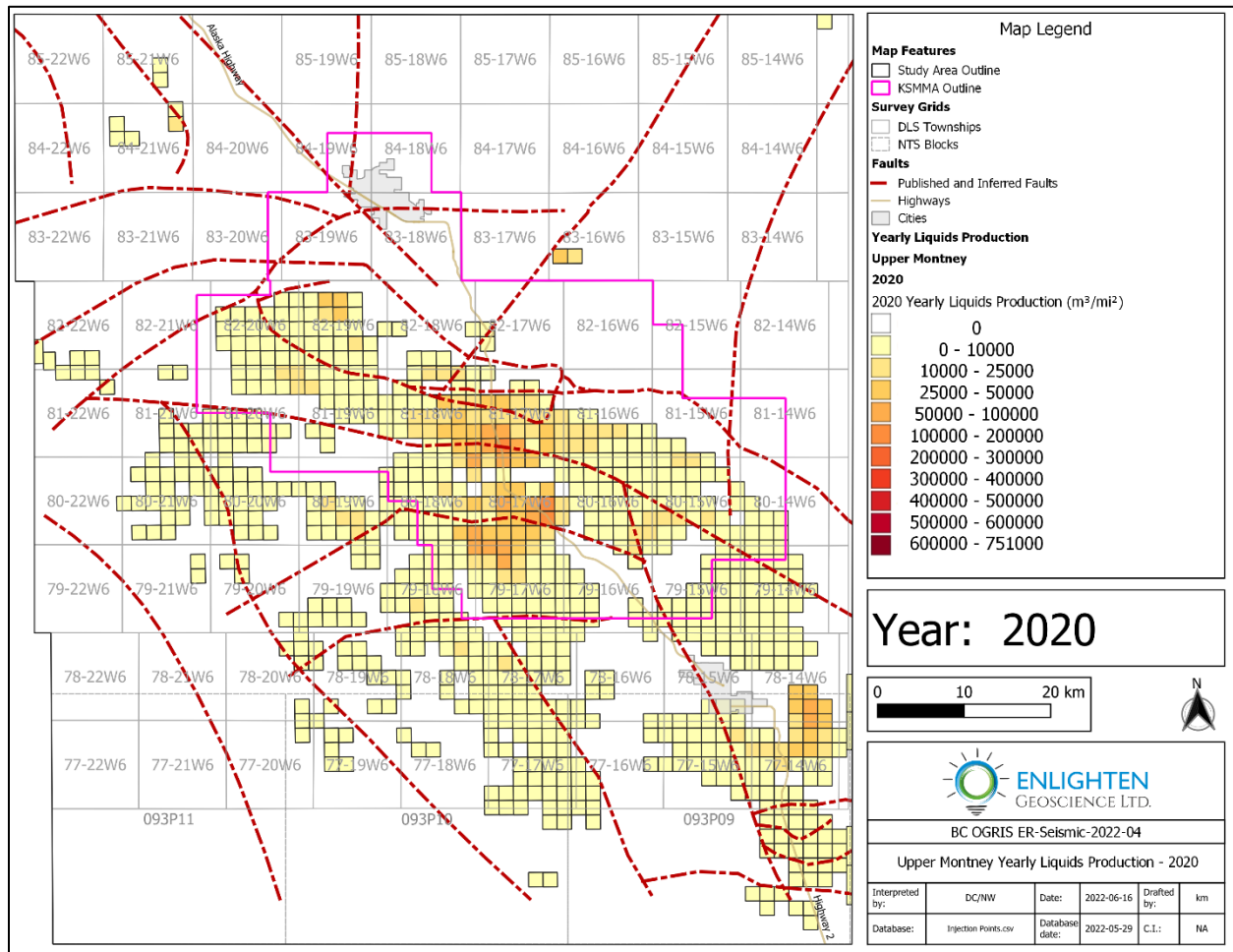


Figure 24. Map of Upper Montney yearly liquids production for 2020.

[Link to map animation of Upper Montney yearly liquids production from 2008 to 2020.](#)

*Geomechanical Effects of Cumulative Fluid Injection through Hydraulic Fracturing in the Kiskatinaw Seismic Monitoring and Mitigation Area, British Columbia (ER-Seismic-2022-04)*

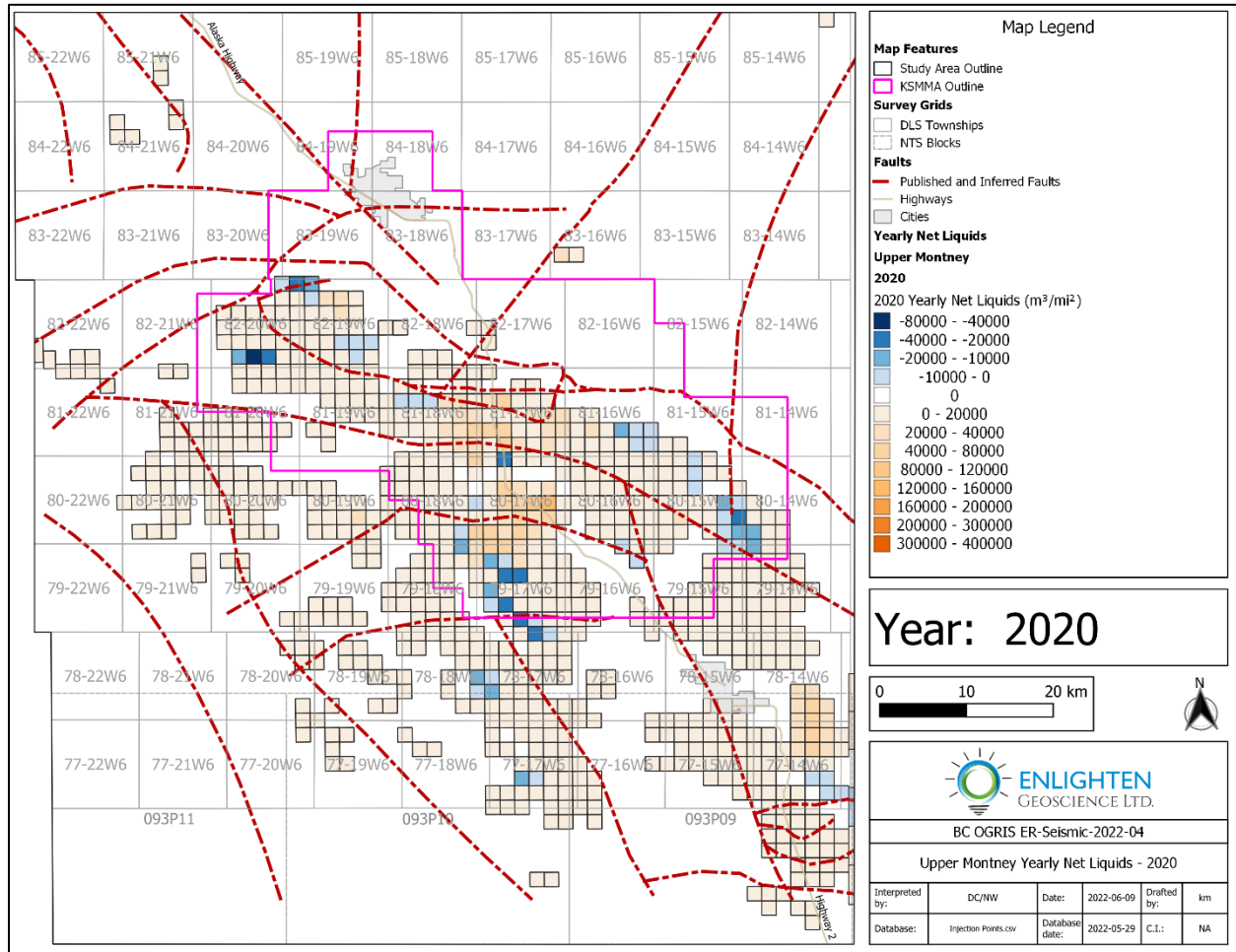


Figure 25. Map of Upper Montney yearly net liquids for 2020.

[Link to map animation of Upper Montney yearly net liquids from 2008 to 2020.](#)

*Geomechanical Effects of Cumulative Fluid Injection through Hydraulic Fracturing in the Kiskatinaw Seismic Monitoring and Mitigation Area, British Columbia (ER-Seismic-2022-04)*

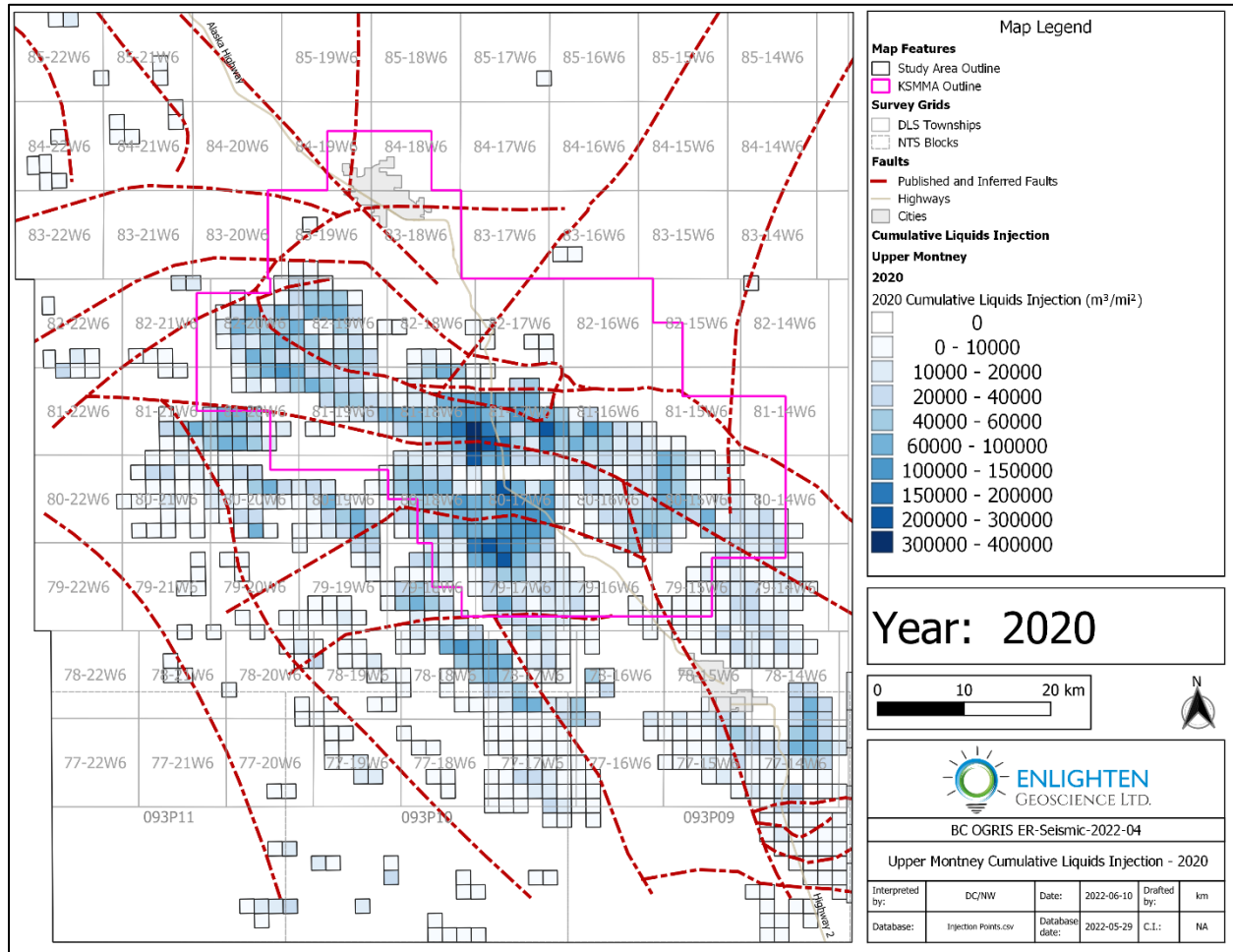


Figure 26. Map of Upper Montney cumulative liquids injection for 2020.

[Link to map animation of Upper Montney cumulative liquids injection from 2008 to 2020.](#)

*Geomechanical Effects of Cumulative Fluid Injection through Hydraulic Fracturing in the Kiskatinaw Seismic Monitoring and Mitigation Area, British Columbia (ER-Seismic-2022-04)*

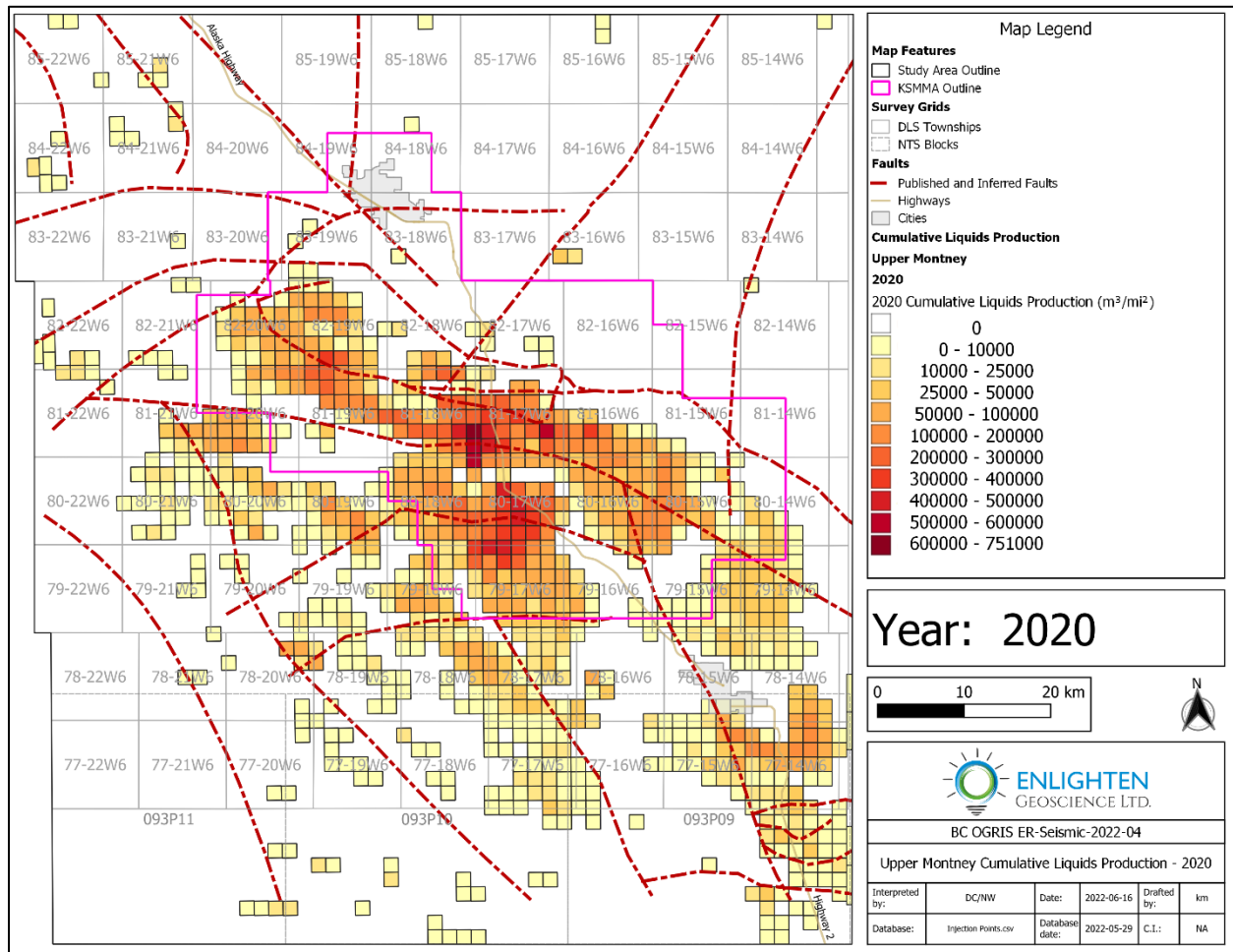


Figure 27. Map of Upper Montney cumulative liquids production for 2020.

[Link to map animation of Upper Montney cumulative liquids production from 2008 to 2020.](#)

*Geomechanical Effects of Cumulative Fluid Injection through Hydraulic Fracturing in the Kiskatinaw Seismic Monitoring and Mitigation Area, British Columbia (ER-Seismic-2022-04)*

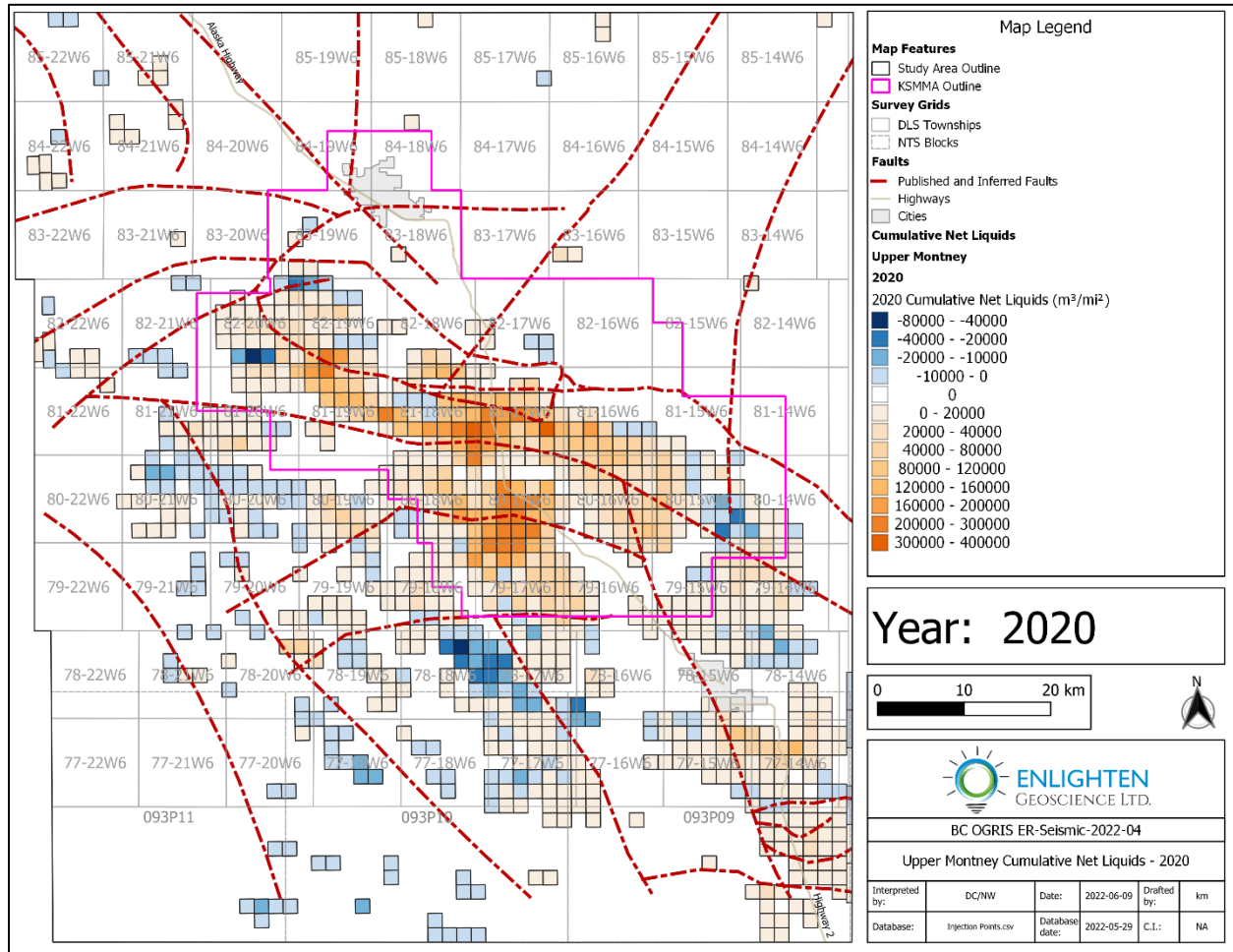


Figure 28. Map of Upper Montney cumulative net liquids for 2020.

[Link to map animation of Upper Montney cumulative net liquids from 2008 to 2020.](#)

## Volumes Summary

The summation of cumulative net liquid injection, liquid production and net liquid injection within the KSMMA for the entire Montney and each stratigraphic interval is provided below in Table 3. Although the UM has experienced the largest volume of liquid injection over a broad area, wells completed in the UM have experienced relatively low levels of associated HFIS events (M. Gaucher, personal communication). This is contrary to what would be expected if the volume of liquids injected were the primary driver behind HFIS.

Stratigraphic Interval	Cumulative Liquids Injection (m <sup>3</sup> ) up to 2020	Cumulative Liquids Production (m <sup>3</sup> ) up to 2020	Cumulative Net Liquids Injection (m <sup>3</sup> ) up to 2020
Montney	19,753,324	41,048,119	-21,294,795
UM	16,220,175	36,203,454	-19,983,278
uMM	826,199	881,410	-55,212
IMM	2,311,831	3,461,915	-1,150,083
LM	395,119	501,341	-106,222

Table 3. Summary of cumulative liquids for the KSMMA.

## Montney Pressure vs Depth

Mapping out the changes in the Pressure vs Depth (PD) Ratios for the entire Montney illustrates the range of pressure decline across the Study Area. Although the effect of any pressure decrease is expected to be localized and slow to communicate across larger, inter-well distances due to the very low permeability of the Montney, a sense of the magnitude of PID can be developed.

PD ratios for 2020 for the entire Montney, IMM, uMM and UM are shown in Figures 29 to 32. Links to animations illustrating the changes from 2008 to 2020 are provided below each map. As with the liquids injection and production maps, the LM PD maps are not presented here but are provided in Appendix C.

As illustrated by the liquids injection history, most of the early IMM development occurred to the south and southeast of the KSMMA. As a result, the primary pressure depletion in the IMM is seen in this region.

Given that the development of the uMM has only recently begun to expand, the level of PID as not been very significant to date in this interval.

As the interval first brought on the production and the most widely exploited, the UM displays the most localities of reduced pressure. These areas of lowered pressures are not attributed to migration along trends of increased permeability due to faulting or sedimentological factors, which is believed to have caused the development of the pressure compartmentalization (Euzen et al. ( 2021). Instead, they represent areas of depletion. As noted earlier, hydraulic fracturing of the UM has not been determined to be a significant contributor of HFIS events. Decreasing pore pressure would, in fact, serve to lower the risk of induced seismicity through a corresponding increase in effective normal stress on pre-existing fractures and faults.

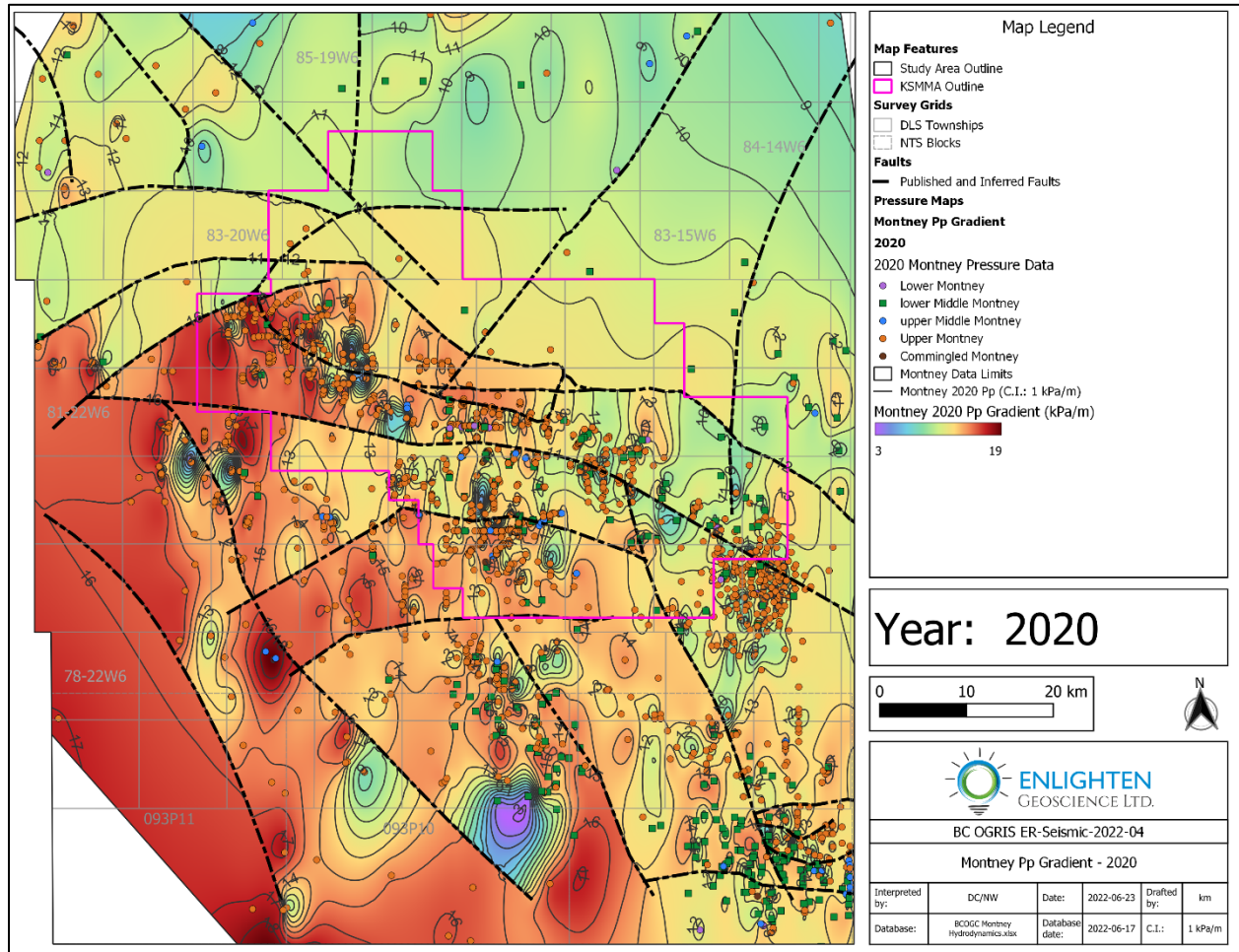


Figure 29. Map of Montney pressure vs depth gradient for 2020.

[Link to map animation of Montney pressure vs depth gradient from 2008 to 2020.](#)

[Link to map animation of Lower Montney pressure vs depth gradient from 2008 to 2020.](#)

*Geomechanical Effects of Cumulative Fluid Injection through Hydraulic Fracturing in the Kiskatinaw Seismic Monitoring and Mitigation Area, British Columbia (ER-Seismic-2022-04)*

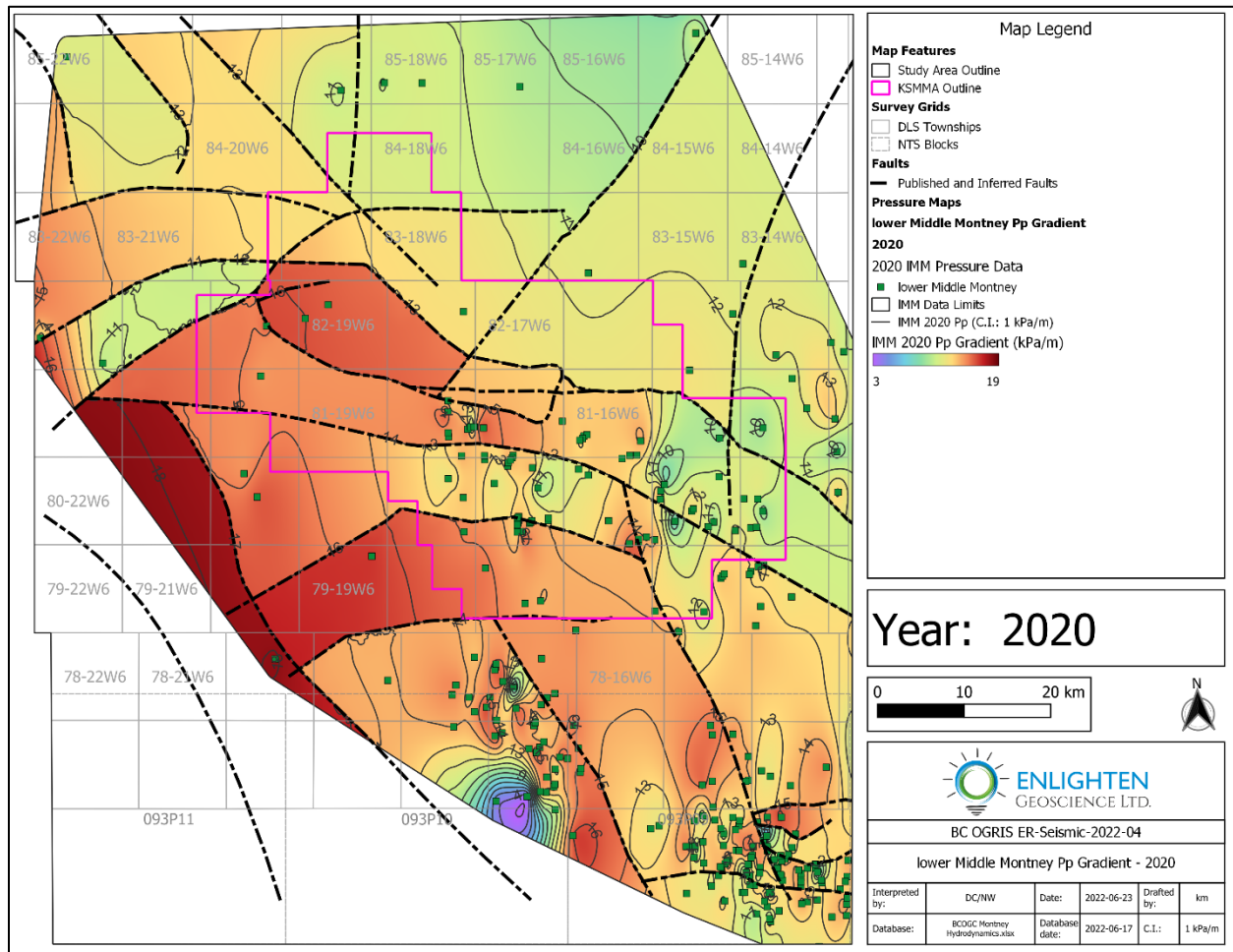


Figure 30. Map of lower Middle Montney pressure vs depth gradient for 2020.

[Link to map animation of lower Middle Montney pressure vs depth gradient from 2008 to 2020.](#)

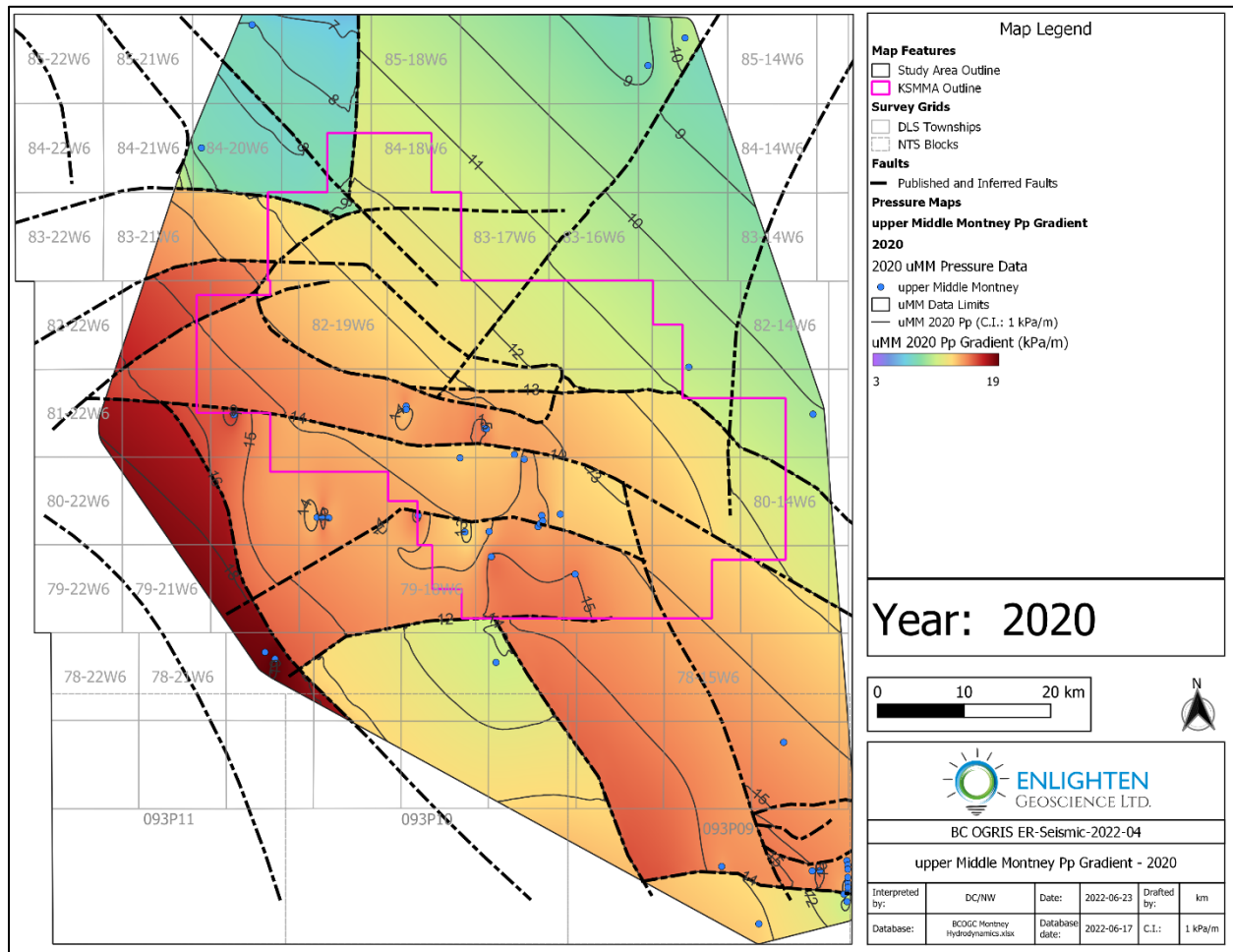


Figure 31. Map of upper Middle Montney pressure vs depth gradient for 2020.

[Link to map animation of upper Middle Montney pressure vs depth gradient from 2008 to 2020.](#)

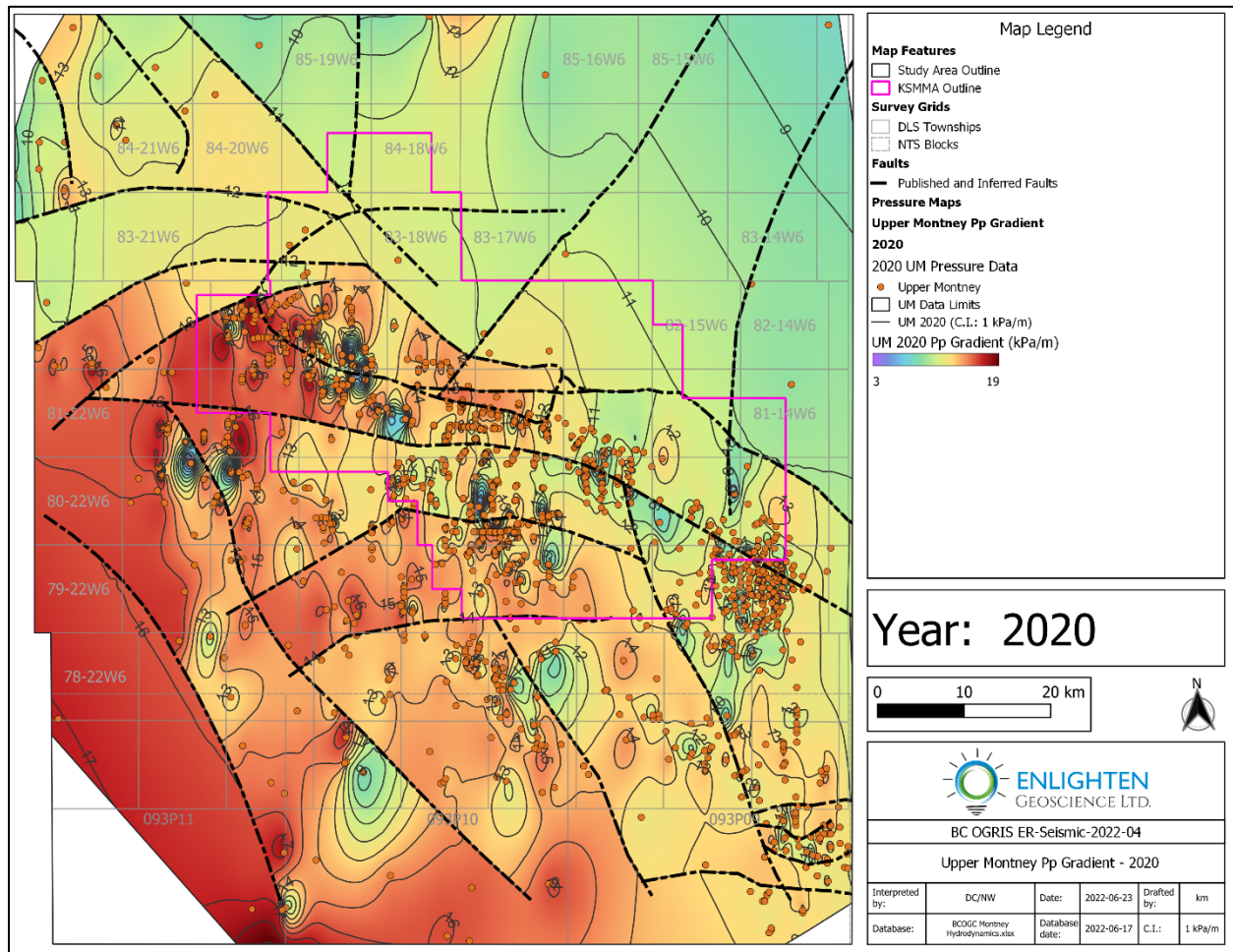


Figure 32. Map of Upper Montney pressure vs depth gradient for 2020.

[Link to map animation of Upper Montney pressure vs depth gradient from 2008 to 2020.](#)

## Montney Seismicity

Consistent with the other data types presented so far, earthquake data for the KSMMA can be displayed in an annual time series revealing trends in the number of earthquakes, their distribution and frequency over time. The yearly maps were generated using the entire earthquake catalogue, and no distinction is made between natural and induced seismic events. Due to the very large number of smaller events, the seismicity maps and animations were filtered so that only events with a magnitude greater than 2 are displayed. The map for 2020 is shown in Figure 33, while the link below the map is for the animation for the time period 2008 to 2020. The animation reveals an increasing level of events greater than magnitude 2 that accompanied the increased development in the KSMMA up to the end of 2017. There is then a noticeable decrease in the number of larger events for 2018 through 2020. Although industry activity levels might have been a contributing factor, the mitigation efforts resulting from the establishment of the KSMMA in 2018 are likely a significant contributor to a reduction in larger induced events, even in the context of an increase of hydraulic fracturing over the same period.

*Geomechanical Effects of Cumulative Fluid Injection through Hydraulic Fracturing in the Kiskatinaw Seismic Monitoring and Mitigation Area, British Columbia (ER-Seismic-2022-04)*

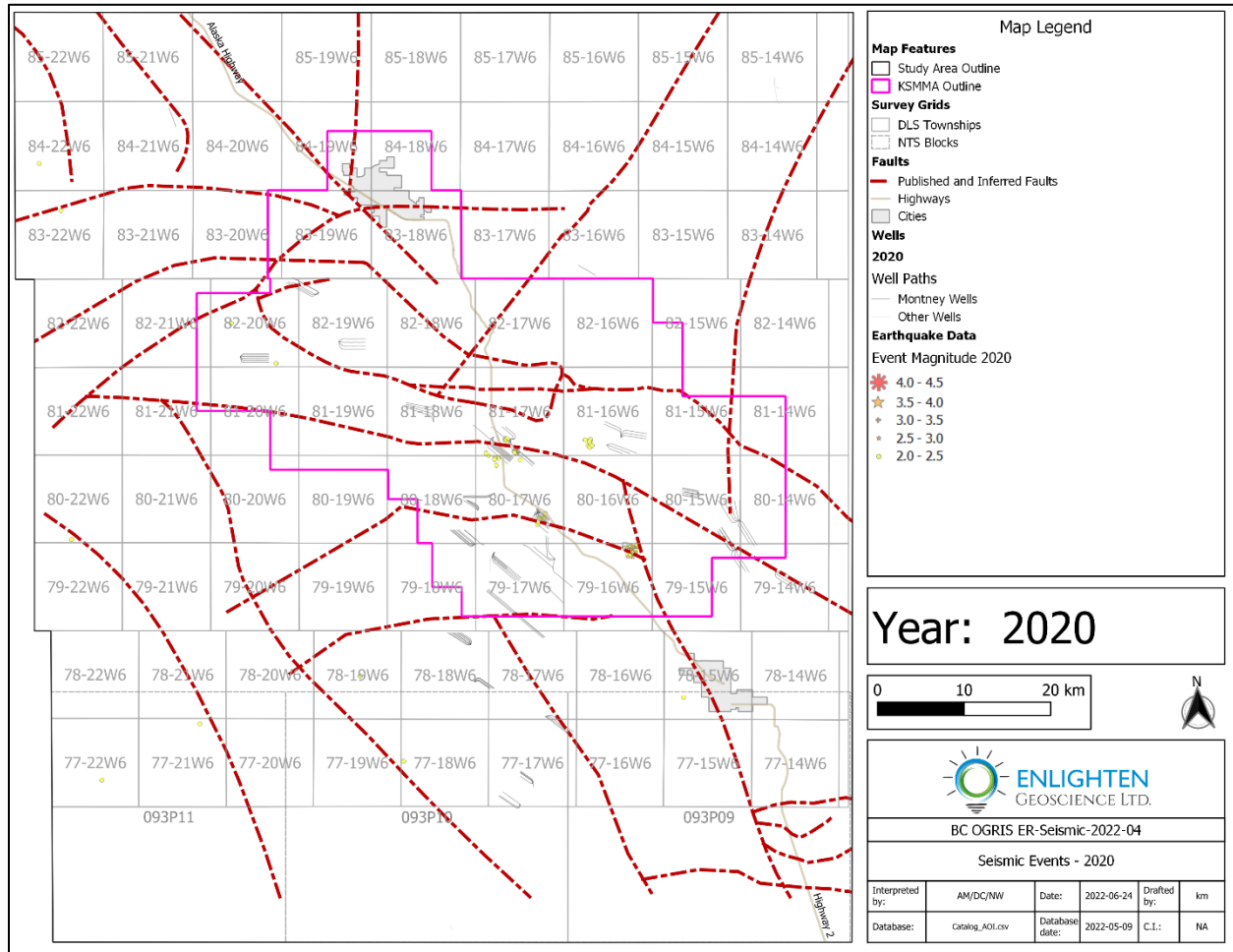


Figure 33. Map of Montney earthquakes greater than magnitude 2 for 2020.

[Link to map animation of Montney induced seismic events from 2008 to 2020.](#)

## V. 3-9 Pad Analysis

The pad-specific analysis was undertaken to better understand temporal changes in stress and seismicity in a limited area with extensive horizontal, hydraulically fractured Montney well development, possibly in multiple stratigraphic intervals, where there was associated induced seismic events. As discussed in Section II, the 3-9 pad chosen for the analysis was selected in coordination with the BC OGC. Two primary analyses were performed, one focused on the information provided from DFIT and hydraulic fracturing stage data, and the other focused on earthquake b-values.

### DFIT and Hydraulic Fracturing Stage Data Analysis

DFIT and hydraulic fracturing stage data were analyzed to identify possible stress changes during the development of wells on the 3-9 pad. Data availability for this analysis was discussed in Section III.

DFITs have become an extremely common test run in tight reservoirs such as the Montney. They are typically performed at the toe of a horizontal well and are commonly referred to as Stage 0, 1 or 1a of a multi-stage hydraulic fracturing completion in that well. Like a hydraulic fracture but smaller in scale, the tests pump fluid into the formation in order to induce an opening mode (tensile, or Mode I) fracture, then the pumps are shut off and data continue to be recorded as the induced fracture closes and the reservoir responds. The tests are generally interpreted for three main reservoir properties: minimum principal stress, reservoir permeability and reservoir (pore) pressure. A DFIT is of fairly long duration; it can take on the order of 100's of hours after the induced fracture is created and the pump is shut off to get data sufficient for accurate reservoir permeability and pressure estimates. In contrast, interpretation for minimum principal stress is done on relatively early part of the test data, shortly after pumping has stopped, as the induced fracture closes when the pressure inside the fracture reduces to the minimum principal in situ stress acting on the rock. The point at which this occurs is called the closure pressure and is typically considered a good estimate of the minimum principal stress. Various methods have evolved to best determine the closure pressure along with other key pressure indicators such as the instantaneous shut-in pressure (ISIP), which is the pressure once the pumps have been turned off and system friction effects dissipate. For much more detail on DFIT interpretation methods and their relative drawbacks and merits, the reader is referred to Enlighten's previous KSSMA study in which hundreds of these tests were used to map minimum principal stress across the entire KSMMA (Enlighten Geoscience, 2021, particularly Section II and Appendix A). In that study, it was demonstrated that operator-reported ISIP correlates very poorly with closure pressure. Far-field fracture extension pressure (FFEP) determined using Pressure Transient Analysis (PTA) based techniques, however, correlates very well with closure pressure. This is true for the 3-9 pad, as illustrated in Figure 34, where operator-reported ISIP correlates poorly with closure pressure (blue dots), while FFEP correlates very closely to closure pressure (orange dots). In this case, the closure pressure is an average  $(0.5 * (\text{Compliance} + \text{Tangent}))$  of that found using the compliance and tangent methods.

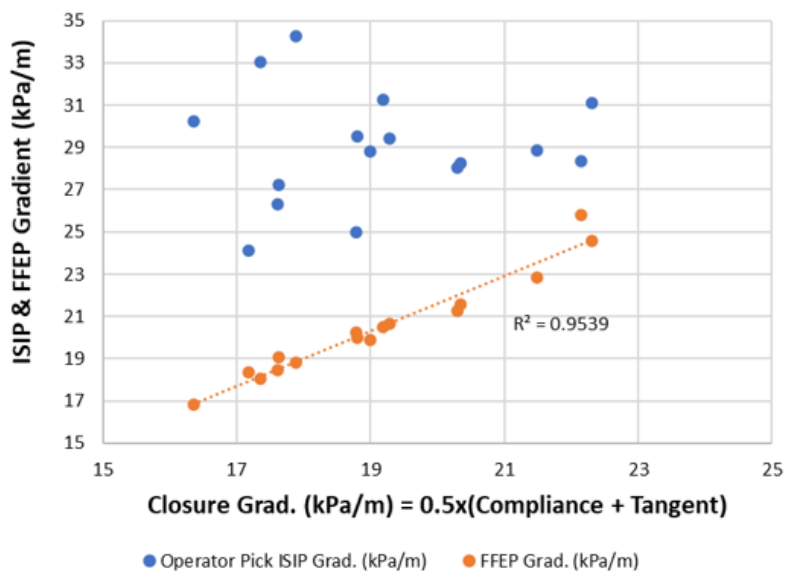


Figure 34. Comparison of how operator-picked ISIP values and PTA-based FFEP values correlate with closure pressure for the 3-9 DFITs.

While ISIP is considered a highly subjective interpretation point, it has historically been and continues to be one of the most commonly reported values from both DFIT tests and hydraulic fracturing treatments. A possible reason for this is that in the past some operators were able to establish consistent relationships between ISIP and minimum principal stress in specific areas. In addition, fracture closure is not identified on hydraulic fracturing stage data, so ISIP represent one of the only ways to estimate stress data from a hydraulic fracture treatment. With ISIP data from any source, consistency in how the value is interpreted/picked from the test data is very important. For the 3-9 Pad hydraulic fracturing treatment data set, all of the ISIPs were picked by the same analyst. For the purpose of this analysis, it is therefore assumed they were picked with a consistent methodology, meaning relative changes likely reflect real changes in minimum principal stress.

Figure 35 presents the DFIT FFEP values (large squares positioned at stage 0), operator-picked DFIT ISIP values (small squares positioned at stage 0.5), and hydraulic fracturing ISIP values (small symbols plotted at stages 1 and up) for all stages of the wells with DFITs on the 3-9 pad. The purple, horizontal line at 25 kPa/m represents the value of the vertical stress gradient at this location (Enlighten Geoscience, 2021). Square symbols represent wells drilled to the northwest from the pad, while circles represent wells drilled to the southeast. The five wells with DFITs that also had associated induced seismicity are all southeast-oriented wells (circles) and have larger symbols than the others. They are 102/16-34 (yellow), 100/16-34 (red), 103/16-34 (light blue), 103/09-34 (green) and 104/09-34 (black).

The first observation from Figure 35 is that DFIT FFEP aligns much better with stage 1 hydraulic fracturing ISIP than does DFIT ISIP. The second is that all of the wells associated with induced events, and many of the wells that are not, show a clear trend of increasing hydraulic fracturing stage ISIP with increasing stage number. For two of the seismogenic wells, ISIP values eventually reach and exceed the vertical stress. For several of the non-seismogenic wells that don't show this increasing trend, early

stage ISIPs start out higher than the vertical stress and remain high. Interestingly, these wells tended to experience completion problems such as screen-outs.

Figure 36 presents the number of induced seismic events as a function of stage number for the seismogenic wells on the 3-9 pad. Comparing Figure 36 with Figure 35, it appears that event numbers are higher as stage ISIP increases, and the highest numbers of events are associated with the wells where the stage ISIP eventually exceeds the vertical stress.

Taking a closer look at well 104/09-34-080-17W6/00, the well with the highest number of associated induced seismic events (194), Figure 37 shows hydraulic fracturing stage ISIP, event count per stage, event magnitude distribution (min, max and mean) and a small region along the well where it intersects the mapped trace of the Ft St John Graben South Fault. This further illustrates the increase in seismicity rate as ISIP approaches the vertical stress and shows that this occurs in the region of the mapped fault. The map in Figure 38 shows the locations of the induced events (above the magnitude of completeness for that year – see next section) relative to the well and fault trace.

Figures 39 and 40 present a similar plot and map for well 103/16-34-080-17W6/00. This well differs from 104/09-34 in that the event counts are considerably lower and it is the magnitudes, not numbers that seem to correlate with the increase in ISIP above the vertical stress and the location of the Ft. St. John Graben South Fault.

Plots like those in Figures 37 and 39 for all of the other wells on the 3-9 pad are available in Appendix D.

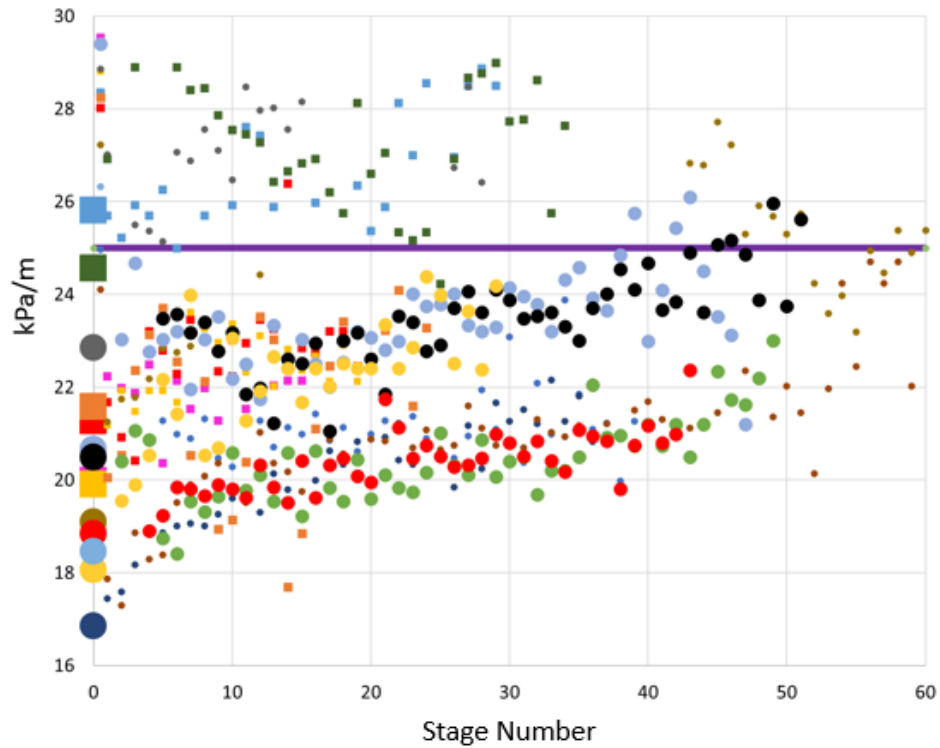


Figure 35. DFIT FFEP (stage 0), operator-picked DFIT ISIP (stage 0.5) and hydraulic fracturing stage ISIP as a function of fracture stage. See text for symbols explanation.

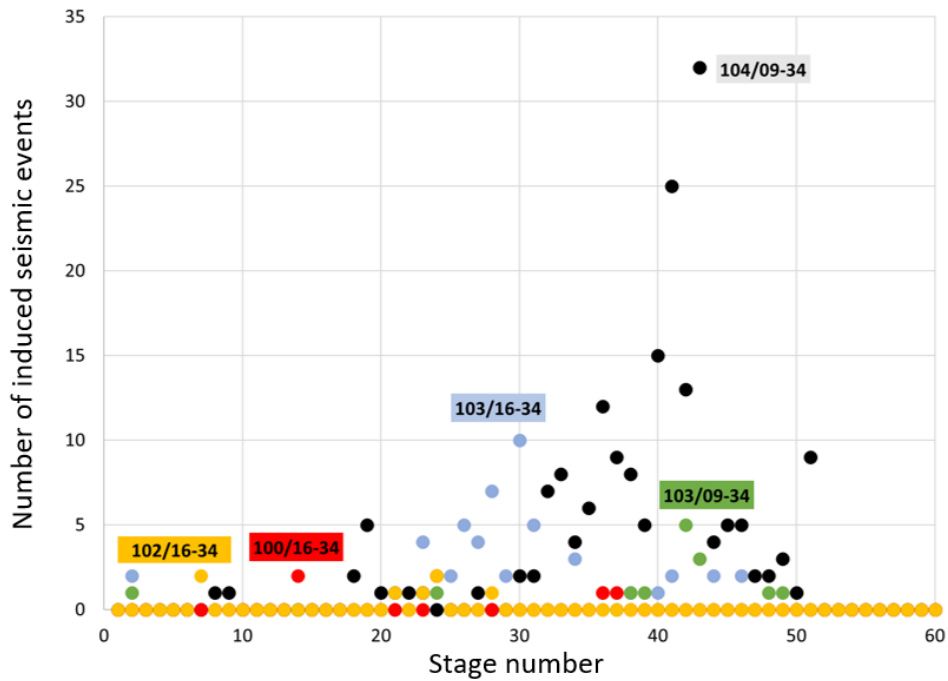


Figure 36. Number of induced seismic events as a function of stage number for the seismogenic wells on the 3-9 pad.

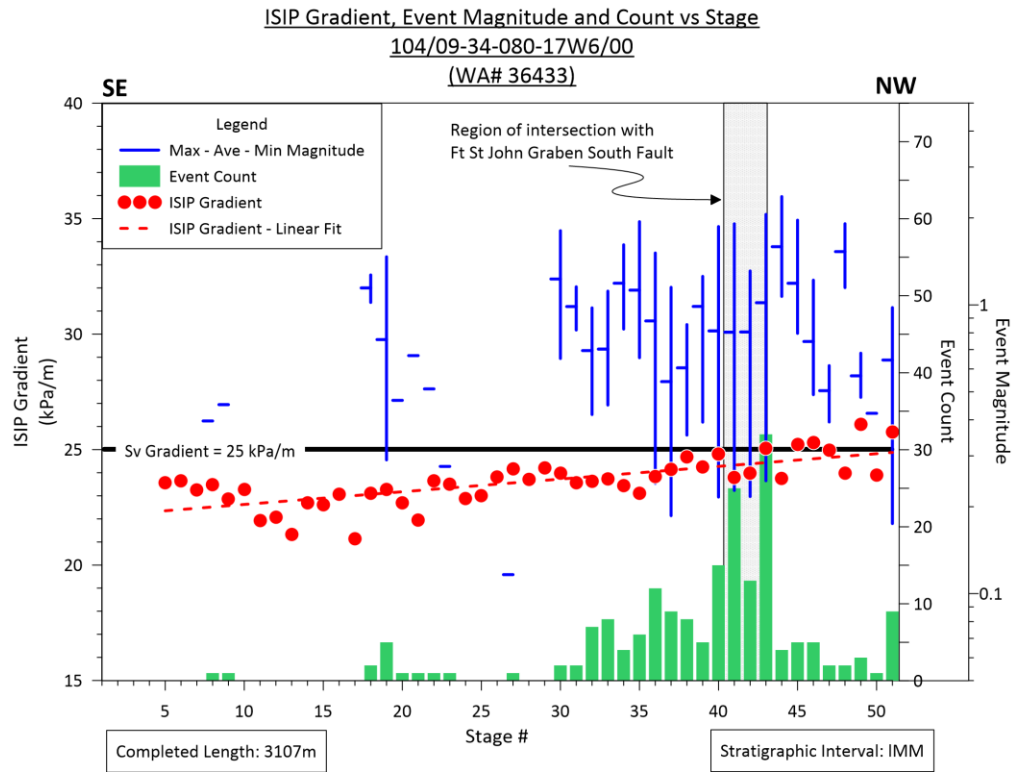


Figure 37. ISIP, induced seismic event count and event magnitude distribution as a function of stage number in well 104/09-34-080-17W6/00, with mapped location of the Ft. St. John Graben South Fault indicated.

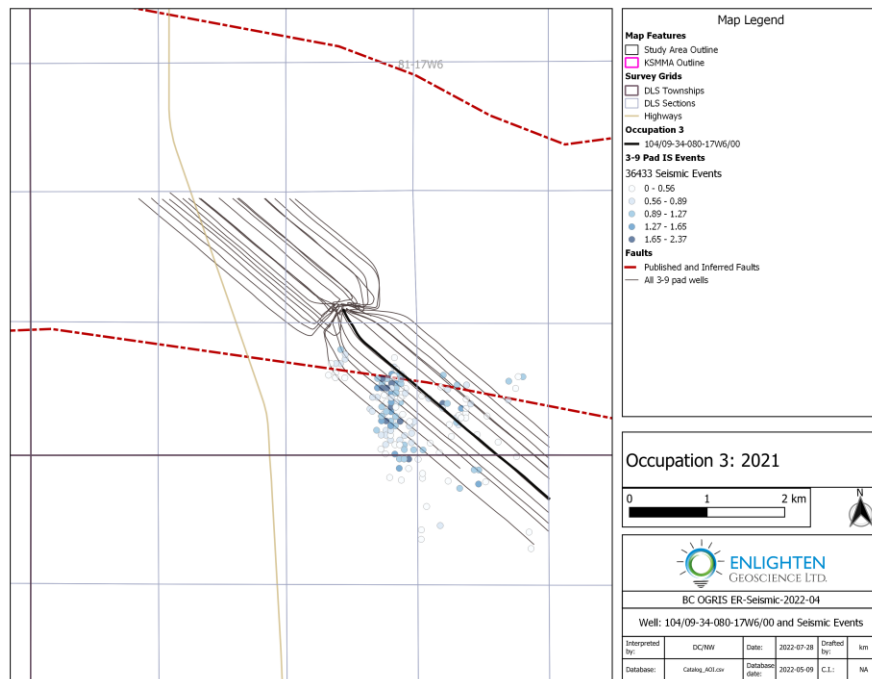


Figure 38. Map of well 104/09-34-080-17W6/00, its associated induced seismic events and the Ft. St. John Graben South Fault (as mapped).

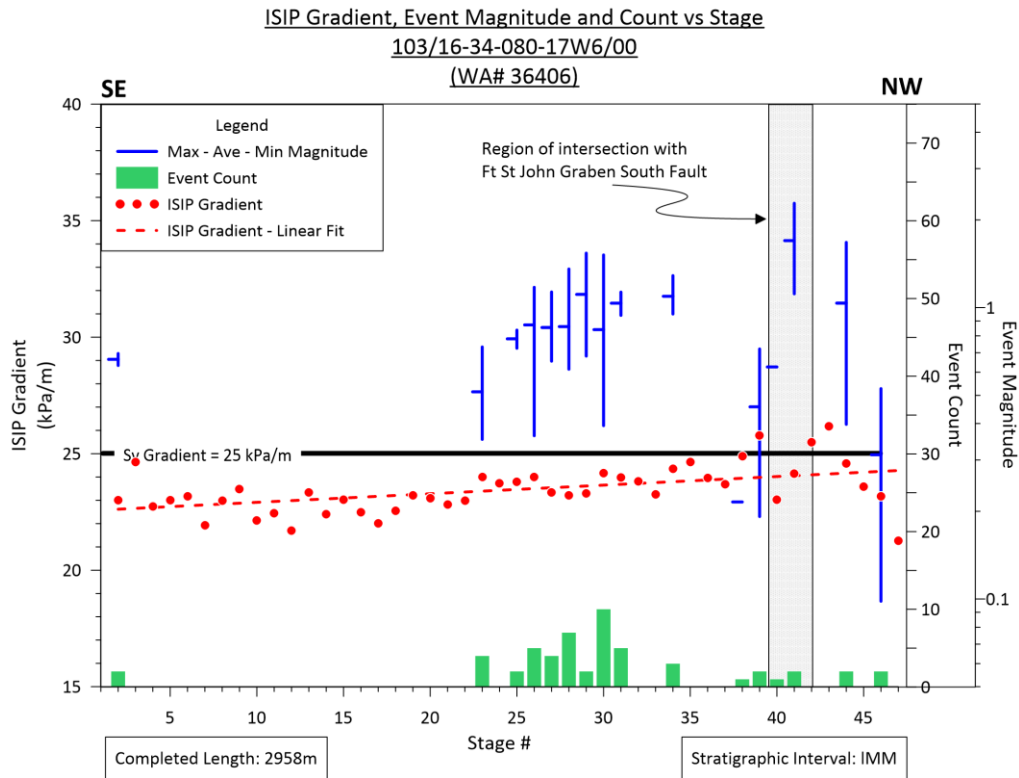


Figure 39. ISIP, induced seismic event count and event magnitude distribution as a function of stage number in well 103/16-34-080-17W6/00, with mapped location of the Ft. St. John Graben South Fault indicated.

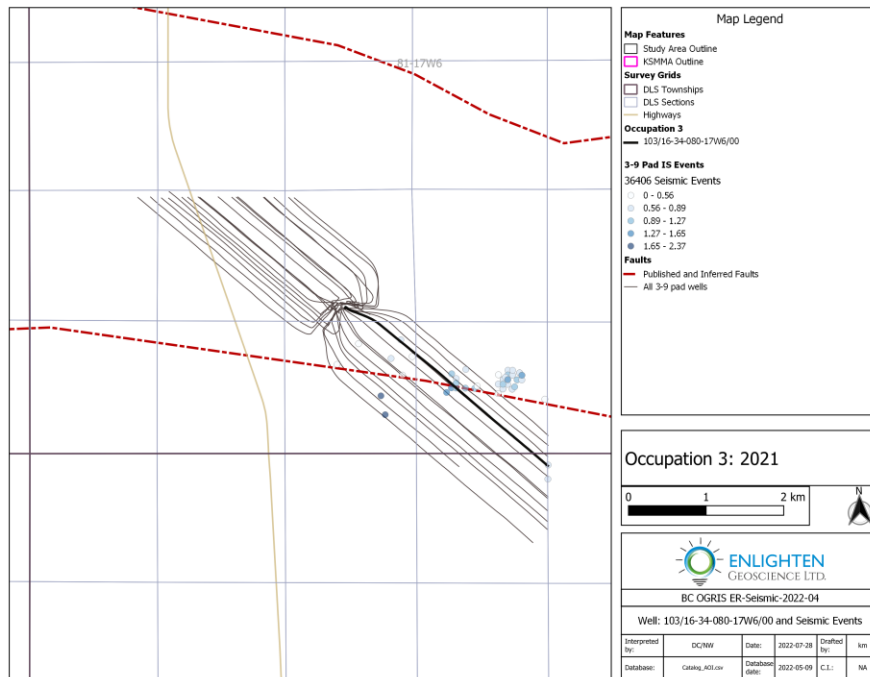


Figure 40. Map of well 103/16-34-080-17W6/00, its associated induced seismic events and the Ft. St. John Graben South Fault (as mapped).

A general increase in treating pressures with an increasing number of stages is not uncommon in horizontal wells with multi-stage hydraulic fracturing completions. It is often attributed to an increase in stress caused by the fracturing itself, a phenomenon frequently referred to as stress shadowing (Roussel, 2017). It is well known that stress shadowing may lead to some operational difficulties and sub-optimal hydraulic fracture geometries, but it has not previously been linked directly to induced seismicity.

It appears that for some of the wells on the 3-9 pad, stress shadowing, particularly when it leads to pressures close to the vertical stress, may be related to induced seismicity when a fault is present. Although it is not documented publicly, similar behavior has been seen in the Montney and Duvernay plays in Alberta (K. Nicholson, personal communication). At this point it can only be speculated as to what may be happening in the subsurface when these wells are being completed. Certainly, it is expected that as pressures approach the vertical stress, there is the possibility of creating sub-horizontal fractures by slight lifting of the overburden, most likely along bedding planes. Bedding-plane parallel natural fractures have been noted in Montney cores, with some showing clear evidence of past slip in the form of slickensides (Davies et al., 2018). Horizontal planes of weakness caused by differing rock mechanical properties are believed to contribute to “stair-step” hydraulic fracture growth, and potential casing shear, in parts of the Upper Montney in the Altares Field, north of the KSMMA (Sanders et al., 2018). How this might contribute to induced seismicity risk is not directly evident, but it is possible that a complex fracture network may increase the risk of the fluid pressure increase from the hydraulic fracture reaching a fault. PTA-based DFIT interpretation techniques can reveal evidence of induced fracture complexity through the identification of the presence and duration of different flow regimes. The same approach can be used on hydraulic fracturing stage fall-off data in real-time if it is expected that this fracture complexity is somehow related to induced seismicity risk.

As noted previously, some of the wells on the 3-9 pad have ISIP values higher than the vertical stress even in the early stages. Interestingly, these wells had numerous and severe problems during their completions. The 104/13-08-081-17W6/00 well (WA# 36412) provides a good example. In addition to difficulty experienced in keeping the well to the preferred target window during the drilling phase (to the point where the preferred horizon was abandoned) the completion phase experienced the following difficulties:

- Stage 4: Screen out. Unable to flush. Flowback the well.
- Stage 7: Pressure out on flush.
- Stage 9: Screen out. Flow to tester.
- Stage 13: Tagged obstruction during plug pump down. Decision to condense perf interval.
- Stage 14-15: Tagged workstring. Pump down with plug. No movement. POOH. Did fluid injectivity test and move to stage 16.
- Stage 16: Tool tagged obstruction. Decision to set plug as deep as possible.
- Stage 17: Flush early due to pressure. Flow to tank. Con't frac.
- Stage 18: Screen out on flush.
- Stage 19: Tagged obstruction during plug pumping down. Unable to pull free. Set plug @ 3224 mKB.
- Stage 21: Cut the sand short due to rising pressure.

- Stage 25: Tool string stuck. Tried fishing. Recovered Schlumberger perforating toolstring.

Similar issues were encountered in completing 100/13-34-080-17W6/00 (WA# 36430), including:

- Stage 1: Screened out performed a flush with a rate of 2m<sup>3</sup>/min @ 46.5 MPa.
- Stage 2: RIH w/ perf string and got stuck @ 4346 mKB. Set BP @ 4342 mKB and perf interval 2 and disconnect from perforating string. No Frac.
- Stage 3: Screened out after 13.5m<sup>3</sup> flush. Flushed well with 90m<sup>3</sup> of produced.
- Stage 5: Wireline tool stuck in hole @ 4184.2 mKB unable to free. Shot 3 guns and disconnect from tools and POOH. No Frac. Performed fishing operations and retrieved fish.
- Stage 15: Plug stuck @ 3369.9 mKB set plug and POOH. Flowed well back to testers and spot acid over plug squeeze 250 L every hour past plug. Perform high rate flush.
- Stage 15-25: Stage omitted. No Frac.
- Stage 25: Stuck in hole with BP @ 3289 mKB perf the interval and displaced acid into perforations. Decided not to frac.

A small percentage of induced seismicity in the KSMMA is from reverse faults (Roth et al., 2022; Babaie Mahani et al., 2020). ISIP values starting above the vertical stress may indicate a reverse faulting environment where the vertical stress is the minimum principal stress. ISIP values starting below the vertical stress but then later exceeding it may indicate a change in faulting regime from strike-slip or normal, where the horizontal stress is the minimum principal stress to reverse. The concept that a stress state can switch from one to another is not unheard of. There are well-documented cases where oil and gas activity has promoted a normal-faulting stress regime, where the vertical stress is the maximum horizontal stress, due to the poroelastic reduction in horizontal stresses with depletion (Zoback, 2010). In the 3-9 pad well, horizontal stresses may be increasing with increasing pressure, but only in a very localized area and probably only temporarily. Although the data set is limited, the DFITs from the 3-9 pad show a decreasing trend in FFEP over time from about 22 kPa/m to 19 kPa/m over the three occupations, as shown in Figure 41. If this is a poroelastic effect due to a pore pressure decrease over time from ongoing production, it implies a pore pressure change on the order of 4-5 kPa/m. In terms of Coulomb shear failure, both the pore pressure reduction and the decrease in stress magnitude would reduce fault slip risk overall. Dvory and Zoback (2021) demonstrated that due to poroelastic stress response in the Delaware Basin of Texas and New Mexico, induced seismicity has become less likely over time.

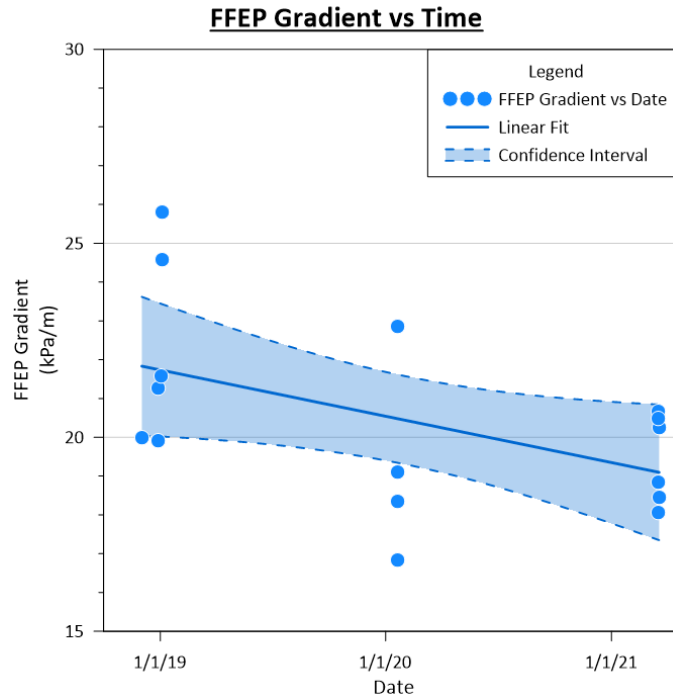


Figure 41. FFEF values from the 3-9 DFITs as a function of time.

### Earthquake b-value Analysis

One of the most commonly used models in seismology is the Gutenberg-Richter relationship (Gutenberg and Richter, 1944), which provides the relationship between magnitude and frequency of earthquakes as

$$\log_{10}(N) = a - bM$$

where  $N$  is the cumulative number of earthquakes with magnitudes equal to or greater than  $M$ , and  $a$  and  $b$  are the seismicity parameters; specifically,  $a$  is a measure of the level of seismicity (also known as seismic productivity), and  $b$ , which is the slope of the linear relationship and is commonly referred to as the b-value, describes the ratio between the number of small and large events. In an area with a higher b-value there is a proportionally higher number of small events than large events. For natural seismicity, the average b-value is generally close to 1.

Estimation of the b-value and its error can be achieved through a variety of methods (see Babaie Mahani, 2021). For this study, b-value was calculated using the magnitude interval approach (Utsu 1965; Bender, 1983):

$$b = \frac{1}{\ln(10) \left[ \mu - \left( M_c - \frac{\Delta M}{2} \right) \right]}$$

Where  $\mu$  is the average of magnitudes,  $\Delta M = 0.1$  and  $M_c$  is the magnitude of completeness of the seismic catalogue, which was calculated for this analysis using the maximum curvature technique of

Wiemer and Wyss (2000).  $M_c$  is dependent on the seismic recording network; events with magnitudes below  $M_c$  are not necessarily fully captured by the network.

Magnitude of completeness, b-value and error in the b-value were calculated for 17 scenarios as explained in Table 4. Scenario 1 is the full earthquake catalog used in the analysis, including events not associated with the 3-9 pad. Scenario 2 includes all earthquakes associated with the 3-9 pad wells. Scenarios 3 through 5 include all earthquakes associated with the 3-9 pad wells for occupations in January 2019, February 2020 and March to April 2021, respectively. The rest of the scenarios are for the 3-9 pad and events assigned to wells targeting specific Montney stratigraphic intervals. It is important to note that the seismic events themselves are not assigned to specific Montney intervals because of the large uncertainty in their hypocenter depths.

Figure 42 shows the magnitude of completeness, number of events with magnitudes above  $M_c$  and b-values (with error bars) for all of the scenarios listed in Table 4. Figures 43, 44 and 45 provide details for each of the pad occupations including event magnitudes,  $M_c$  and b-value as a function of time. For  $M_c$  and b-value, a moving window of 50 induced events was used, with a step of 10 events, therefore the calculated values start after the first 50 events. These figures also include a map of the induced events which includes a representation of a structural corridor discussed in Wozniakowska et al. (2021). Note that the maps in Figures 43 through 45 use a slightly different geographic projection than the other maps in this report and that the overall display is different as a result.

Scenario Number	Earthquakes	Completion Target(s)	Occupation Year(s)
1	Full catalogue	All	All
2	All associated with 3-9 pad wells	All	All
3	All associated with 3-9 pad wells	All	2019
4	All associated with 3-9 pad wells	All	2020
5	All associated with 3-9 pad wells	All	2021
6	All associated with 3-9 pad wells	lower Middle Montney	All
7	All associated with 3-9 pad wells	lower Middle Montney	2019
8	All associated with 3-9 pad wells	lower Middle Montney	2020
9	All associated with 3-9 pad wells	lower Middle Montney	2021
10	All associated with 3-9 pad wells	upper Middle Montney	All
11	All associated with 3-9 pad wells	upper Middle Montney	2019
12	All associated with 3-9 pad wells	upper Middle Montney	2020
13	All associated with 3-9 pad wells	upper Middle Montney	2021
14	All associated with 3-9 pad wells	Upper Montney	All
15	All associated with 3-9 pad wells	Upper Montney	2019
16	All associated with 3-9 pad wells	Upper Montney	2020
17	All associated with 3-9 pad wells	Upper Montney	2021

*Table 4. Scenario descriptions for the b-value analysis.*

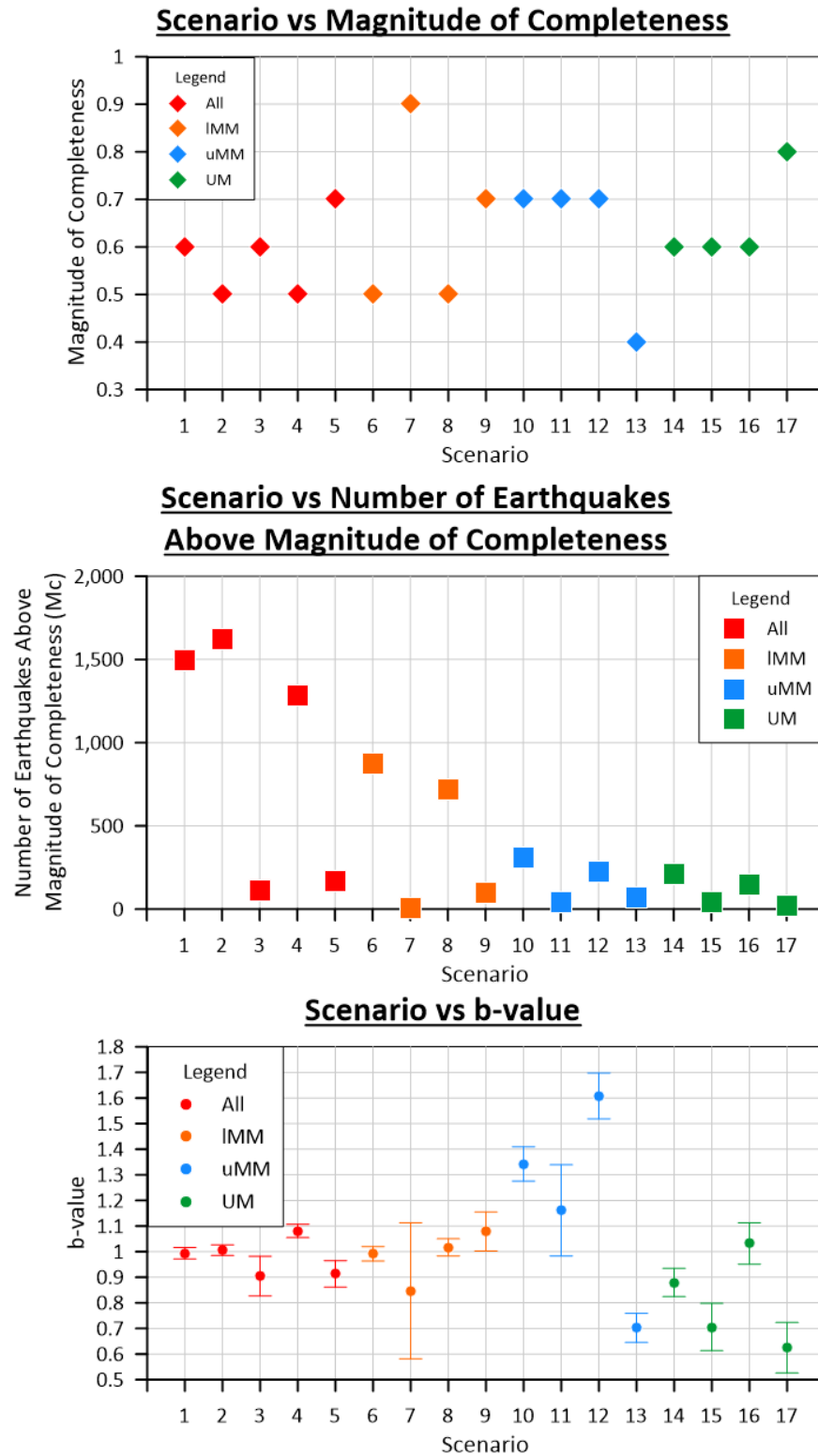
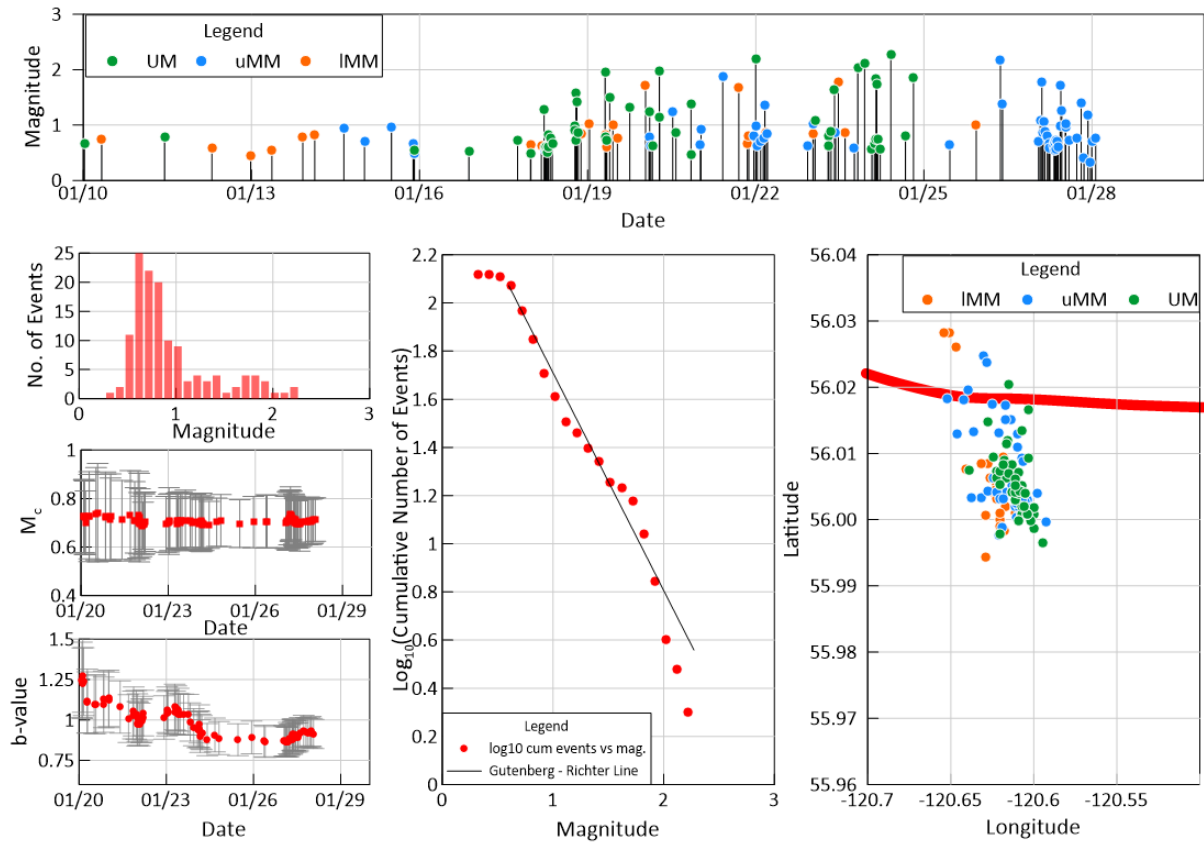


Figure 42. Magnitude of completeness ( $M_c$ ), number of events with magnitudes above  $M_c$  and  $b$ -values (with error bars) for all of the scenarios listed in Table 4. Points are coloured according to the target interval of the associated well(s).

*Geomechanical Effects of Cumulative Fluid Injection through Hydraulic Fracturing in the Kiskatinaw Seismic Monitoring and Mitigation Area, British Columbia (ER-Seismic-2022-04)*



*Figure 43. Details for the 2019 occupation of the 3-9 pad. Coloured data points refer to the target interval of the well associated with the seismic event.*

*Geomechanical Effects of Cumulative Fluid Injection through Hydraulic Fracturing in the Kiskatinaw Seismic Monitoring and Mitigation Area, British Columbia (ER-Seismic-2022-04)*

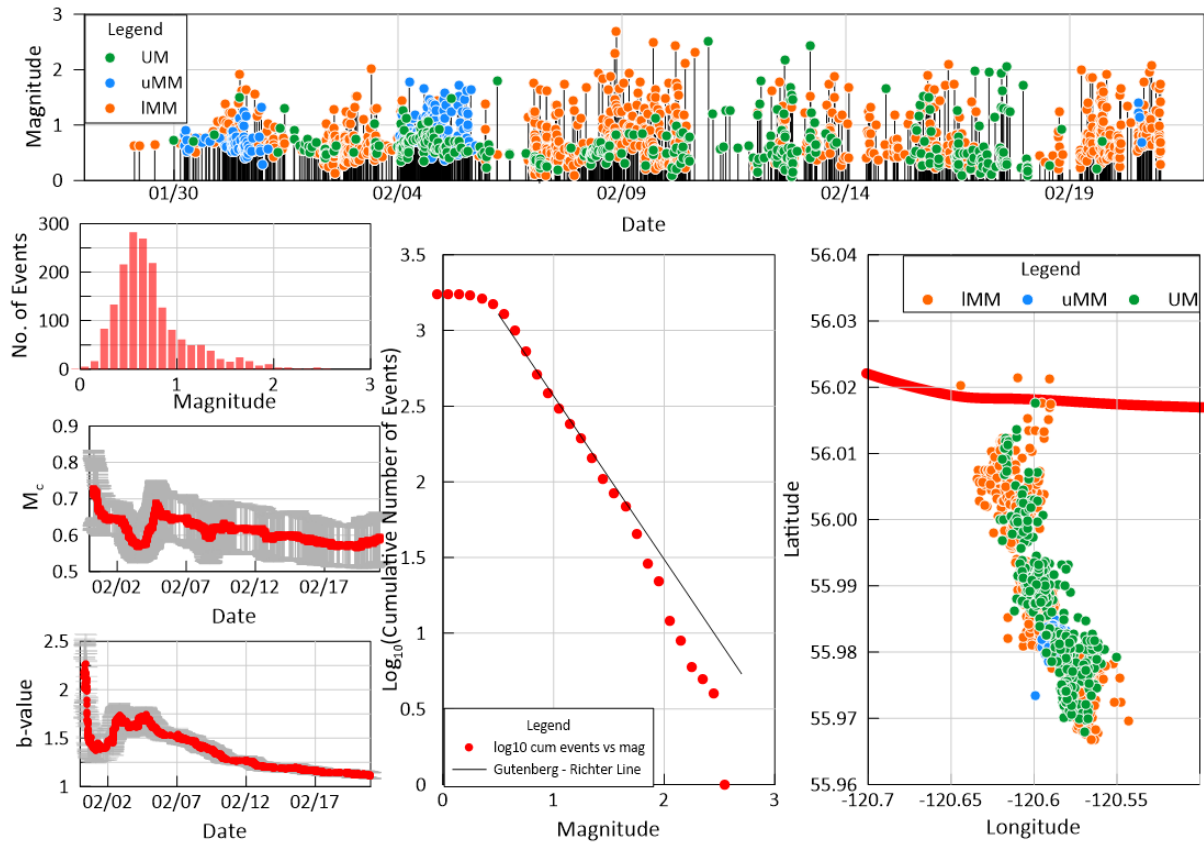


*Figure 44. Details for the 2020 occupation of the 3-9 pad. Coloured data points refer to the target interval of the well associated with the seismic event.*

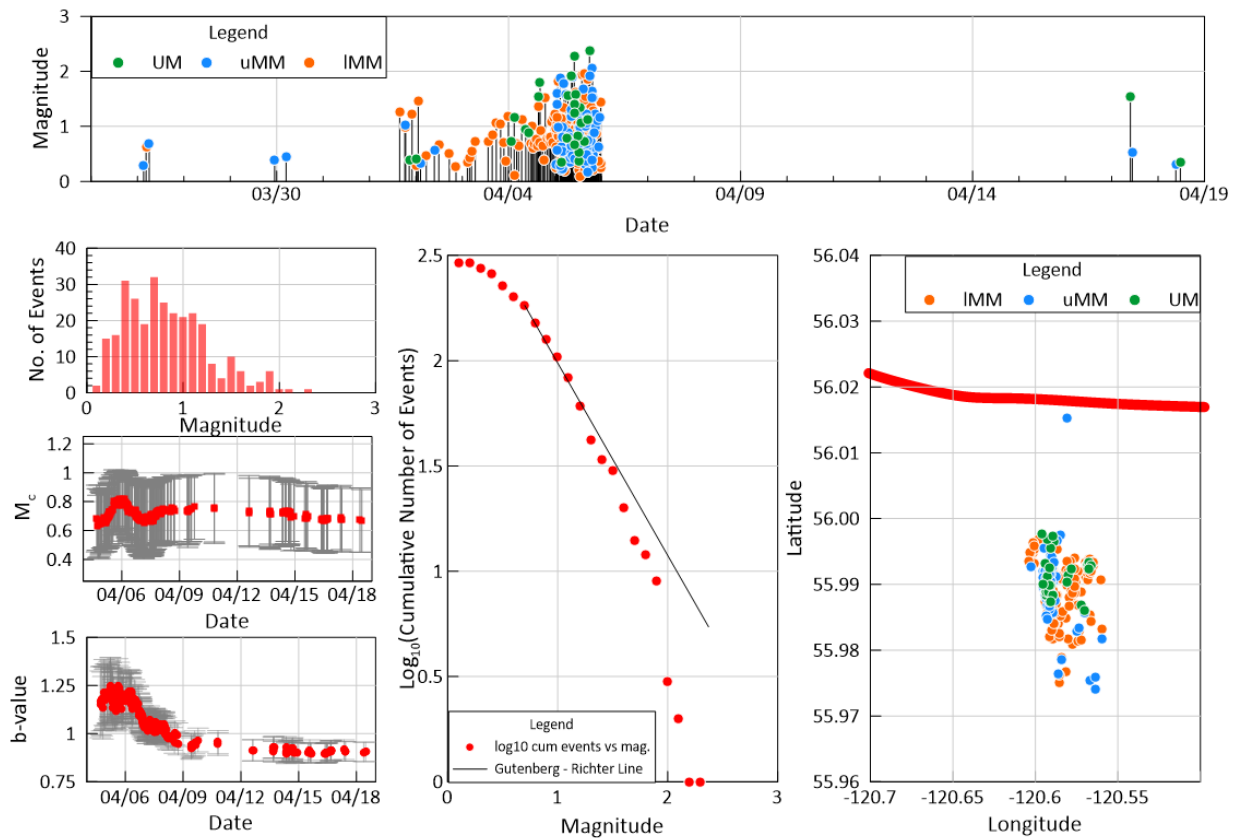


Figure 45. Details for the 2021 occupation of the 3-9 pad. Coloured data points refer to the target interval of the well associated with the seismic event.

The frequency–magnitude scaling relationship quantified by the b-value has been shown to hold down to very small ( $M = 0$  or less) seismic events (Abercrombie, 1996) and is controlled at least partly by the relative distribution of fault lengths in a given region (Wesnousky et al., 1983). The contribution of small seismic events in distributing elastic stress in the crust has been demonstrated by Hanks (1992) and Marsan (2005, 2006), who showed that small earthquakes are equally as important as large ones, redistributing stress over shorter wavelengths but in greater numbers.

Local b-values often deviate significantly from the global average value of 1. The cause is unclear, but it may be related to factors such as situ stress regime (Schorlemmer et al., 2005), regional stress magnitudes (Huang and Turcotte, 1988), or fault strength heterogeneity (Steady et al. 1996). Day-Lewis et al. (2010) attributed differences in b-values adjacent to sections of the San Andreas fault in California to differences in the scaling of local stress heterogeneity as observed in wellbore data. In general, based on observations of induced seismicity in different types of environments, it is expected that b-values for induced events will be higher than those for natural seismicity, but any meaningful interpretation remains difficult due to the problems inherent in analyzing data sets that are small in number and dynamic range (Geffers et al., 2022).

Babaie Mahani (2021) investigated Montney earthquake b-values across northeastern BC for the period between 2014 and 2018. For the south Montney data set, which is essentially equivalent to the KSMMA

area, it was found that the b-value over-estimated small earthquakes (approximately magnitudes 2 to 4) and underestimated larger events. The magnitudes of the events in this study are all less than 3. For the 2019 occupation (Figure 43), the b-value appears to underestimate events with magnitude 1.5 to 2, then overestimate events with magnitude greater than 2. In both other occupations, the b-value overestimates events with magnitude greater than 1.5.

Of all of the scenarios, the upper Middle Montney completion zone overall (scenario 10), and in just the 2019 (scenario 11) and 2020 (scenario 12) occupations, has by far the highest b-values. This is consistent with a relatively greater number of smaller magnitude events than larger ones, which is similar to the KSMMA-wide experience for wells targeting this stratigraphic interval. In all three pad occupations, b-values decrease over time. In 2020 and 2021 the drop-off is steep at first and then more gradual.

In all three occupations the highest magnitude events are in the middle of the occupation. It is during this period when seismic events necessitated, due to the mitigation measures enforced by the BC OGC in the KSMMA, that the operator implement operational changes such as rest time or skipping stages. It is likely that such measures resulted in the reduction of seismic events. In the 2019 and 2021 occupations it could potentially be argued that b-values show a small increase at the time of the largest events, but the significance of this observation, if any, is unclear.

The 2020 occupation clearly had the highest number of associated seismic events. On the map in Figure 44, these seem to delineate a broad NW-SE trending feature, which would be approximately perpendicular to the known, NE-SW orientation of the maximum horizontal tectonic stress in this region (Enlighten Geoscience, 2021). Closer investigation of these events, however, reveals a series of probable NE-SW oriented faults. Figure 46 presents the same population of seismic events as the map in Figure 44 but coloured according to the completion targets of the associated wells (the wells associated with induced seismicity are shown as black). This partially illustrates the individual NE-SW clusters of seismic events, but these are made even more clear in the associated animations (links below the figure). The first animation shows events for each day of activity on the pad, while the second shows the cumulative development of the daily events.

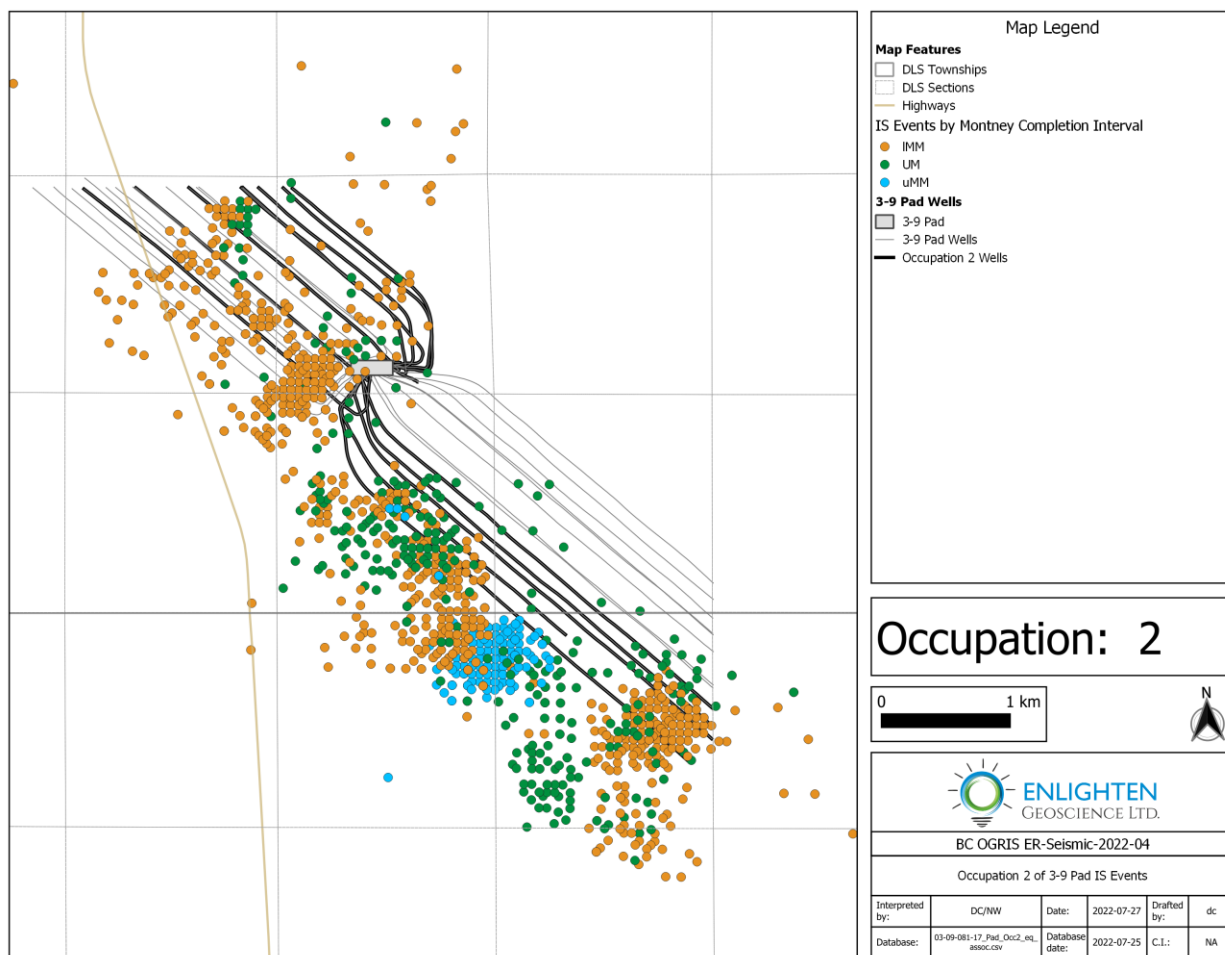


Figure 46. Map of seismic events during the 2020 pad occupation, coloured by target interval of the associated wells (shown in black).

[Link to map animation of daily seismic events \(greater than  \$M\_c\$ \) for the 2020 occupation of the 3-9 pad.](#)

[Link to map animation of cumulative seismic events \(greater than  \$M\_c\$ \) for the 2020 occupation of the 3-9 pad.](#)

Figure 47 shows events associated with a single completion interval (Stage 51) of well 104/09-34-080-17W6/00 (WA 36433), with a hypothetical, small fault trace defined by the events. The associated animation (link below the figure) presents a time-lapse view of all of the well completion stages, the associated seismic events, and corresponding fault interpretations. These smaller faults are at a more optimal orientation to the maximum horizontal stress for failure as strike-slip faults. Most of the induced earthquake events in the area have been found to be strike-slip events (Roth et al., 2022; Babaie Mahani et al., 2020), and the overall stress state has been shown to be strike-slip with the vertical stress magnitude intermediate between the minimum and maximum horizontal stress magnitudes (Enlighten Geoscience, 2021).

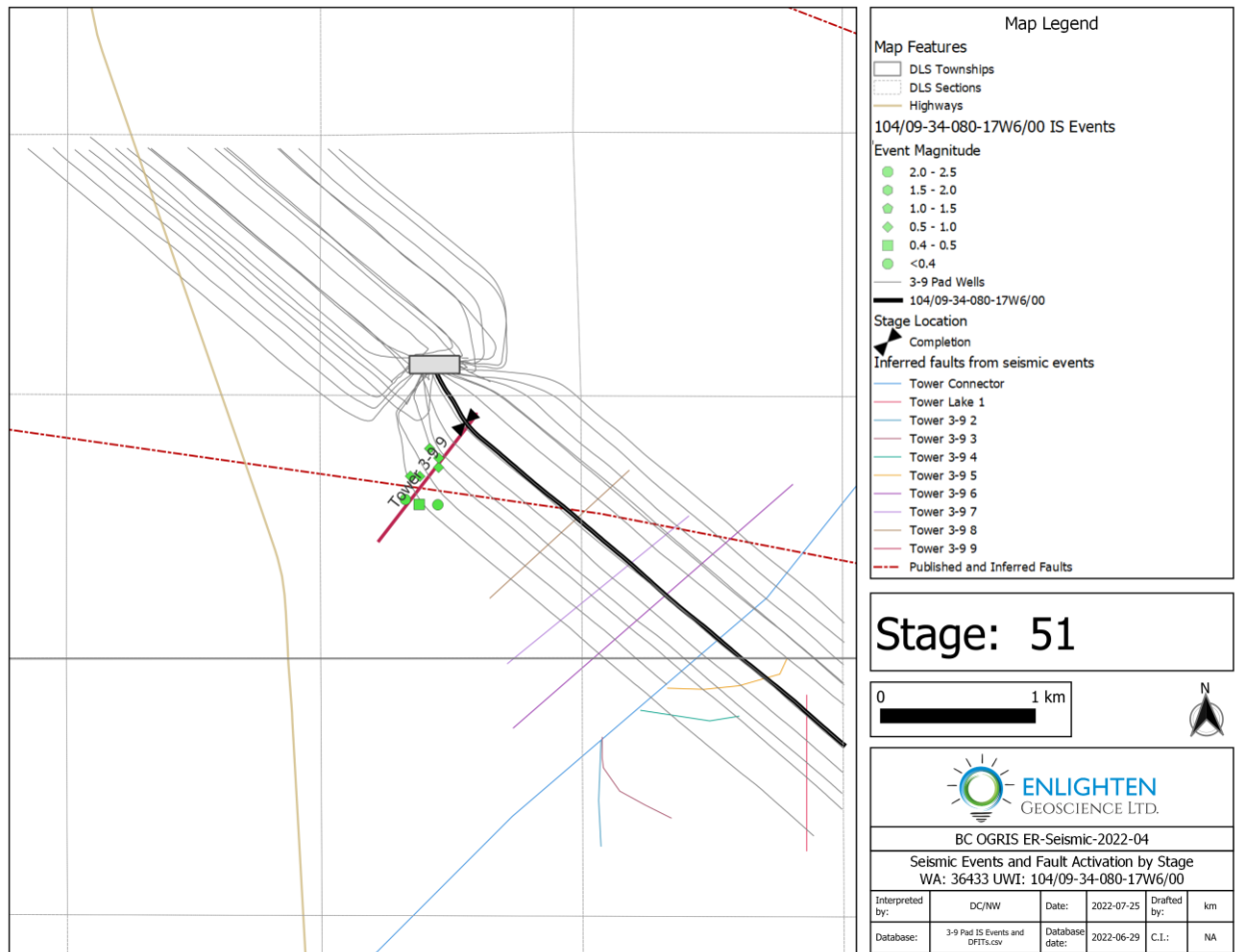


Figure 47. Map of seismic events associated with Stage 51 of the completion of 104/09-34-080-17W6/00 (WA 36433) during the 2020 occupation of the 3-9 pad, with interpreted potential fault trace superimposed (red). Additional potential fault traces defined by other completion stages (see the animation) are shown in additional colours.

[Link to map animation of WA 36433 completion summary and associated induced seismic events.](#)

## VI. Conclusions and Recommendations

The study detailed in this report provided an opportunity to investigate induced seismicity in the KSMMA in several novel and unique ways. The mapping workflow developed to illustrate cumulative fluid injection and withdrawal from the Montney combined with the analysis of the 3-9 Pad reinforced the proposition that temporary increases in pore pressure related to hydraulic fracturing in areas proximal to critically stressed faults is the primary driver of IS rather than continuously increasing fluid volumes.

Although the accepted understanding of the causes of induced seismicity point to the increase in pore pressure above the critical perturbation pressure of critically stressed faults, concern also arises with regards the volumes of liquids injected into the subsurface. While the volumes are very large in

aggregate, it is important to recognize that the pore space volume of the KSMMA Montney is three orders of magnitude larger than the injected fluids. Other factors offsetting the injected liquids volume include:

- The fluid is being injected into reservoirs in which the primary phase is compressible
- The injection has happened at discrete and different locations, intervals and time periods
- After load fluid recovery and produced fluids are considered, the net cumulative liquids injection in a particular area is generally negative

Several sources of data, including the mapping of seismicity over time, revealed the locations of probable faults that have not been previously published. Fault slip potential analysis, as was performed in Enlighten's previous study (Enlighten Geoscience, 2021), requires knowledge of the locations and orientations existing faults.

The analysis of the 3-9 pad demonstrated the information and insights that can be obtained by looking at detailed data from individual wells and induced earthquakes associated with them. DFIT and hydraulic fracturing treating pressures may be revealing information about changes in the subsurface stress state during completions and the development of induced seismicity risk. Such an analysis could be performed in real-time through the monitoring of hydraulic fracturing stage fall-off data for indications of increasing pressures and/or fracture complexity, especially approaching a known fault.

Some authors have suggested that the rate of induced seismicity, and induced event magnitudes, will increase over time with ongoing hydraulic fracture-based field development (e.g., Chapman, 2021). This concept is erroneous in the KSMMA and elsewhere. The work presented here demonstrates that the effects of Montney hydraulic fracturing flowback and production more than offset the cumulative effect of fluid injection during hydraulic fracturing. In addition, the stress drop associated with cumulative seismicity (Roth et al., 2022) would likely serve to reduce seismic risk. At the Coso geothermal field in California, for example, a large earthquake generated relatively few aftershocks, and no major aftershocks, within the Coso field itself because of prior stress relief by small earthquakes generated by the geothermal activity (Im et al., 2021).

The results of this work should be of interest to many stakeholders including the regulators, oil and gas operators and the public. Through sharing of the data generated during this work, it is hoped that other researchers will be able to build on the results presented here to better mitigate induced seismicity in the KSMMA and elsewhere. In particular, the following work is recommended:

- Develop a more detailed structural model for the KSMMA incorporating all available wellbore, seismic event, geophysical and other data.
- Expand the understanding of pressure-induced drawdown and depletion over time through more detailed pressure evaluation.
- Re-apply the fault slip potential workflow to the faults mapped in the structural model and applying the insights in the advanced pressure analysis.
- Continue to develop an understanding of the implications and applications of anomalous hydraulic fracture ISIP data, particularly with regards background levels of stress shadowing, and encroachment on known faults.

## VII. Acknowledgements

We are grateful for the financial support of BC OGRIS and the technical support of the BC Oil and Gas Commission, particularly Michelle Gaucher and Stuart Venables. The cooperation and encouragement the authors continue to receive from the OGC is always appreciated and serves as a model for regulators in other jurisdictions. We also wish to thank Ryan Visser for providing the associations of the induced seismic events to the completions activity on the 3-9 pad and Amanda Grieg and Sobhi Alhaswa of Ovintiv for their comments on a draft of this report.

## VIII. Appendices

### [Appendix A: Databases](#)

#### Appendix A1: DFIT Database

This is folder containing an updated database of DFIT data from across the KSMMA. The database filename is **DFIT Database 07-04-2022 with redactions.xlsx**. There is also a README file: **DFIT Database Read Me.pdf**.

#### Appendix A2: Earthquake Databases

This is a folder containing the full earthquake catalog used in the study (filename **Catalog\_AOI csv**) and the databases of events assigned to the 3-9 pad analysis (filename **03-09-081-17\_PadRun1\_eq\_assoc.csv**, **03-09-081-17\_PadRun2\_eq\_assoc.csv** and **03-09-081-17\_PadRun3\_eq\_assoc.csv**). There is also an explanation of how the event assignments were achieved (filename **R Visser notes on assigning IS events to stages.pdf**).

### [Appendix B: Data Sources and Software](#)

This appendix outlines the data sources and software products utilized in this study. The filename is **Appendix B - Data Sources and Software.PDF**.

### [Appendix C: Maps and Mapping Data](#)

#### Appendix C1: Large-format Maps

This appendix is a folder containing full-size (91.4 cm x 104.6 cm) copies of selected maps shown and discussed in this report. The maps are individual PDF files with self-explanatory file names.

#### Appendix C2: Map Shapefiles

This appendix is a folder containing ESRI Shapefiles of the contours and data for each map in Appendix C1.

#### Appendix C3: Mapping Data Files

This appendix is a folder containing the grid files and associated .csv files for the maps included in Appendix C1, shapefiles in Appendix C2 and image files in Appendix C4.

#### Appendix C4: Image and Animation Files

This appendix is a folder containing subfolders with the .MOV files of the time series animations and the .PNG files used to create the animations, respectively.

#### [Appendix D: 3-9 Pad ISIP and Seismicity Plots](#)

This appendix is a folder containing additional figures like those in Figures 37 to 40 for the other wells on the 3-9 pad.

## IX. References

- Abercrombie, R. E., The magnitude-frequency distribution of earthquakes recorded with deep seismometers at Cajon Pass, southern California, *Tectonophysics*, v. 261, p. 1–7, 1996 ([https://sites.bu.edu/rea/files/2016/02/cjp\\_ml\\_tectonophys96.pdf](https://sites.bu.edu/rea/files/2016/02/cjp_ml_tectonophys96.pdf))
- Babaie Mahani, A., Seismic b value within the Montney play of northeastern British Columbia, Canada, *Canadian Journal of Earth Sciences*, v. 58, no. 8, p. 720–730, <https://doi.org/10.1139/cjes-2020-0157>, 2021
- Babaie Mahani, A., F. Esfahani, H. Kao, M. Gaucher, M. Hayes, R. Visser and S. Venables, A Systematic Study of Earthquake Source Mechanism and Regional Stress Field in the Southern Montney Unconventional Play of Northeast British Columbia, Canada, *Seismological Research Letters*, v. 91, n.1, p. 195–206, <https://doi.org/10.1785/0220190230>, 2020
- Barclay, J.E., F. F. Krause, R. J. Campbell and J. Utting, Dynamic casting and growth faulting: Dawson Creek Graben Complex, Carboniferous-Permian Peace River Embayment, western Canada. *Bulletin of Canadian Petroleum Geology*, v. 38A, p. 115–145, 1990
- Bender, B., Maximum likelihood estimation of b values for magnitude grouped data, *Bulletin of Seismological Society of America*, v. 73, p. 831–851, <https://doi.org/10.1785/BSSA0730030831>, 1983
- Berger, Z., M. Boast and M. Mushayandebvu, The contribution of integrated HRAM studies to exploration and exploitation of unconventional plays in North America, *CSPG Reservoir*, v. 35, no. 10, p. 42–47, 2008
- Berger, Z., M. Boast and M. Mushayandebvu, The contribution of integrated HRAM studies to exploration and exploitation of unconventional plays in North America. Part 2. Basement structures control on the development of the Peace River Arch's Montney/Doig resource plays, *CSPG Reservoir*, v. 36, p. 40–45, 2009
- British Columbia Oil and Gas Commission Data Centre. Drilling Kicks and Blowouts by Area [BCOGC-41720] [https://iris.bcogc.ca/reports/rwservlet?prd\\_ogcr708](https://iris.bcogc.ca/reports/rwservlet?prd_ogcr708) [accessed 05-13-2022]
- British Columbia Oil and Gas Commission, 2020, 2020-Gas-Reserves.csv, <https://www.bcogc.ca/files/operations-documentation/Reservoir-Management/Reserves/2020-Gas-Reserves.csv> [accessed 07-01-2022]
- British Columbia Oil and Gas Commission eLibrary, 2022, <https://www.bcogc.ca/energy-professionals/online-systems/elibrary/> [accessed 06-01-2022]

Chapman, A. R., Hydraulic Fracturing, Cumulative Development and Earthquakes in the Peace River Region of British Columbia, Canada, *Journal of Geoscience and Environment Protection*, v. 9, p. 55–82, <https://doi.org/10.4236/gep.2021.95006>, 2021

Davies, G., N. Watson, T. Moslow and J. MacEachern, Regional Subdivisions, Sequences, Correlations and Facies Relationships of the Lower Triassic Montney Formation, West-Central Alberta to Northeastern British Columbia, Canada — with Emphasis on Role of Paleostucture, *Bulletin of Canadian Petroleum Geology*, v. 66, n. 1, p. 23–92, 2018

Day-Lewis, A., M. Zoback, and S. Hickman, Scale-invariant stress orientations and seismicity rates near the San Andreas Fault, *Geophysical Research Letters*, v. 37, no. L24304, <https://doi.org/10.1029/2010GL045025>, 2010

Enlighten Geoscience Ltd., Pressure, Stress and Fault Slip Risk Mapping in the Kiskatinaw Seismic Monitoring and Mitigation Area, British Columbia, Report for BC Oil and Gas Research and Innovation Society, Project ER-Seismic-2020-01, February 2021 (<https://www.bcogris.ca/projects/complete>)

Euzen, T., T. Moslow, V. Crombez and S. Rohais, Regional Stratigraphic Architecture of the Spathian Deposits in Western Canada — Implications for the Montney Resource Play, *Bulletin of Canadian Petroleum Geology*. v. 66, n. 1, p. 175–192, 2018

Euzen, T., N. Watson, M. Fowler, A. Mort and T. Moslow, Petroleum distribution in the Montney hybrid play: Source, carrier bed, and structural controls, *AAPG Bulletin*, v. 105, n. 9, p. 1867-1892, <https://doi.org/10.1306/12222020088>, 2021

Fox, A. D. and N. D. Watson, Induced Seismicity Study in the Kiskatinaw Seismic Monitoring and Mitigation Area, British Columbia, report to the BC Oil and Gas Commission, 2019 (<https://www.bcogc.ca/data-reports/reports/>)

gDC Web™, geOLOGIC systems Ltd., 2022, <https://gdcweb.geologic.com> [accessed 05-13-2022]

Geffers, G.-M., I. G. Main and M. Naylor, Biases in estimating b-values from small earthquake catalogues: how high are high b-values?, *Geophysical Journal International*, v. 229, p. 1840-1855, <https://doi.org/10.1093/gji/ggac028>, 2022

Gutenberg, B. and C. F. Richter, Frequency of earthquakes in California, *Bulletin of the Seismological Society of America*, v. 34, p. 185–188, 1944 (<https://authors.library.caltech.edu/47734/1/185.full.pdf>)

Hayes, B., H. Anderson, M. Cooper, P. McLellan and B. Rostron, Wastewater Disposal in the Maturing Montney Play Fairway of NEBC, *Geoscience BC*, 2021 (<https://www.geosciencebc.com/projects/2019-004/>)

Im, K., J.-P. Avouac, E. Heimisson and D. Elsworth, Ridgecrest aftershocks at Coso suppressed by thermal destressing, *Nature*, v. 595, p. 7–74, <https://doi.org/10.1038/s41586-021-03601-4>, 2021

Kijko, A. and A. Smit, Extension of the Aki-Utsu b-value estimator for incomplete catalogs, *Bulletin of the Seismological Society of America*, v. 102, p. 1283–1287, <https://doi.org/10.1785/0120110226>, 2012

Koohzare, A., P. Vaníček and M. Santos, Pattern of recent vertical crustal movements in Canada. *Journal of Geodynamics* v. 45, p. 133–145, 2008

([http://www2.unb.ca/gge/Personnel/Santos/JGeodyn2007\\_final.pdf](http://www2.unb.ca/gge/Personnel/Santos/JGeodyn2007_final.pdf))

Lagenbruch, C., M. Weingarten and M. D. Zoback, Physics-based forecasting of man-made earthquake hazards in Oklahoma and Kansas, *nature communications*, <https://doi.org/10.1038/s41467-018-06167-4>, 2018

Moslow, T., B. Haverslew and C. Henderson, Sedimentary Facies, Petrology, Reservoir Characteristics, Conodont Biostratigraphy and Sequence Stratigraphic Framework of a Continuous (395m) Full Diameter Core of the Lower Triassic Montney Fm, Northeastern British Columbia, *Bulletin of Canadian Petroleum Geology*, v. 66, no. 1, p. 259–287, 2018

Norgard, G.T., Structural inversion of the Middle Triassic Halfway Formation, Monias Field, northeast British Columbia, *Bulletin of Canadian Petroleum Geology*, v. 45, p. 614–623, 1997

O'Connell, S.C., Geological history of the Peace River Arch, in *Geological Atlas of the Western Canada Sedimentary Basin*, G.D. Mossop and I. Shetsen (comps.), Canadian Society of Petroleum Geologists and Alberta Research Council, ch. 28, 1994 (<https://ags.aer.ca/reports/atlas-western-canada-sedimentary-basin>)

Roth, M. P., K. B. Kemna, R. M. Harrington and Y. Liu, Source properties of hydraulic-fracturing induced earthquakes in the Kiskatinaw area, British Columbia, Canada, *Journal of Geophysical Research: Solid Earth*, v. 127, no. e2021JB022750, <https://doi.org/10.1029/2021JB022750>, 2022

Roussel, N. P., Analyzing ISIP Stage-by-Stage Escalation to Determine Fracture Height and Horizontal-Stress Anisotropy, paper presented at the SPE Hydraulic Fracturing Technology Conference and Exhibition, The Woodlands, Texas, USA, January 2017, Paper Number SPE-184865-MS, <https://doi.org/10.2118/184865-MS>

Sanders, S., C. Etienne, A. Gogolick, E. Kelly and J.-P. Zonneveld, The Middle Montney Altares Member: lithology, depositional setting and significance for horizontal drilling and completion in the Altares Field, British Columbia, *Bulletin of Canadian Petroleum Geology*, v. 66, no. 1, p. 318–337, 2018

Schorlemmer, D., S. Wiemer, and M. Wyss, Variations in earthquake–size distribution across different stress regimes, *Nature*, v. 437, p. 539–542, <https://doi.org/10.1038/nature04094>, 2005

Schultz, R., G. Atkinson, D. W. Eaton, Y. J. Gu and H. Kao, Hydraulic fracturing volume is associated with induced earthquake productivity in the Duvernay play, *Science*, v. 359, p. 304–308, <https://doi.org/10.1126/science.aao0159>, 2018

Stacy, S. J., J. McCloskey, C. J. Bean and J. Ren, Heterogeneity in a self-organised critical earthquake model, *Geophysical Research Letters* v. 23, p. 383–386, <https://doi.org/10.1029/96GL00257>, 1996

Utsu, T., A method for determining the value of b in the formula  $\log n = a - bM$  showing the magnitude-frequency relation for earthquakes (with English summary), *Geophysical Bulletin of Hokkaido University*, v. 13, p. 99-103, 1965

Wesnousky, S. G., C. H. Scholz, K. Shimazaki, and T. Matsuda, Earthquake frequency distribution and the mechanics of faulting, *Journal of Geophysical Research*, v. B88, p. 9331–9340, <https://doi.org/10.1029/JB088iB11p09331>, 1983

Wiemer, S. and M. Wyss, Minimum magnitude of completeness in earthquake catalogs: examples from Alaska, the western United States, and Japan, *Bulletin of Seismological Society of America*, v. 90, p. 859–869, <http://dx.doi.org/10.1785/0119990114>, 2000

Wozniakowska, P., D. W. Eaton, C. Deblonde, A. Mort and O. H. Ardakani, Identification of regional structural corridors in the Montney play using trend surface analysis combined with geophysical imaging, British Columbia and Alberta, Geological Survey of Canada Open File 8814 <https://doi.org/10.4095/328850>, 2021

Zoback, M. D., *Reservoir Geomechanics*, Cambridge University Press, Cambridge, UK, 449 p., 2010

Zonneveld, J.-P. and T. Moslow, Palaeogeographic Setting, Lithostratigraphy, and Sedimentary Framework of the Lower Triassic Montney Formation of Western Alberta and Northeastern British Columbia, *Bulletin of Canadian Petroleum Geology*, v. 66, n. 1, p. 93–127, 2018